DETERMINATION OF FIELD SCALE DISPERSIVITIES BY MATHEMATICAL MODELING

by

ROBERT DEAN RAVNAAS, B.S.

THESIS

Presented to the Faculty of the Graduate School of

The University of Texas at Austin

in Partial Fulfillment

of the Requirements

for the Degree of

MASTER OF SCIENCE IN ENGINEERING

THE UNIVERSITY OF TEXAS AT AUSTIN

August 1981

ACKNOWLEDGEMENTS

The author would like to thank INTERCOMP for their financial support of this project.

Gratitude is extended to the University of Texas Engineering Foundation and the Texas Mining and Mineral Resources Research Institute for their respective fellowships.

A very special appreciation is extended to Dr. Larry Lake, the supervising professor in this project. His patience with this substantially less than "ideal" graduate student will never be forgotten. The author would also like to thank the other member of his committee, Dr. Gary Pope, for his instructive comments and recommendations.

Robert Dean Ravnaas

The University of Texas
Austin, Texas 78712
August 1981

ABSTRACT

Dispersion in heterogeneous porous media results from the simultaneous action of a mechanical phenomenon and molecular diffusion. The mechanical contribution arises from discrepancies in flow streamlines caused by inhomogeneities within the system.

A two dimensional computer simulator based upon the moving point method was written. This method accurately described all levels of numerical dispersion.

Observation well data from the El Dorado field in Kansas were effluent history matched with corresponding simulator runs. Longitudinal dispersivities ranged from 12 ft to 20 ft while transverse dispersivities ranged from 0.00 ft to 0.06 ft. An "ideal" sampling scheme is proposed for future field wide dispersion tests, enabling more accurate determinations of history matched dispersivities.

The Lake and Hirasaki method of grouping layered systems producing effective one-dimensional dispersivities, was found to be a relatively quick, approximate, procedure. This method takes into account the oftentimes important relative spatial ordering of reservoir layers.

TABLE OF CONTENTS

LIST OF TABLES

LIST OF FIGURES

CHAPTER 1. INTRODUCTION

1.1 General Discussion of Dispersion in Porous Media

Dispersion in porous media fluid flow is the occurrence and evolution of a transition zone between two domains of the fluid phase with different concentrations.[1,2] For example, let us consider a porous medium saturated with pure water contained in a cylindrical tube. At time zero, a chemical liquid compound mixed with water at concentration C_o is injected into the tube. The concentration is a step function at time zero (Figure (1-1)). The movement is unidirectional and the injection rate is constant. The concentration of the injected chemical compound varies with time and position. The variation of concentration with position at fixed time has the typical aspect of an S-curve. The transition zone is frequently defined as the zone where the concentration of injected liquid varies from $0.1C_o$ to $0.9C_o$. The width of the transition zone varies with the square root of time, which is a typical effect of dispersion.

Dispersion results from the simultaneous action of both a purely mechanical phenomenom and a molecular diffusion phenomenom.[1,2,3]

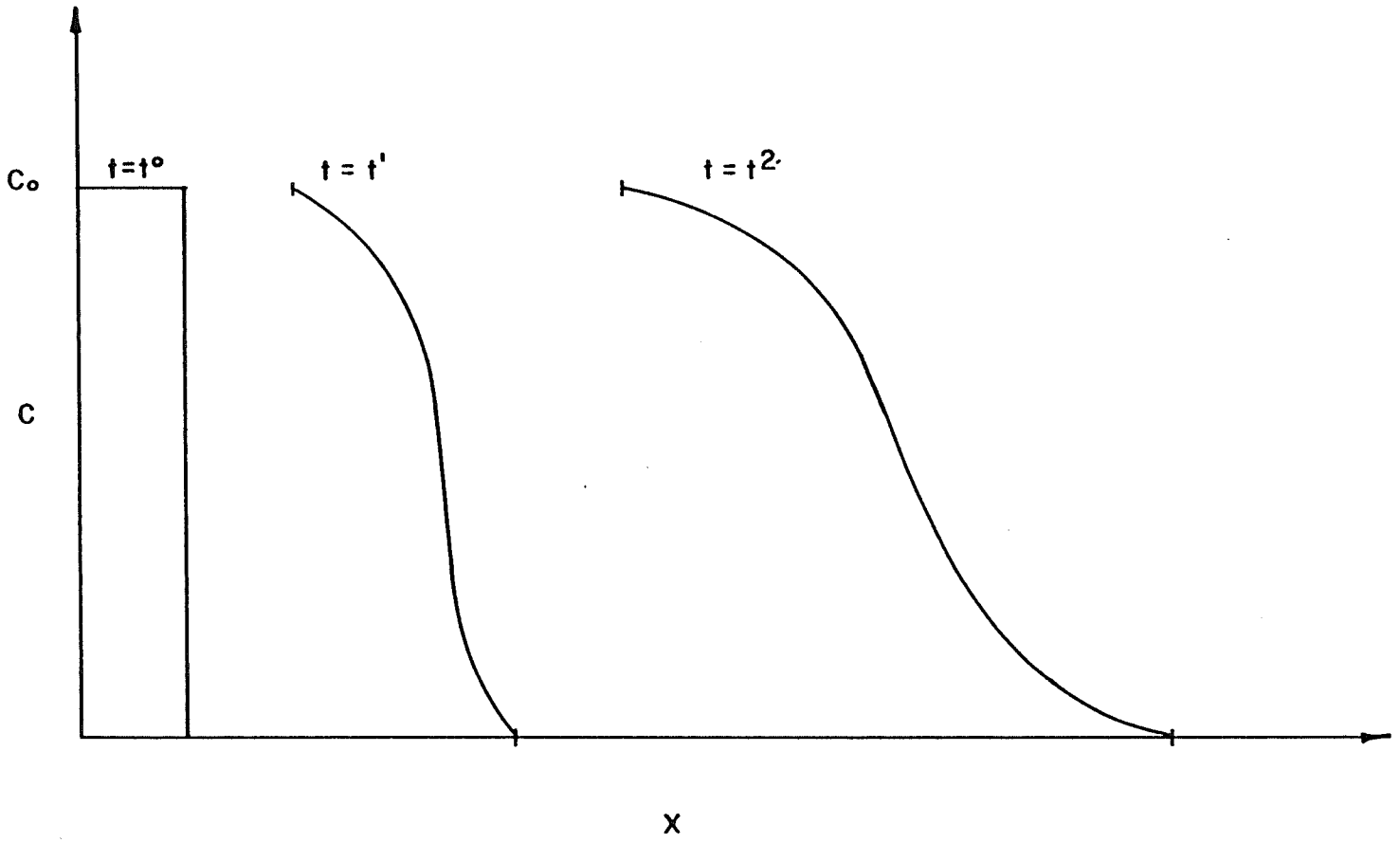

Figure 1-1. Evolution of transition zone with time.

1.1a Mechanical action

The velocity distribution of a fluid flowing through a porous medium is not microscopically uniform. Variations of pore dimensions create discrepancies between the flow streamlines yielding mechanical dispersion (Figure (1-2)). For quantitative purposes, mechanical dispersion is classified as consisting of two parts, one in the direction of mean fluid velocity and another in the plane orthogonal to fluid flow. These are respectively termed longitudinal and transverse dispersion.

1.1b Diffusion action

Molecular diffusion results when a concentration gradient exists between two miscible fluids in contact, whether they are in motion or at rest. Fick[1,4] performed the first quantitative study of diffusion in 1855. He noticed an anology between diffusion and heat transfer, and stated that the rate of diffusive transfer of a substance through a unit area is proportional to the concentration gradient normal to the area. This is expressed mathematically as:

$$N_A = -D_o \frac{dC_A}{d_x} \qquad (1\text{-}1)$$

where

$N_A \equiv$ flux of component A

$D_o \equiv$ diffusion coefficient

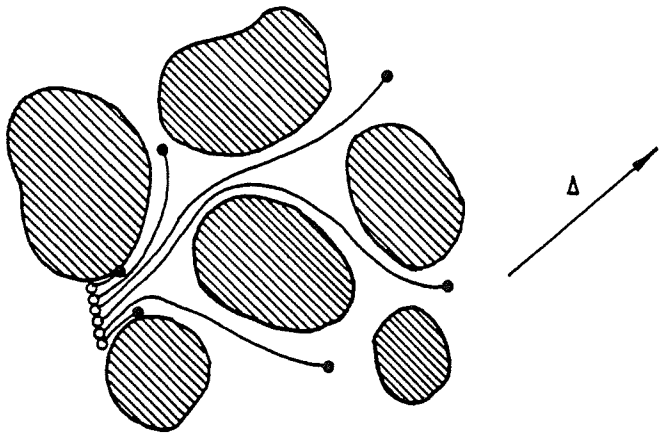

Figure 1-2. Phenomena of mechanical dispersion.

$C_A \equiv$ concentration of component A in fluid

$x \equiv$ position with respect to the x-direction

1.2 Conceptual Representation of Dispersion in Porous Media

In order to represent mathematically the dispersion of two miscible fluids in a porous medium, several models have been derived and discussed extensively in the literature.(1-3,5-10) Presented here are the early geometric models of Taylor and Aris and the macroscopic equation of dispersion which is used widely at the present time.

1.2a Geometric models

The geometric models were the first simplistic approach to dispersion problems and are not very representative of actual flow in porous media. The two discussed below link the porous medium with a model of bundles of capillaries.

1.2ai Taylor's approach. Taylor showed that under certain restrictions, flow through a cylindrical straight capillary obeys Fick's law.(6) These restrictions are:

1. Concentration changes along the tube due to molecular diffusion are negligible compared to those by convective transport.

2. Radial variations of concentrations are reduced by molecular diffusion much more quickly than for significant effects to appear due to convective transport.

Condition (2) needs further explanation. The distribution of velocities, v, in a cylindrical cross section is parabolic.[29] Without diffusion and if, at time equal to zero, the displacing fluid is on one side of a cross section, the displacing fluid distribution at times greater than zero obeys the same parabolic distribution law (Figure (1-3)). When diffusion occurs radially, it tends to equalize concentrations across a cross section, thus opposing the formation of a parabolic surface of separation between the fluids. The curvature of the resulting transition zone straightens with increasing diffusion velocities (Figure (1-4)). Condition (2) applies to the case of a high diffusion velocity as illustrated in figure (1-4b), whereby the radial diffusion has suppressed the effect of the longitudinal velocity profile resulting in a diffusion-like phenomenon.

Taylor derived the equation of axial dispersion along a capillary as:

$$\frac{\partial C}{\partial t} = \frac{a^2 \, v_{max}^2}{192 \, D_o} \frac{\partial^2 C}{\partial x^2} \qquad (1\text{-}2)$$

where

a ≡ capillary radius

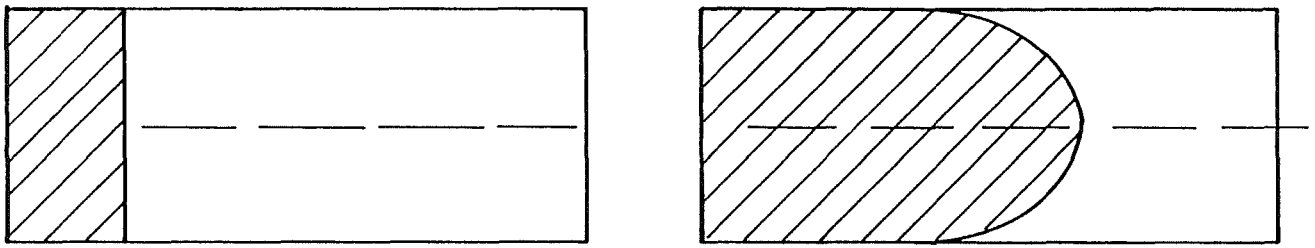

Figure 1-3. Propagation of two immiscible fluids, showing shape of interface.

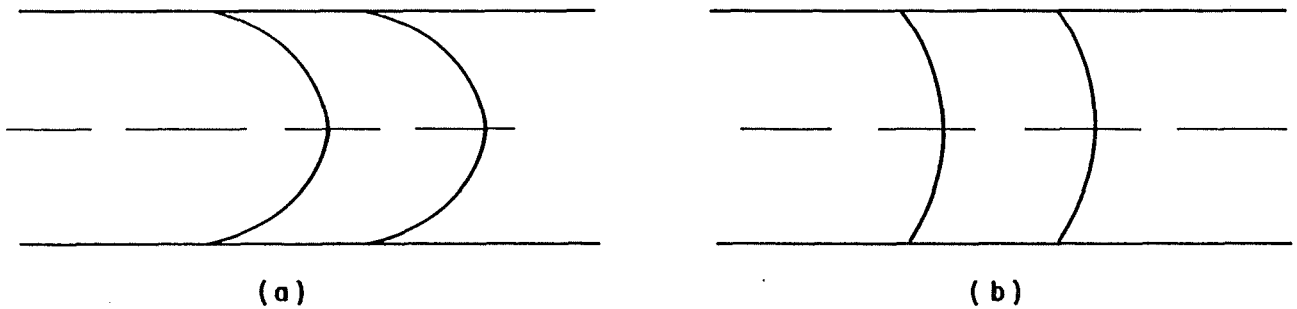

Figure 1-4. Miscible displacement in cylindrical capillary for a) low diffusion velocity, b) high diffusion velocity.

$v_{max} \equiv$ maximum velocity (on axis of capillary)

Therefore, he showed that Fick's law applies in cylindrical straight capillaries under the given conditions and the effective dispersion coefficient is:

$$K = \frac{a^2 \, v_{max}^2}{192 \, D_o} \tag{1-3}$$

1.2aii Aris' approach. Aris generalized Taylors method to handle irregularly shaped capillaries.[10] He noticed the asymptotic behavior of the moments of the concentration distribution acted like the normal law of probability. He stated that the mean concentration is dispersed according to a Gaussian distribution about a point moving at the mean velocity of flow. The effective diffusion coefficient takes the form:

$$K = D_o + \beta \, [a^2 \, \bar{v}^2 / D_o] \tag{1-4}$$

where

$\bar{v} \equiv$ thickness weighted mean velocity of flow

$\beta \equiv$ dimensionless constant, a function of capillary cross section

1.2aiii Summary. The works of Taylor and Aris were instructive as they were the first attempts toward understanding the phenomena of dispersion in porous media. Unfortunately, flow in porous media is not very similar to flow in capillary tubes. The meandering of streamlines and local cell mixing is the dominant reason for disper-

sion in porous media, while velocity distributions were the major contributors in capillary tube flow.

1.2b Macroscopic View of Dispersion in Porous Media

By various methods[1,4,24] an equation called the general equation of dispersion has been derived and is given by (all assumptions listed in section 2.1):

$$\vec{\nabla}\cdot(\phi\vec{\vec{K}} - \vec{\nabla}C) - \vec{\nabla}\cdot(\vec{u}C) = \phi\frac{\partial C}{\partial t} \qquad (1\text{-}5)$$

where

$\vec{u}$ ≡ superficial fluid velocity

$\vec{\vec{K}}$ ≡ dispersion coefficient tensor

ϕ ≡ porosity

The dispersion coefficient is given in tensorial form to keep equation (1-5) as general as possible. This allows K to vary with direction, and its principle axis to be unalligned with respect to the coordinate axis.[24]

The equation of dispersion (1-5) is the mathematical model currently used to account for dispersion in porous media flow. Most experimental work is based upon the equation and computation of its dispersion coefficients. No assumptions have to be made as to the internal geometrical structure of the media, though boundary conditions must be prescribed on the macroscopic porous media boundary.[23,24]

1.3 Experimental Determination of the Dispersion Coefficients

Under the assumption of bulk flow only in the x-direction, equation (1-5) becomes:

$$\frac{\partial}{\partial x}\left(\phi K_{xx}\frac{\partial C}{\partial x}\right)+\frac{\partial}{\partial y}\left(\phi K_{yy}\frac{\partial C}{\partial y}\right)-\frac{\partial(u_x C)}{\partial x}=\phi\frac{\partial C}{\partial t} \qquad (1\text{-}6)$$

where

$K_{xx} \equiv$ longitudinal dispersion coefficient = K_ℓ

$K_{yy} \equiv$ transverse dispersion coefficient = K_t

Longitudinal and transverse dispersion in packs of granular material have been studied in the laboratory.[3,11-14] Most investigators studied longitudinal dispersion by filling a column of packed material with one fluid, displacing it with another and measuring the subsequent effluent concentrations as a function of fluid injected.

Bringham et al.[12] have shown a convenient method for determining the dispersion coefficient for this type of data. In a slight modification of their method,[3] the function λ,

$$\lambda = \frac{PVI - 1}{\sqrt{PVI}} \qquad (1\text{-}7)$$

where

PVI $\equiv$ pore volumes of injected fluid

is plotted versus percent displacing fluid in the effluent on arithmetic-probability paper. The longitudinal dispersion coefficient is then calculated by:

$$K_{xx} = K_{\ell} = v_x L \frac{(\lambda_{90} - \lambda_{10})^2}{3.625} \qquad (1\text{-}8)$$

where

$L \equiv$ system length

$\lambda_{90} \equiv \lambda$ value at 90% displacing fluid

$\lambda_{10} \equiv \lambda$ value at 10% displacing fluid

The longitudinal dispersion coefficient has been found experimentally to have additive components of diffusion and convection;[3] with the convective part varying approximately as the first power of the interstitial velocity, v.

$$K_{xx} = \frac{D_o}{F\phi} + 0.5\sigma d_p v_x \qquad (1\text{-}9)$$

where

$\sigma \equiv$ constant, a measure of inhomogeneity in the pack

$d_p \equiv$ particle diameter

Often, the $(0.5\sigma d_p)$ term is replaced by a constant referred to as the longitudinal dispersivity, α_{ℓ}.[16] This results in:

$$K_{xx} = \frac{D_o}{F\phi} + \alpha_{\ell} v_x \qquad (1\text{-}10)$$

The transverse dispersion coefficient is measured in a tube filled with packed granular material and fluids are injected simultaneously in a so-called stream splitting technique. (Figure (1-5)). Fluid A with concentration C = 1 is injected in the top half of the

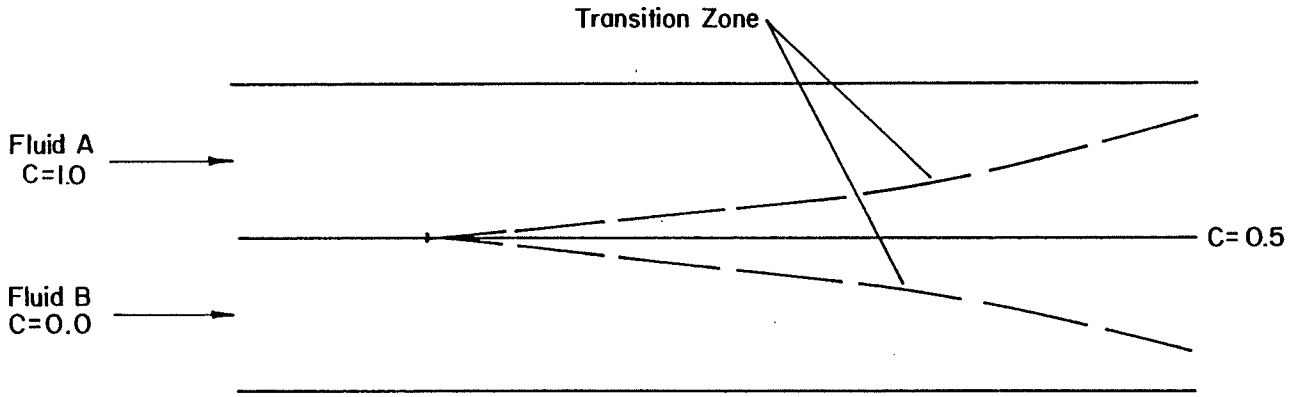

Figure 1-5. Stream-splitting technique for transverse dispersion determination.

cylinder, while fluid B with a concentration of 0 is injected into the bottom half. As the fluid travels through the tube, a mixed zone will grow in a direction transverse to the direction of fluid movement. If a profile of fluid composition is made along a line perpendicular to the axis of the tube, an S-shaped concentration profile will be observed. The transverse dispersion coefficient is calculated by plotting distance from the 50% composition line (axis of cylinder) versus percent composition on arithmetic-probability paper. The transverse dispersion coefficient is calculated by[3]

$$K_{yy} = \frac{v_x}{L} \left(\frac{y_{90} - y_{10}}{3.625}\right)^2 \qquad (1\text{-}11)$$

where

y_{90} ≡ transverse distance from 50% composition line to point where fluid concentration is 90%, cm

y_{10} ≡ transverse distance from 50% composition line to point where fluid concentration is 10%, cm

K_{yy} was also found to vary as the first power of the interstitial velocity in the longitudinal direction:

$$K_{yy} = \frac{D_o}{F\phi} + 0.0157\sigma d_p v_x \qquad (1\text{-}12)$$

Replacing $(0.0157\sigma d_p)$ by a constant called the transverse dispersivity, α_t,[16] in the same manner described above, results in:

$$K_{yy} = \frac{D_o}{F\phi} + \alpha_t v_x \qquad (1\text{-}13)$$

1.4 Dispersion in Heterogeneous Porous Media

Dispersion coefficients have been found to be affected by inhomogeneities in cemented outcrop or reservoir rocks. Part of the inhomogeneity is of a small, pore to pore scale which is accounted for by the (σ) terms in equations (1-9) and (1-12). However, there are larger scale inhomogeneities in natural sandstone. Permeability can vary in such rocks by orders of magnitude over a few inches, several feet, or even greater distances.

1.4a Lab scale

Dispersion in lab size (less than a few feet in size) outcrop rocks has been studied by several investigators.[11-14] They all find that dispersion is greater than one might have suspected from particle size alone. Values for the quantity (σd_p) have been measured on a laboratory scale in outcrop sandstones and are listed in Table (1-1). Only one value for the case of transverse dispersion was found in the literature and was given as 0.25 cm. Values of (σd_p) for longitudinal dispersion varied from 0.17 cm to 0.55 cm with an average of 0.393 cm.

1.4b Field scale

The same mechanism causing dispersion coefficients to be larger than expected in lab scale sandstones having dimensions of a few feet causes even larger field wide

Table 1-1. (σd_p) Values in Outcrop Sandstones

Source	Dispersion	Rock	(σd_p) (cm)
Grane and Gardner[11]	Transverse	Berea	0.25
Brigham[12]	Longitudinal	Berea	0.39
	Longitudinal	Torpedo	0.17
Raimondi[13]	Longitudinal	Berea	0.46
Handy[14]	Longitudinal	Boise	0.55

Average Longitudinal = .393 cm

dispersion coefficients. That is, there is a scale effect in that as the system size increases, the observed dispersivities increase.(15)

Dieuhlin(15) compiled data of observed longitudinal dispersivities in field displacements. He plotted dispersivities of various types of reservoir rocks versus system length (Figure (1-6)). Dispersivities as low as 0.2 m are reported for systems of length around 5 m, while systems nearly 5000 m long exhibited dispersivities of over 100 meters.

1.5 Heterogeneous Porous Media Flow Models

The simplest model of a heterogeneous medium is a stratified system.(2) This is often not a bad representation because sedimentary formations are sometimes found to be stratified, composed of plane strata, of different porosities and permeabilities. Flow is assumed as unidirectional and parallel to the layers with the x-axis taken along the flow direction and the y-axis transverse to the strata. The dispersion tensor reduces to two components, K_{xx} and K_{yy}, and ϕ is assumed to be dependent on y. Equation (1-5) then becomes:

$$\phi K_{xx} \frac{\partial^2 C}{\partial x^2} + \frac{\partial}{\partial y}\left(\phi K_{yy} \frac{\partial C}{\partial y}\right) - u_x \frac{\partial C}{\partial x} = \phi \frac{\partial C}{\partial t} \qquad (1\text{-}14)$$

Investigators(1,2) have shown that under special conditions, it is possible to replace equation (1-14) with

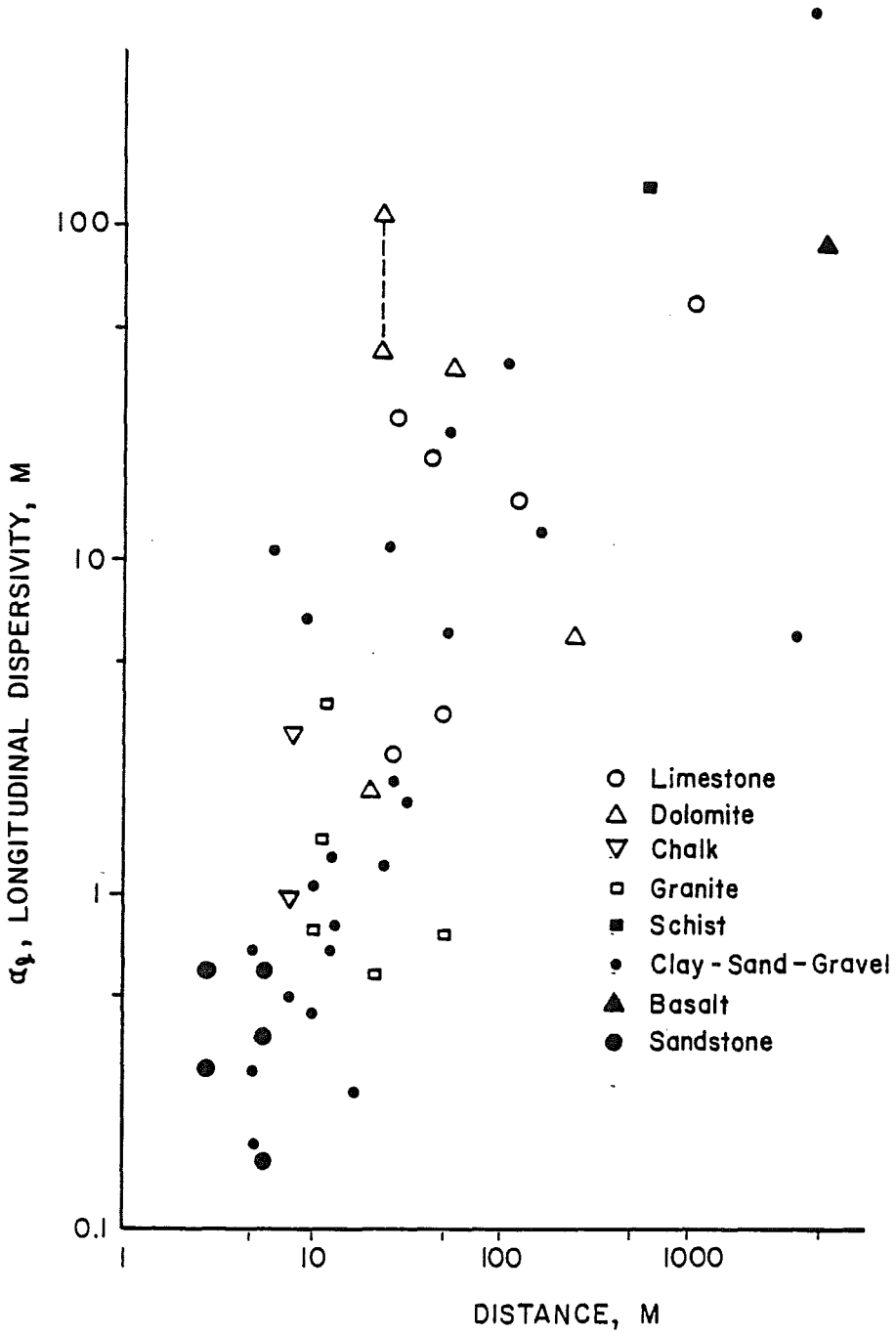

Figure 1-6. Field measured longitudinal dispersivities plotted as a function of system length.

the unidimensional equation:[1]

$$K_{EFF} \frac{\partial^2 \bar{C}}{\partial x^2} - \bar{v}_x \frac{\partial \bar{C}}{\partial x} = \frac{\partial \bar{C}}{\partial t} \qquad (1\text{-}15)$$

where

K_{EFF} ≡ effective dispersion coefficient

$\bar{C}$ ≡ flow rate-averaged concentration

$\bar{v}_x$ ≡ thickness averaged interstitial fluid velocity in x-direction

1.5a Fried and Combarnous Method

The solution of equation (1-14) is a concentration distribution $C(x,y,t)$.[1] The solution may be approached by deriving the moments $C^{(\eta)}(y,t)$ with respect to x of the distribution $C(x,y,t)$. These moments are defined as

$$C^{\eta}(y,t) = \int_{-\infty}^{+\infty} x^{\eta} C(x,y,t)dx \qquad (1\text{-}16)$$

The moments $C^{(\eta)}$ of equation (1-14) are compared, at the asymptotic (long time) regime, to the moments of the simpler system given by equation (1-15). The moments were found by Fried & Combarnous[1] to be identical when:

$$K_{EFF} = \frac{1}{\bar{\phi}H} \int_o^H K_{xx}\phi dy + \int_o^H \frac{\Phi^2}{K_{yy}\phi} dy \qquad (1\text{-}17)$$

and

$$\Phi = \int_{y_m}^{y} \phi_m(v_{x_m} - \bar{v}_x)dy \qquad (1\text{-}18)$$

where

H ≡ total system height

$\bar{\phi}$ ≡ thickness weighted average porosity

y_m ≡ y-coordinate of bottom of layer m

v_{x_m} ≡ interstitial fluid velocity in layer m in x-direction

Thus the asymptotic behavior of a stratified porous medium is identical to the behavior of an equivalent homogeneous medium having a dispersion coefficient given by equation (1-17).

1.5b Lake and Hirasaki Method

Lake and Hirasaki derived an analytical method to determine K_{EFF} for an equivalent one dimensional system.[16] This longitudinal dispersion is greater than normally existing in a corresponding homogeneous system.

They found that effective longitudinal dispersion will result between two adjacent layers when their transverse dispersion number, N_{TD}, is greater than 5.

$$N_{TD} = 14\ (L/H)\ \frac{K_{yy2}}{H\ v_{x_1}} \tag{1-19}$$

where

$K_{yy_2} \equiv$ transverse dispersion of slower layer

$v_{x_1} \equiv$ x-direction velocity of fast layer

When this condition is met, the two layers will behave as one layer, for flow purposes, with a resulting effective longitudinal coefficient of

$$K_{EFF} = \bar{K}_{xx} + \frac{1}{3}\left(\frac{(\bar{v}_x H)^2}{1 + \frac{\phi_1 h_1}{\phi_2 h_2}}\right)\left(\frac{\frac{k_1 h_1}{k_2 h_2} - \frac{\phi_1 h_1}{\phi_2 h_2}}{\frac{k_1 h_1}{k_2 h_2} + 1}\right)^2 \cdot \left(\frac{\frac{h_1}{h_1 + h_2}}{\frac{\phi_1 h_1}{\phi_2 h_2}\ K_{yy_1}} + \frac{\left(1 - \frac{h_1}{h_1 + h_2}\right)^2}{K_{yy_2}}\right) \tag{1-20}$$

and

$$\alpha_{EFF} = \frac{K_{EFF}}{\bar{v}_x} \qquad (1\text{-}21)$$

where

$\bar{K}_{xx}$ ≡ thickness weighted average K_{xx}

1 ≡ subscript denoting faster layer

2 ≡ subscript denoting slower layer

This procedure can easily be extended to more than two layers through the following grouping method:

1. Calculate N_{TD} for each adjacent layer pair.
2. Locate maximum N_{TD}.
3. Combine layer pair and average properties.
4. Re-index layers and continue until no layer pair has a N_{TD} greater than 5.

1.6 Goals of Research

The primary goals of this research are:

1. To write a simulator(s) that will accurately model all levels of two-dimensional physical dispersion in porous media.
2. Calculate field scale dispersivities found in the El Dorado field through history matching data sampled from observation wells. Contribution of vertical flow near the wellbore (coning) will be taken into account and will be eliminated from dispersivity determinations.

3. Investigate methods of grouping layered systems presented by Fried and Combarnous (F&C), and Lake and Hirasaki (L&H) to determine which procedure is superior for flow modeling purposes.
4. From the knowledge gained during the course of this investigation, present an "ideal" sampling procedure to determine field wide dispersivities.

CHAPTER 2. MATHEMATICAL MODELING

2.1 Fluid Flow Equations

Computer modeling of dispersion centers around the mass conservation equation for isothermal fluid flow in permeable media. For our conditions of single phase flow with one dispersing component, this equation is given by:(17)

$$\frac{\partial W}{\partial t} + \vec{\nabla}\cdot\vec{N} = R \qquad (2\text{-}1)$$

where

$$W = \phi\rho C + (1 - \phi)\rho_s C_s \qquad (2\text{-}2)$$

$$\vec{N} = \rho C\,\vec{u} - \phi\rho\vec{\vec{K}}\cdot\vec{\nabla}C \qquad (2\text{-}3)$$

$$R = \phi r + (1 - \phi)\, r_s \qquad (2\text{-}4)$$

$\phi \equiv$ porosity

$\rho \equiv$ fluid density

$\rho_s \equiv$ rock density

$C \equiv$ concentration of dispersing component in the fluid

$C_s \equiv$ concentration of dispersing component in rock

$\vec{u} \equiv$ superficial fluid velocity

$\vec{\vec{K}} \equiv$ dispersion coefficient tensor

$r \equiv$ kinetic reaction rate of dispersing component in fluid

$r_s \equiv$ kinetic reaction rate of dispersing component on rock surface

Given the following assumptions:

1. No chemical reaction of dispersing component.
2. No adsorption of dispersing component on rock.
3. Incompressible fluid.
4. Porosity of rock remains constant through time.

Equation (2-1) now takes the form of:

$$\phi \frac{\partial C}{\partial t} + \vec{\nabla} \cdot (\vec{u}C - \phi \vec{\vec{K}} \cdot \vec{\nabla} C) = 0 \qquad (2\text{-}5)$$

Peaceman[18] showed that for two dimensional, flow, the correct dispersion term is:

$$\vec{\nabla} \cdot (\phi \vec{\vec{K}} \cdot \vec{\nabla} C) = \frac{\partial}{\partial x} \left(\phi K_{xx} \frac{\partial C}{\partial x} + \phi K_{xy} \frac{\partial C}{\partial y} \right) + \frac{\partial}{\partial y} \left(\phi K_{yy} \frac{\partial C}{\partial y} + \phi K_{yx} \frac{\partial C}{\partial x} \right) \qquad (2\text{-}6)$$

where (if we assume isotropic flow)

$$K_{xx} = \frac{D_o}{F} + \alpha_\ell \frac{v_x^2}{|\vec{v}|} + \alpha_t \frac{v_y^2}{|\vec{v}|} \qquad (2\text{-}7)$$

$$K_{xy} = K_{yx} = (\alpha_\ell - \alpha_t) \frac{|v_x \cdot v_y|}{|\vec{v}|} \qquad (2\text{-}8)$$

$$K_{yy} = \frac{D_o}{F\phi} + \alpha_\ell \frac{v_y^2}{|\vec{v}|} + \alpha_t \frac{v_x^2}{|\vec{v}|} \qquad (2\text{-}9)$$

$v_x \equiv$ x-direction interstitial fluid velocity

$v_y \equiv$ y-direction interstitial fluid velocity

$|\vec{v}| \equiv$ magnitude of interstitial fluid velocity,

$$|\vec{v}| = \sqrt{v_x^2 + v_y^2}$$

Note that for flow only in the x-direction, the off-diagonal dispersion terms, K_{yx} and K_{xy} are zero, and equations (2-7) and (2-9) reduce to equations (1-10) and

(1-13), respectively, for K_{xx} and K_{yy} as given in Chapter 1.

The cross derivative terms can be neglected even for flow in both directions if dispersion is small or if $\alpha_\ell \cong \alpha_t$. For our purposes, large dispersion was displayed by the field data, as will be discussed later, and $\alpha_\ell >> \alpha_t$. However, Settari, Price, and Dupont,[31] have shown that neglecting the cross derivative terms causes distortion of the fronts similar to grid-orientation effect, which is a numerical phenomenon causing preferential flow along grid lines. In addition, the cross derivative terms become significant only when the vertical velocity components approach the horizontal velocity components in magnitude. Since this occurs only near the wellbore for the systems modeled during our research (Chapter 4), if at all, we feel that K_{xy} and K_{yx} do not have to be taken into account to prevent serious error and were not used in our simulation.

For two dimensional flow, equation (2-5) can now be written as:

$$\phi \frac{\partial C}{\partial t} + \frac{\partial (u_x C)}{\partial x} + \frac{\partial (u_y C)}{\partial y} - \frac{\partial}{\partial x}\left(\phi K_{xx} \frac{\partial C}{\partial x}\right) - \frac{\partial}{\partial y}\left(\phi K_{yy} \frac{\partial C}{\partial y}\right) = 0 \qquad (2\text{-}10)$$

2.1a Velocity determination with no vertical flow

Most of our model runs were performed with no flow in the vertical or y-direction. For flow in the x-direction, it was assumed fluid is injected into individual layers according to:

$$v_{x_m} = Q \frac{(k_{x_m} h_m)}{\sum_{m=1}^{M} (k_{x_m} h_m) \phi_m A} \qquad (2\text{-}11)$$

where

$v_{x_m} \equiv$ interstitial velocity in x-direction in reservoir layer m

$Q \equiv$ total volumetric flow rate into all reservoir layers

$k_{x_m} \equiv$ horizontal (x-direction) permeability of reservoir layer m

$h_m \equiv$ height of reservoir layer m

$\phi_m \equiv$ porosity of reservoir layer m

$M \equiv$ total number of reservoir layers

$A \equiv$ cross sectional area of all layers

Equation (2-11) assumes D'arcy's Law is valid and neglects gravity effects.

2.1b Velocity determination with vertical flow

Under actual field conditions, the assumption of fluid entering all layers according to their (kh) product is not always accurate. Consider the case, which will be explored during our research, of fluid injection or withdrawal through a limited perforated interval, intro-

ducing vertical flow. The basic pressure equation, derived from the continuity equation, must be used to determine velocities throughout the system.[19] For an incompressible system with no gravity or capillary pressure effects:

$$\nabla \cdot (\vec{\vec{T}} \cdot \vec{\nabla} P) - Q = 0 \qquad (2\text{-}12)$$

where

$\vec{\vec{T}} \equiv$ fluid transmissibility tensor $= \vec{\vec{k}} A/\mu$

$P \equiv$ pressure

$Q \equiv$ sink or source term (volumetric flow rate)

The principle axis of the transmissibility tensor is assumed to be alligned with the coordinate axis. This assumption eliminates off-diagonal terms.[17] In two dimensions, equation (2-12) now takes the form

$$T_x \frac{\partial^2 P}{\partial x^2} + T_y \frac{\partial^2 P}{\partial y^2} - Q = 0 \qquad (2\text{-}13)$$

where

$T_x \equiv$ transmissibility in x-direction $= k_x A_x/\mu$

$T_y \equiv$ transmissibility in y-direction $= k_y A_y/\mu$

Details of the finite difference form of equation (2-13), boundary conditions, and its solution are given in Appendix A.

2.1bi Use of source and sink terms. The source and sink terms, Q, are utilized at the system's inflow and outflow boundaries, respectively. The program was written

so that the perforated intervals could be set independently at both the injection boundary at x = 0 and the production boundary at x = L (Figure (2-1)). The fraction of the total injected flow rate going into the perforated interval at x = 0 is given by f_I with the remaining fraction $(1 - f_I)$ being injected into the other non-perforated layers. The specified flow rates going into the perforated interval and the non-perforated interval are distributed into each layer according to their respective (kh) product as compared to the sum of the entire group of layers.

For example, the layers in the perforated injection interval will receive fluid according to:

$$Q_{m_I} = \frac{k_{x_m} h_m}{\sum_{m=PIT}^{PIB} (k_{x_m} h_m)} Q \cdot f_I \qquad (2\text{-}14)$$

where

PIT ≡ top layer of injection perforated interval

PIB ≡ bottom layer of injection perforated interval

Q_{m_I} ≡ injected volumetric flowrate into reservoir layer m

The layers in the non-perforated interval will receive fluid in the following amount:

$$Q_{m_I} = \frac{k_{x_m} h_m}{\sum_{m=1}^{PIT-1} (k_{x_m} h_m) + \sum_{m=PIB+1}^{M} (k_{x_m} h_m)} Q \cdot (1 - f_I) \qquad (2\text{-}15)$$

The perforated and non-perforated production intervals receive fluid in exactly the same manner as

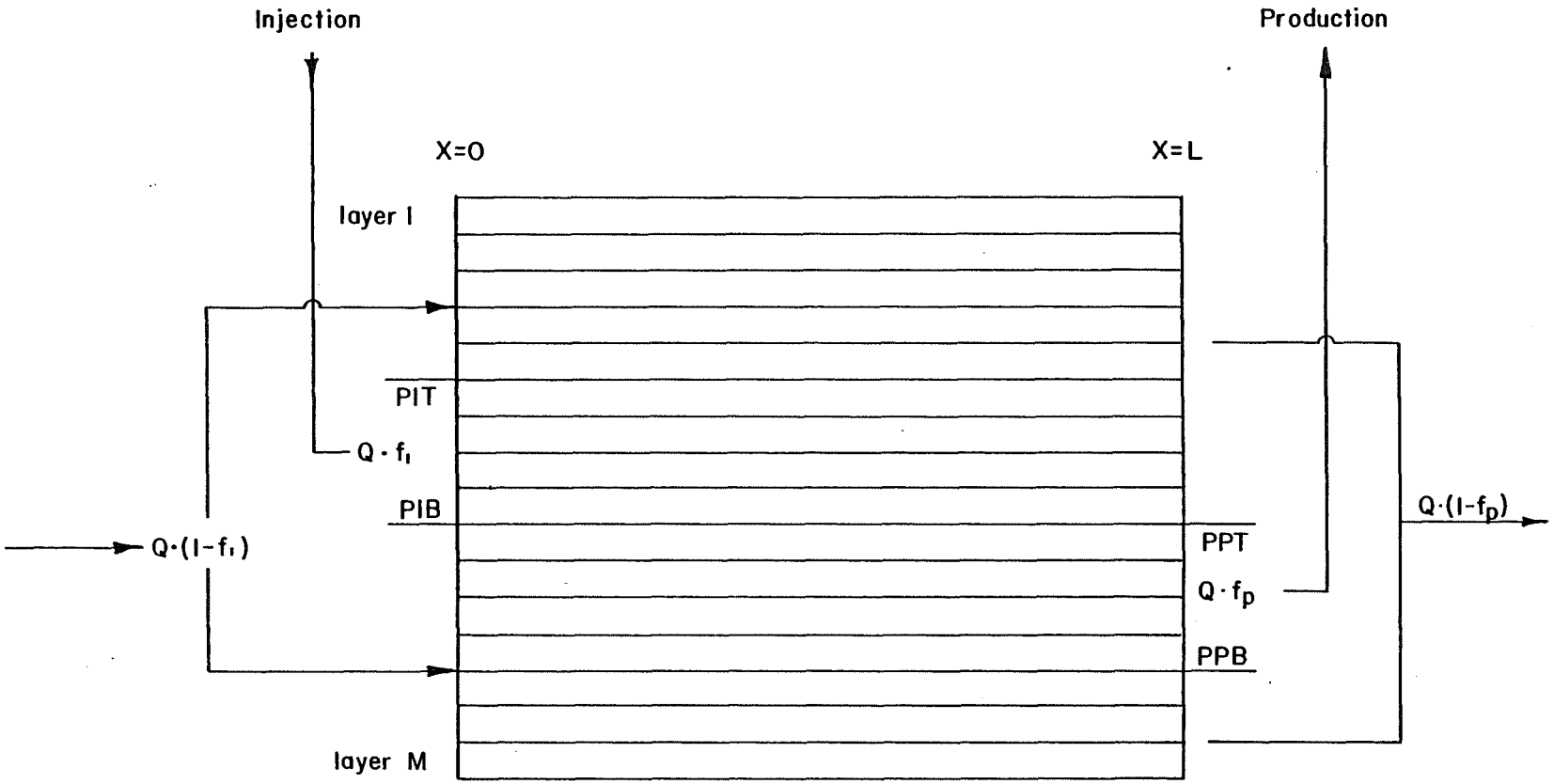

Figure 2-1. Diagram of production and injection scheme.

discussed above, with the fraction of the total flow rate through the production perforated interval given by f_P.

For the production perforated layers,

$$Q_{m_P} = \frac{k_{x_m} h_m}{\sum_{m=PPT}^{PPB} (k_{x_m} h_m)} Q \cdot f_P \qquad (2\text{-}16)$$

where

PPT ≡ top layer of the perforated production layer

PPB ≡ bottom layer of the perforated production interval

Q_{m_P} ≡ produced volumetric flowrate from reservoir layer m

The flow rates produced from the non-perforated layers are:

$$Q_{m_P} = \frac{k_{x_m} h_m}{\sum_{m=1}^{PPT-1} (k_{x_m} h_m) + \sum_{m=PPB+1}^{M} (k_{x_m} h_m)} Q \cdot (1 - f_P) \qquad (2\text{-}17)$$

For the sake of thoroughness and clarity, let us relate mathematically the flow rates into and out of the individual finite difference grid blocks at the inflow and outflow faces, respectively, to the reservoir layer volumetric flow rates they fall within:

$$q_{1,j} = \frac{Q_{m_I}}{N_{G/L}} \qquad (2\text{-}18)$$

and

$$q_{N_x,j} = \frac{Q_{m_P}}{N_{G/L}} \qquad (2\text{-}19)$$

where

$q_{1,j}$ ≡ volumetric flowrate into the finite difference grid block (1,j)

$q_{N_x,j}$ ≡ volumetric flowrate out of the finite difference grid block (N_x,j)

Q_{m_I} ≡ injection volumetric flowrate in reservoir layer m containing grid block (1,j)

Q_{m_p} ≡ production volumetric flowrate out of reservoir layer m containing grid block (N_x,j)

$N_{G/L}$ ≡ the number of grid blocks in the vertical (y) direction per reservoir layer

It should also be pointed out that further references to the total number of reservoir layers will be represented by M, while the number of grids in the vertical direction denoted by N_y.

2.1bii Velocity determination within system from calculated nodal pressures. Pressures at each node in the system are calculated from equation (2-13) and D'arcy's Law is utilized to find velocities, v_x and v_y, at mid-points through the node network shown in figure (2-2).(20)

For example,

$$v_{x_{i+1/2,j}} = -\left(\frac{k_x}{\phi}\right)_{i+1/2,j} \frac{1}{\mu} \frac{P_{i+1,j} - P_{i,j}}{\Delta x} \qquad (2\text{-}20)$$

$$v_{y_{i,j+1/2}} = -\left(\frac{k_y}{\phi}\right)_{i,j+1/2} \frac{1}{\mu} \frac{P_{i,j+1} - P_{i,j}}{\Delta y} \qquad (2\text{-}21)$$

where

i ≡ x-direction node index

j ≡ y-direction node index

μ ≡ fluid viscosity

$\left(\frac{k_x}{\phi}\right)_{i+1/2,j}$ ≡ geometric average of (k_x/ϕ) terms in grid blocks (i,j) and (i+1,j)

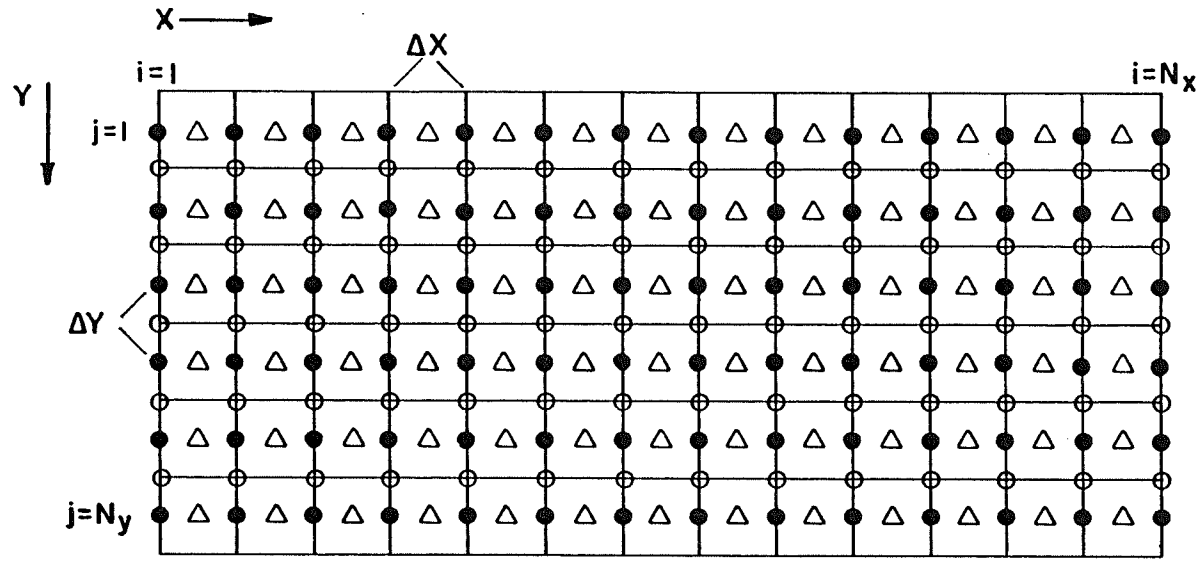

● Nodes at which pressures are computed

△ Midpoints where V_x components are computed from pressures

o Midpoints where V_y componets are computed from pressures

Figure 2-2. Pressure node network and relative positions of v_x and v_y components.

$$\left(\frac{k_x}{\phi}\right)_{i+1/2,j} = 2.0 \cdot \frac{\left(\frac{k_x}{\phi}\right)_{i+1,j} \cdot \left(\frac{k_x}{\phi}\right)_{i,j}}{\left(\frac{k_x}{\phi}\right)_{i+1,j} + \left(\frac{k_x}{\phi}\right)_{i,j}}$$

Notice that the nodes of the system are positioned on the boundaries with regard to the x-direction (inflow and outflow boundaries) but are ½ spacing off the upper and lower boundaries in the y-direction. This is referred to as being face centered in the x-direction and block centered in the y-direction. The nodes are positioned in this manner for the moving point simulation and reasons for this arrangement are detailed later in this chapter.

2.1biii Velocity determination at system boundaries. The system is assumed to be bounded above and below by impermeable strata. The vertical velocity components, $v_{y_{i,j}}$, at $j = 1/2$ and $j = N_y + 1/2$ are therefore set equal to zero. The horizontal velocity components, $v_{x_{i,j}}$, at $i = 1$ and $i = N_x$ are based upon the injection and production flow rates, respectively, calculated for each reservoir layer as described previously. The velocities at the inflow and outflow faces are:

$$v_{x_{i,j}} = \frac{q_{1,j}}{\Delta y \; W \; \phi_{1,j}} \qquad (2\text{-}22)$$

$$v_{x_{N_x,j}} = \frac{q_{N_x,j}}{\Delta y \; W \; \phi_{N_x,j}} \qquad (2\text{-}23)$$

$W \equiv$ width of system cross section

$\phi_{1,j} \equiv$ porosity of grid block (1,j)

$\phi_{N_x,j} \equiv$ porosity of grid block (N_x,j)

$y \equiv$ distance of grid spacing in y-direction

2.1biv Velocity determination at any point with system. Velocity components, v_x and v_y, at any point within the system are found by bilinear interpolation of the previously calculated midpoint node and boundary velocities (figure (2-3)). Linear interpolation assumes a property (in our case velocity) varies linearly with respect to a specified direction between two known properties at given locations. The value of the property at a location between the known values is solved by multiplying the values by appropriate fractions based upon their distances to the point and to one another with regard to the given direction.(24) Bilinear interpolation for our purposes involves linear interpolation, with respect to the direction of the desired component (x or y), of the given grid velocities the point falls within. Linear interpolation based upon the same direction and distance is again performed on the velocities of the grid adjacent to and in the transverse direction of the given grid. Finally, the two calculated interpolated velocities are again linearly interpolated but with respect to their transverse direc-

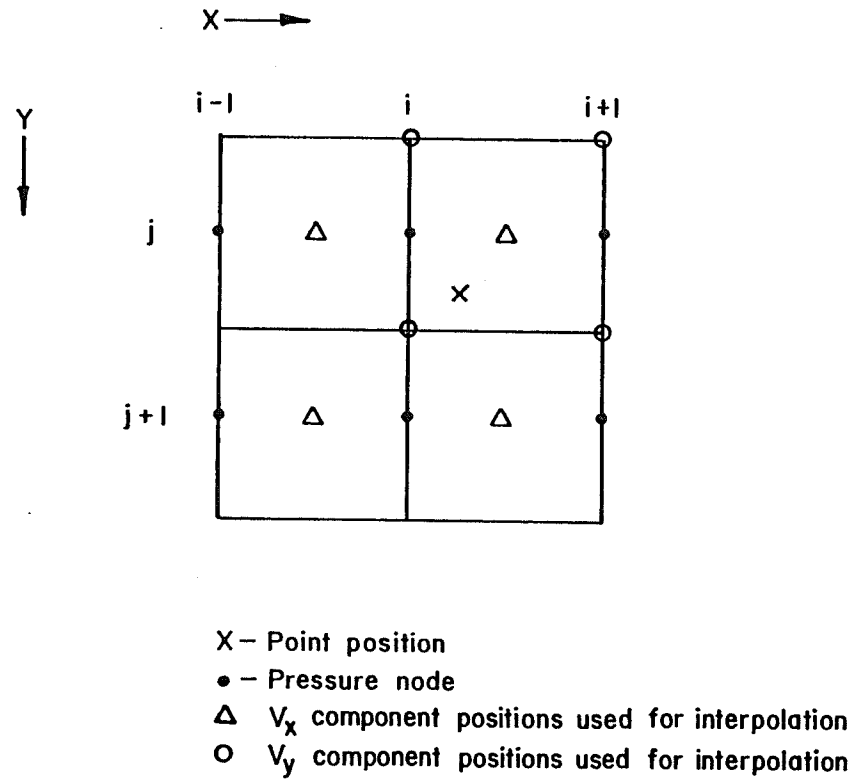

Figure 2-3. Positions of v_x and v_y components used for bilinear interpolation of a point's velocities.

tion and distance to the point. This process is best described mathematically. For the point in figure (2-3):

$$v_{x_p} = \left(1 - \frac{y_p - y_j}{\Delta y}\right)\left[\frac{x_p - x_{i-1/2}}{\Delta x} v_{x_{i+1/2},j} + \left(1 - \frac{x_p - x_{i-1/2}}{\Delta x}\right) \cdot v_{x_{i-1/2},j}\right] + \left(\frac{y_p - y_j}{\Delta y}\right)\left[\frac{x_p - x_{i-1/2}}{\Delta x} v_{x_{i+1/2},j+1} + \left(1 - \frac{x_p - x_{i-1/2}}{\Delta x}\right) v_{x_{i-1/2},j+1}\right] \quad (2\text{-}24)$$

$$v_{y_p} = \left(1 - \frac{x_p - x_i}{\Delta x}\right)\left[\frac{y_p - y_{j-1/2}}{\Delta y} v_{y_i,j+1/2} + \left(1 - \frac{y_p - y_{j-1/2}}{\Delta y}\right) \cdot v_{y_i,j-1/2}\right] + \left(\frac{x_p - x_i}{\Delta x}\right)\left[\frac{y_p - y_{j-1/2}}{\Delta y} v_{y_{i+1},j+1/2} + \left(1 - \frac{y_p - y_{j-1/2}}{\Delta y}\right) v_{y_{i+1},j-1/2}\right] \quad (2\text{-}25)$$

where

$y_p \equiv$ y-coordinate of point

$x_p \equiv$ x-coordinate of point

$y_j \equiv$ y-coordinate of grid index j

$y_{j-1/2} \equiv$ y-coordinate of grid index j-1/2

$x_i \equiv$ x-coordinate of grid index i

$x_{i-1/2} \equiv$ x-coordinate of grid index i-1/2

2.2 Fixed grid finite difference

Fixed grid finite difference techniques are well established for simulation of the two dimensional dispersion equation (2-10)[21,22] and were initially used to model flow for our purposes. Three general forms of finite difference approximations have to be used and include the approximations of the convective first deriva-

tive terms, the second derivative dispersion terms, and the time derivative term.

2.2a Finite difference approximations

There are three main ways to approximate the convective, first derivative terms:

1. Upstream weighting

$$\left(\frac{\partial C}{\partial x}\right)_{i,j} \cong \frac{C_{i,j} - C_{i-1,j}}{\Delta x} \tag{2-26}$$

2. Central difference

$$\left(\frac{\partial C}{\partial x}\right)_{i,j} \cong \frac{C_{i+1,j} - C_{i-1,j}}{2\Delta x} \tag{2-27}$$

3. Downstream weighting

$$\left(\frac{\partial C}{\partial x}\right)_{i,j} \cong \frac{C_{i+1,j} - C_{i,j}}{\Delta x} \tag{2-28}$$

All three methods were studied by use of a weighting factor, WF, which can be input as a constant.

$$\left(\frac{\partial C}{\partial x}\right)_{i,j} \cong \frac{(C_{i,j} - C_{i-1,j})\ WF + (C_{i+1,j} - C_{i,j})\ (1-WF)}{\Delta x} \tag{2-29}$$

WF ranges in value from 0 to 1, with 1 corresponding to upstream, ½ to central, and 0 corresponding to downstream.

The finite difference approximation of the second derivative, dispersion part of equation (2-10) is:

$$\left(\frac{\partial}{\partial x}\ \phi K_{xx}\ \frac{\partial C}{\partial x}\right)_{i,j} \cong (\phi K_{xx})_{i+1/2,j}\ \frac{C_{i+1,j} - C_{i,j}}{\Delta x^2}$$

$$- (\phi K_{xx})_{i-1/2,j}\ \frac{C_{i,j} - C_{i-1,j}}{\Delta x^2}$$

(2-30)

$$\left(\frac{\partial}{\partial y} \quad \phi K_{yy} \frac{\partial C}{\partial y}\right)_{i,j} \cong (\phi K_{yy})_{i,j+1/2} \frac{C_{i,j+1} - C_{i,j}}{\Delta y^2}$$

$$- (\phi K_{yy})_{i,j-1/2} \frac{C_{i,j} - C_{i,j-1}}{\Delta y^2}$$

(2-31)

where the (ϕK) terms at $1/2$ grid spacings are the geometric average of the adjacent (ϕK) block values.

$$(\phi K_{xx})_{i+1/2,j} = 2.0 \cdot \frac{(\phi K_{xx})_{i+1,j} \cdot (\phi K_{xx})_{i,j}}{(\phi K_{xx})_{i+1,j} + (\phi K_{xx})_{i,j}}$$

The calculations are implicit with respect to time. That is, the concentrations of the grids within the system will be solved simultaneously at the new time step $(n + 1)$. The time derivative is approximated by:

$$\left(\frac{\partial C}{\partial t}\right)_{i,j} \cong \frac{C^{n+1}_{i,j} - C^{n}_{i,j}}{\Delta t} \qquad (2\text{-}32)$$

The fixed grid finite difference simulator was written for flow only in the x-direction (no vertical flow) and the resulting implicit finite difference form is:

$$- \left(\frac{v_{x_{i-1,j}} \, WF}{\Delta x} + \frac{(\phi K_{xx})_{i-1/2,j}}{\Delta x^2 \ \phi_{i,j}}\right) C^{n+1}_{i-1,j} + \left(\frac{1}{\Delta t} + \frac{(2WF - 1) \, v_{x_{i,j}}}{\Delta x}\right.$$

$$\left. + \frac{(\phi K_{xx})_{i-1/2,j}}{\phi_{i,j} \ \Delta x^2} + \frac{(\phi K_{xx})_{i+1/2,j}}{\phi_{i,j} \ \Delta x^2} + \frac{(\phi K_{yy})_{i,j-1/2}}{\phi_{i,j} \ \Delta y^2} + \frac{(\phi K_{yy})_{i,j+1/2}}{\phi_{i,j} \ \Delta y^2}\right)$$

$$\cdot C^{n+1}_{i,j} - \left(\frac{(WF - 1) \, v_{x_{i+1,j}}}{\Delta x} + \frac{(\phi K_{xx})_{i+1/2,j}}{\Delta x^2 \ \phi_{i,j}}\right) C^{n+1}_{i+1,j} -$$

$$\left(\frac{(\phi K_{yy})_{i,j-1/2}}{\phi_{i,j} \ \Delta y^2}\right) C^{n+1}_{i,j-1} - \left(\frac{(\phi K_{yy})_{i,j+1/2}}{\phi_{i,j} \ \Delta y^2}\right) C^{n+1}_{i,j+1} = \frac{1}{\Delta t} C^{n}_{i,j}$$

(2-33)

Equation (2-33) forms a pentadiagonal solution matrix and was solved with an economized band algorithm[19] which reduced computer storage requirements.

2.2b Boundary conditions

The fixed grid system is block centered in both x and y-directions (Figure (2-4)). The system boundaries are at $j = 1/2$, $j = N_y + 1/2$, $i = 1/2$, and $i = N_x + 1/2$. Because of the impermeable strata assumed above and below the system, no flux exists at $j = 1/2$ and $j = N_y + 1/2$:

$$v_y C - K_{yy} \frac{\partial C}{\partial y} = 0 \qquad (2\text{-}34)$$

Earlier it was shown that v_y at $j = 1/2$ and $j = N_y + 1/2$ is equal to zero (no flow), therefore:

$$\frac{\partial C}{\partial y} = 0 \qquad (2\text{-}34)$$

In finite difference form,

At $j = 1/2$

$$\left(\frac{\partial C}{\partial y}\right)_{i,1/2} \cong \frac{C_{i,1} - C_{i,0}}{\Delta y} = 0 \qquad (2\text{-}36)$$

$$C_{i,1} = C_{i,0} \qquad (2\text{-}37)$$

At $j = N_y + 1/2$

$$\left(\frac{\partial C}{\partial y}\right)_{i,N_y+1/2} \cong \frac{C_{i,N_y+1} - C_{i,N_y}}{\Delta y} = 0 \qquad (2\text{-}38)$$

$$C_{i,N_y+1} = C_{i,N_Y} \qquad (2\text{-}39)$$

At the inflow face ($i = 1/2$), the flux must be equal on both sides of the boundary:

$$\left(v_x C - K_{xx} \frac{\partial C}{\partial x}\right)_{OUT} = \left(v_x C - K_{xx} \frac{\partial C}{\partial x}\right)_{IN} \qquad (2\text{-}40)$$

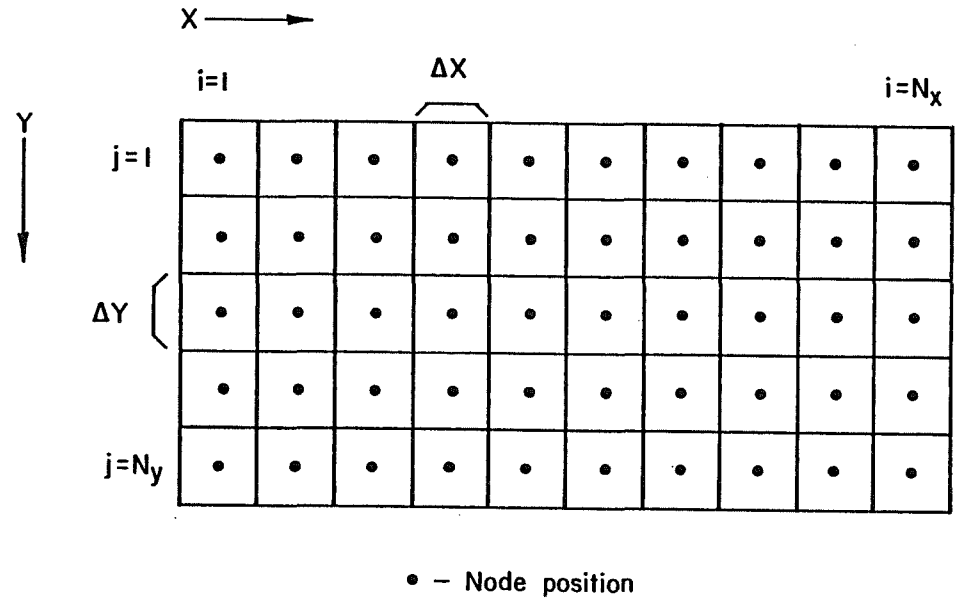

Figure 2-4. Node system for fixed grid finite difference simulator.

where

OUT ≡ outside system boundary at inflow face

IN ≡ inside system boundary at inflow face

If we assume fluid in the wellbore is very well mixed, outside the system $\partial C/\partial x = 0$ and $C_{OUT} = CI$ where CI is the injected concentration. Therefore:

$$v_x\, CI = v_x\, C_{IN} - K_{xx} \frac{\partial C}{\partial x}_{IN} \tag{2-41}$$

In finite difference form,

$$v_{x_{1,j}}\, CI = v_{x_{1,j}}\, C_{0,j} - (K_{xx})_{1/2,j} \frac{C_{1,j} - C_{0,j}}{\Delta x} \tag{2-42}$$

$$C_{0,j} = \frac{v_{x_{1,j}}\, CI + C_{1,j} \dfrac{(K_{xx})_{1/2,j}}{\Delta x}}{v_{x_{1,j}} \quad 1 + \dfrac{(K_{xx})_{1/2,j}}{v_{x_{1,j}}(\Delta x)}} \tag{2-43}$$

At the outflow face ($i = N_x + 1/2$), the flux must also be equal on both sides of the boundary, but there is no way to specify outflow concentration. The concentrations on both sides are assumed to be equal:

$$\left(v_x\, C - K_{xx} \frac{\partial C}{\partial x}\right)_{IN} = \left(v_x\, C - K_{xx} \frac{\partial C}{\partial x}\right)_{OUT} \tag{2-44}$$

and

$$C_{IN} = C_{OUT} \tag{2-45}$$

therefore:

$$\left(K_{xx} \frac{\partial C}{\partial x}\right)_{IN} = \left(K_{xx} \frac{\partial C}{\partial x}\right)_{OUT} \tag{2-46}$$

If we assume that $(K_{xx})_{OUT} >> (K_{xx})_{IN}$ (which appears reasonable since the wellbore is outside the face):

$$\frac{\partial C}{\partial x} = 0 \tag{2-47}$$

In finite difference form,

$$\left(\frac{\partial C}{\partial x}\right)_{N_{x+1/2},j} \cong \frac{C_{N_{x+1,j}} - C_{N_{x,j}}}{\Delta x} = 0 \qquad (2\text{-}48)$$

$$C_{N_{x+1,j}} = C_{N_{x,j}} \qquad (2\text{-}49)$$

2.3 Moving point method

Garder et al.[25] developed a numerical technique for the solution of multidimensional miscible displacement problems. This method uses the usual fixed grid system, but in addition utilizes a system of moving points for which positions and concentrations are computed at each time step. This method can accurately model all levels of physical dispersion without introducing appreciable numerical error. It was added later in the course of the research and was adapted to handle possible two dimensional flow.

2.3a Theory

If we regard the second order dispersion terms of equation (2-10) as given functions of x,y, and t, then we can treat it as a first order equation.[25] The derivation of the characteristic curves is described in detail by Garder,[25] resulting in the following system of ordinary differential equations:

$$\frac{dx}{dt} = v_x \qquad (2\text{-}50)$$

$$\frac{dy}{dt} = v_y \qquad (2\text{-}51)$$

$$\frac{dC}{dt} = \frac{1}{\phi}\vec{\nabla}\cdot(\phi\vec{\vec{K}}\cdot\vec{\nabla}C) \qquad (2\text{-}52)$$

2.3b Convective treatment

As stated above, this method involves a stationary grid and a set of moving points (figure 2-5). The stationary grid is divided into rectangular x-y regions with N_x in the x-direction and N_y in the y-direction. Due to the relatively few grid blocks used with this technique and the importance of history matching in our research, the grid nodes are face centered in the x-direction and block centered with respect to the y-direction (figure (2-5)). This arrangement permits accurate concentration determination at the outflow end because the node point is directly on the boundary and allows the grid points to be in the center of each individual layer of the system.

Around each point, a rectangle R_{ij} is constructed and we say a point having coordinates (x_p, y_p) falls within R_{ij} if:

$$x_i - \tfrac{1}{2}\Delta x \leq x_p < x_i + \tfrac{1}{2}\Delta x \qquad (2\text{-}53)$$

$$y_i - \tfrac{1}{2}\Delta y \leq y_p < y_i + \tfrac{1}{2}\Delta y \qquad (2\text{-}54)$$

where

$$x_i = i\Delta x \quad i = 1, 2, 3, \ldots N_x$$

$$y_i = i\Delta y \quad j = 1, 2, 3, \ldots N_y$$

The moving points are used to solve equations (2-50) through (2-52), with each point corresponding to one characteristic curve. Let p be the index of each

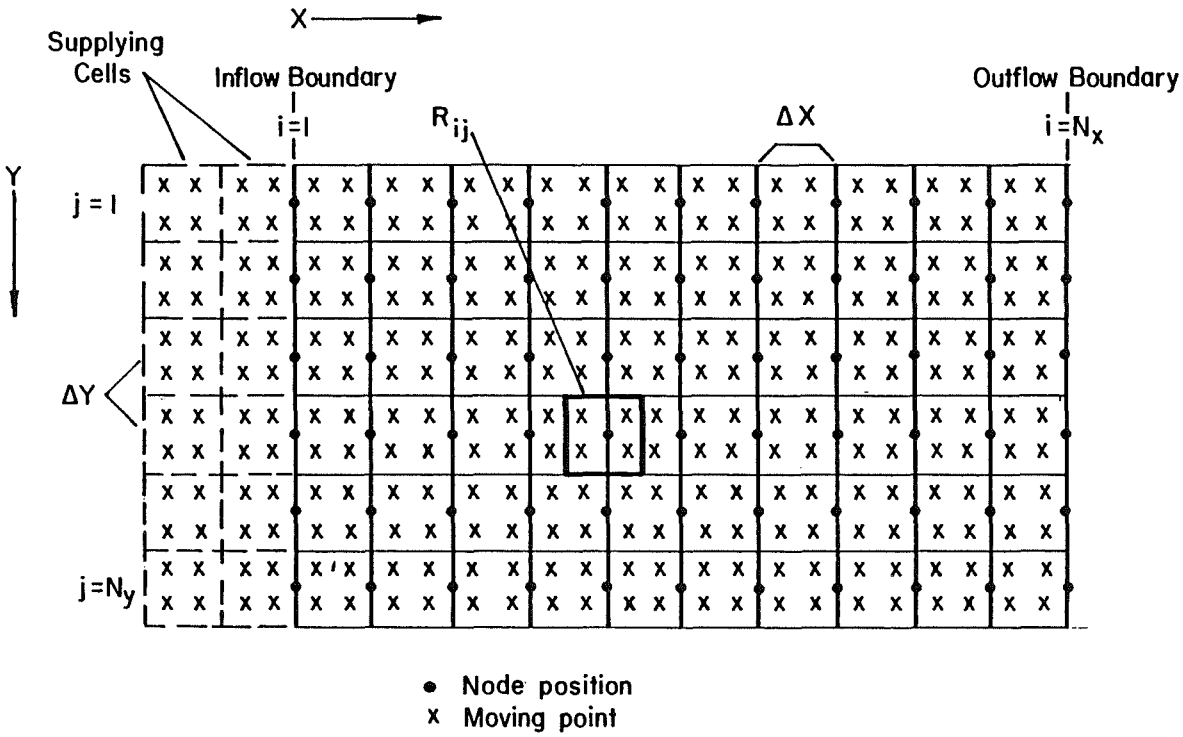

Figure 2-5. Node network and point distribution for the moving point simulator.

point and n the time step. Therefore x_p^n, y_p^n and C_p^n are to be calculated for each point at each time t^n.

The set of moving points are uniformly distributed through the rectangular x-y region at the start of the calculations. The calculation sequence is begun by obtaining pressures throughout the grid network by solution of the pressure equation (2-13), and subsequently velocities are obtained by D'arcy's Law at midpoints between the grid nodes and at the system boundaries as discussed previously. Bilinear interpolations through the use of equations (2-24) and (2-25) determine velocity components, v_x and v_y, for any point within the system.

New positions for the points are calculated by finite difference forms of equations (2-50) and (2-51):

$$x_p^{n+1} = x_p^n + \Delta t \; v_x \; (x_p^n, \; y_p^n) \qquad (2\text{-}55)$$

$$y_p^{n+1} = y_p^n + \Delta t \; v_y \; (x_p^n, \; y_p^n)$$

After the points are moved, they are examined to determine the region each is in by equations (2-53) and (2-54) and the rectangles are assigned a concentration $C_{i,j}^*$, equal to the arithmetic average of the individual points within their area.

2.3c Dispersion calculation

The change in concentration due to dispersion is now calculated for each rectangle. Equation (2-52),

applied to a two dimensional system and assuming the off-diagonal dispersion terms are negligible, becomes:

$$\frac{\partial C}{\partial t} = \frac{1}{\phi}\left[\frac{\partial}{\partial x}\left(\phi K_{xx}\frac{\partial C}{\partial x}\right) + \frac{\partial}{\partial y}\left(\phi K_{yy}\frac{\partial C}{\partial y}\right)\right] \qquad (2\text{-}57)$$

This equation is used to find the change in concentration due to dispersion and can be approximated by either implicit or explicit, with respect to time, finite difference techniques. The implicit method requires the simultaneous solution of a set of equations, while the explicit method consists of a direct calculation based on known concentrations.

Garder et al.[25] illustrated the explicit procedure which takes the finite difference form:

$$\begin{aligned}\Delta C_{i,j} = \frac{\Delta t}{\phi_{i,j}}\Bigg[&(\phi K_{xx})_{i+1/2,j}\,\frac{C^*_{i+1,j} - C^*_{i,j}}{\Delta x^2} \\ &- (\phi K_{xx})_{i-1/2,j}\,\frac{C^*_{i,j} - C^*_{i-1,j}}{\Delta x^2} \\ &+ (\phi K_{yy})_{i,j+1/2}\,\frac{C^*_{i,j+1} - C^*_{i,j}}{\Delta y^2} \\ &- (\phi K_{yy})_{i,j-1/2}\,\frac{C^*_{i,j} - C^*_{i,j-1}}{\Delta y^2}\Bigg]\end{aligned} \qquad (2\text{-}58)$$

The explicit procedure (equation (2-58)) has a time step stability limitation and was changed to an implicit procedure for our purposes.[24]

In finite difference form, the implicit method is:

$$(\phi K_{xx})_{i+1/2,j}\ C^{n+1}_{i+1,j} + (\phi K_{yy})_{i,j+1/2}\ C^{n+1}_{i,j+1} - \left((\phi K_{xx})_{i+1/2,j} + (\phi K_{yy})_{i,j+1/2} + (\phi K_{xx})_{i-1/2,j} + (\phi K_{yy})_{i,j-1/2} + \frac{\phi_{i,j}}{\Delta t} \right) C^{n+1}_{i,j} + (\phi K_{xx})_{i-1/2,j}\ C^{n+1}_{i-1,j} + (\phi K_{yy})_{i,j-1/2}\ C^{n+1}_{i,j-1} = \frac{-\phi_{i,j}}{\Delta t}\ C^{*}_{i,j} \qquad (2\text{-}59)$$

Equation (2-59), as with equation (2-33), forms a pentadiagonal solution matrix and is solved with an economized band algorithm.(19)

The change in concentration, for the implicit procedure, is now determined simply by

$$\Delta C_{i,j} = C^{n+1}_{i,j} - C^{*}_{i,j} \qquad (2\text{-}60)$$

Each point is assigned a new concentration according to the region, R_{ij}, it falls in:

$$C^{n+1}_{p} = C^{n}_{p} + \Delta C_{i,j} \qquad (2\text{-}61)$$

The sequence is now completed for the time step from t^n to t^{n+1} and the procedure is repeated for each subsequent time step.

2.3d Boundary Conditions

Treatment of the boundary conditions at $j = 1/2$ and $j = N_y + 1/2$ for the moving point method is handled identically as the fixed grid system discussed earlier.

At $j = 1/2$

$$\frac{\partial C}{\partial y} \cong \frac{C_{i,0} - C_{i,1}}{\Delta y} = 0 \qquad (2\text{-}62)$$

$$C_{i,0} = C_{i,1} \tag{2-63}$$

At $j = N_y + 1/2$

$$\frac{\partial C}{\partial y} \cong \frac{C_{i,N_{y+1}} - C_{i,N_y}}{\Delta y} = 0 \tag{2-64}$$

$$C_{i,N_{y+1}} = C_{i,N_y} \tag{2-65}$$

The boundary condition at the inflow face, i = 1, is separated into two parts, convective and dispersive.(23) The convection part is treated such that points outside the system in the supplying cells are set equal to the injected concentration, CI. Not until the points have travelled farther than i = 1 (x = 0) will their concentration be allowed to differ from CI.

$$C_p(x,y) = CI \text{ for } x < 0 \tag{2-66}$$

The dispersion portion of the inflow boundary condition is treated by setting concentrations of the $C_{0,j}$ blocks to CI and setting the dispersion coefficient term (ϕK_{xx}) at i = 1/2 equal to (ϕK_{xx}) at i = 3/2.

$$C_{0,j} = CI \tag{2-67}$$

$$(\phi K_{xx})_{1/2,j} = (\phi K_{xx})_{3/2,j} \tag{2-68}$$

2.3e Boundary conditions at outflow end

History matching is an integral part of this research, therefore treatment of the boundary conditions at the outflow end deserves special attention. Two different conditions were tried--reflective and 3 point upstream weighting. The reflective condition is given by

$$\left(\frac{\partial C}{\partial x}\right)_{N_x,j} \cong \frac{C_{N+1,j} - C_{N-1,j}}{\Delta x} = 0 \qquad (2\text{-}69)$$

$$C_{N+1,j} = C_{N-1,j} \qquad (2\text{-}70)$$

Note that face centered reflective conditions require $C_{N+1,j}$ to equal $C_{N-1,j}$ instead of $C_{N,j}$ as with the block centered simulation.

The three point upstream condition is derived by Naiki[23] and is represented as

$$C_{N,j} = 4/3\ C_{N-1,j} - 1/3\ C_{N-2,j} \qquad (2\text{-}71)$$

2.3f Treatment of points at boundaries

Points in the inflow supplying cells are set at the injection concentration, as described in section 2.3d, and have x-velocities equal to their respective inflow boundary velocities and y-velocities of zero. Not until the points cross the inflow face are they assigned interpolated velocities in the manner discussed in section 2.1biv. As points cross the outflow boundary, they are eliminated and placed in the supplying cells, keeping an equal density of points within the system.

2.3g History concentration sampling

Two schemes were tested for outlet concentration sampling for use in history plots. One method is to flow rate average the grid point concentrations on the outflow end. The other scheme involves sampling individual points as they leave the system boundary. An average con-

centration of all points leaving each individual grid block is then calculated. These average concentrations are flow rate averaged in the same manner as the first method. If no points leave the outflow end during a particular time step, the points nearest the end within the system are sampled. This point sampling technique was tried because of the apparent accuracy achieved as to fluid breakthrough, which is important in our history matching applications. The accuracy of breakthrough time in the second method is the result of sampling points as they cross the outflow face (or the nearest set of points within the system). The first method, using nodal concentrations, does not portray the exact arrival time because the nodal concentration will be affected by the points as they cross their grid block region at $i = N_x - 1/2$. The early arrival time error will increase as the number of grids in the x-direction decreases, pushing the $i = N_x - 1/2$ point farther into the system away from the outflow face.

CHAPTER 3. NUMERICAL STUDIES

3.1 Fixed Grid Finite Difference

Numerical dispersion is a problem with finite difference approximations of the dispersion equation.[19,22] With no dispersion present and no reservoir layering, profiles of injected fluid displacements should take the shape of a step function with C equal to the injected concentration behind the front and equal to zero ahead of the front. Conventional simulation of this displacement will exhibit a "spreading" of the front due to numerical dispersion caused by error in the finite difference approximations (figure (3-1)). This error should be kept to a minimum in order to accurately determine proper values of history matched α_ℓ and α_t.

Numerical dispersion was found to be reduced by:[19,22]

1. Reducing time step size.
2. Reducing grid block sizes in the direction of bulk flow (x-direction).
3. Midpoint weighting (WF = 0.5) the convection term of the dispersion equation.

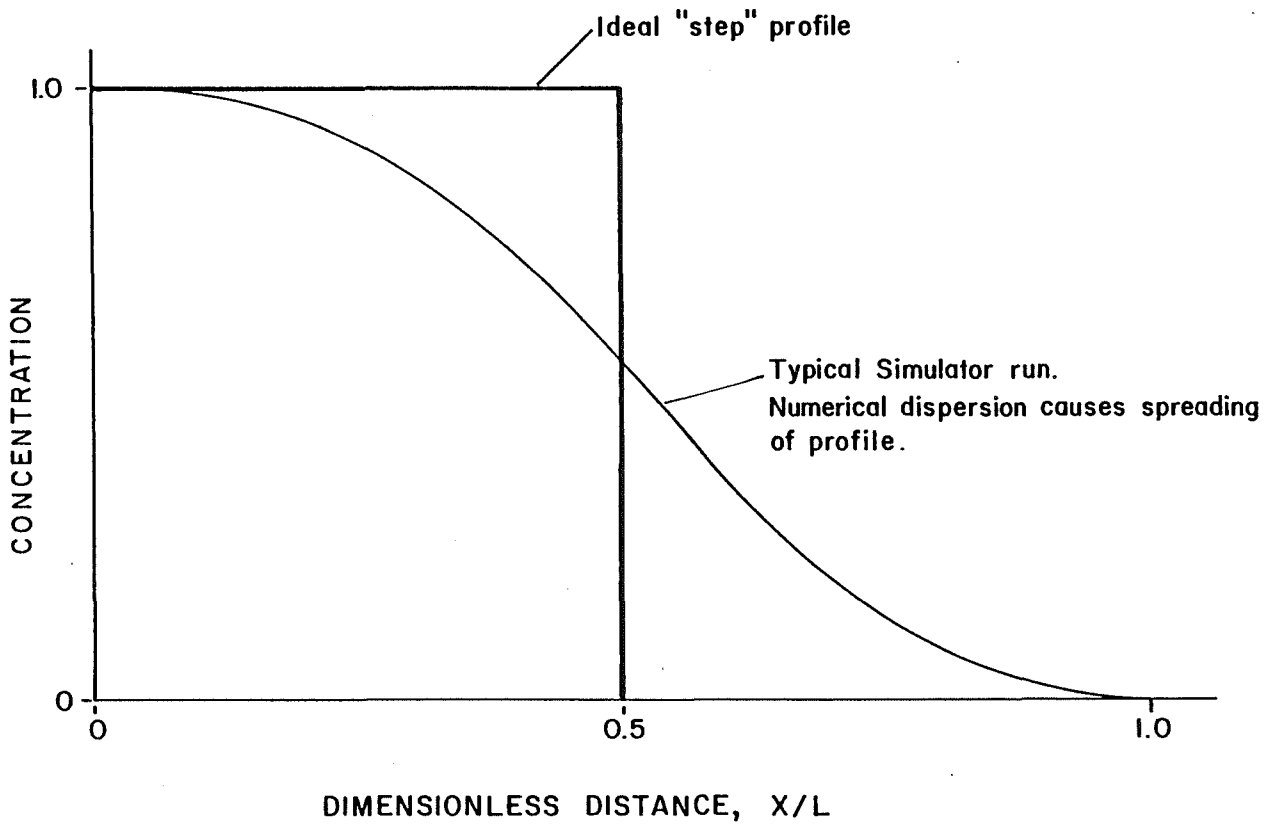

Figure 3-1. Profile of fixed grid simulator with no physical dispersion.

3.1a Effect of grid block size in x-direction

Figure (3-2), showing a concentration profile at 0.5 pore volumes injected, illustrates how spreading is reduced as grid block size in the x-direction is decreased. The simulator was first run with 25 grids over the system length, then again with 100 grids. Much closer fit resulted when 100 grids or a dimensionless grid block size, $\Delta x/L$, of 0.01 was used.

3.1b Weighting of the convection term

Midpoint weighting (WF = 0.5) of the first derivative term of the dispersion equation gives the most accurate results. Midpoint weighting was compared with upstream weighting (WF = 1.0) to determine which method would be best (figure (3-3)). Upstream weighting exhibits no oscillation as does midpoint weighting, but the spreading of the front is more severe. Since the process of history matching to determine values of α_ℓ is dependent upon the curvature of the front, midpoint weighting is superior for our purposes.

3.1c Grid block size in y-direction

After determining the appropriate grid block size in the direction of flow, attention was turned to grid spacing in the transverse or y-direction. The $K_{yy} \frac{\partial^2 C}{\partial y^2}$ term in the dispersion equation is the only contribution

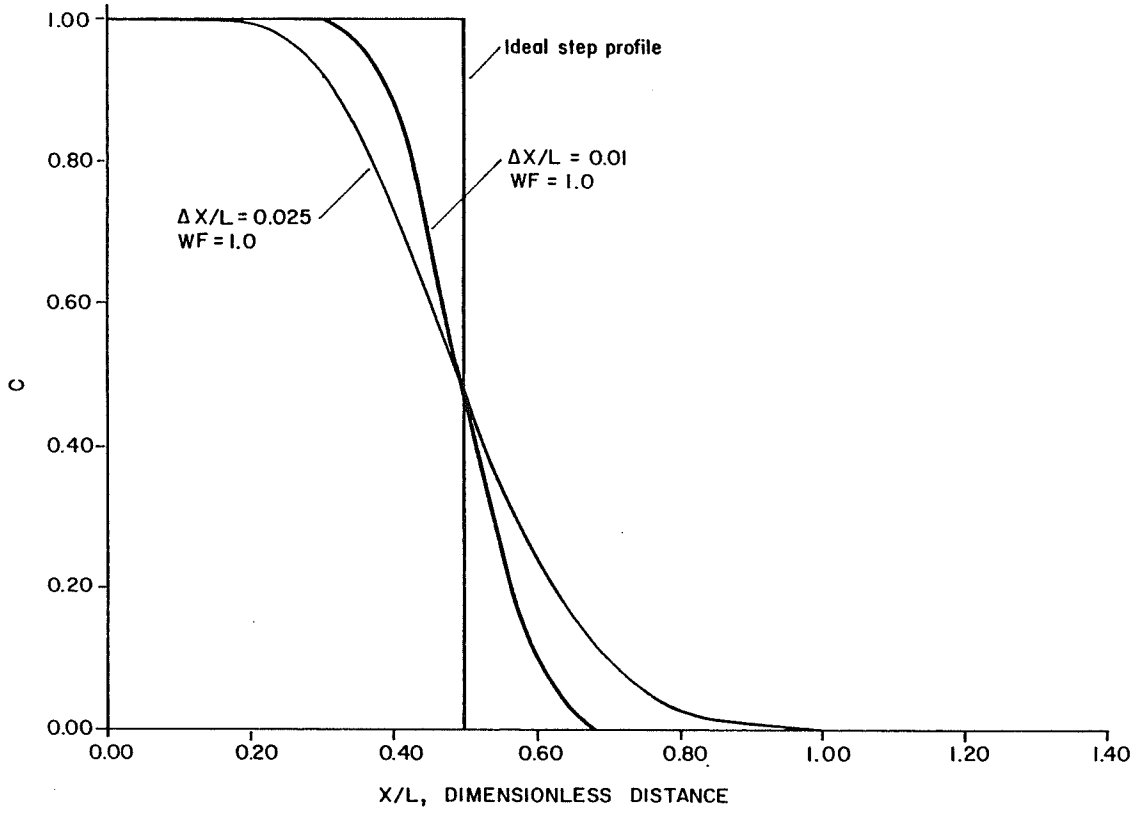

Figure 3-2. Profile showing effect of grid block size in x-direction for fixed grid simulation.

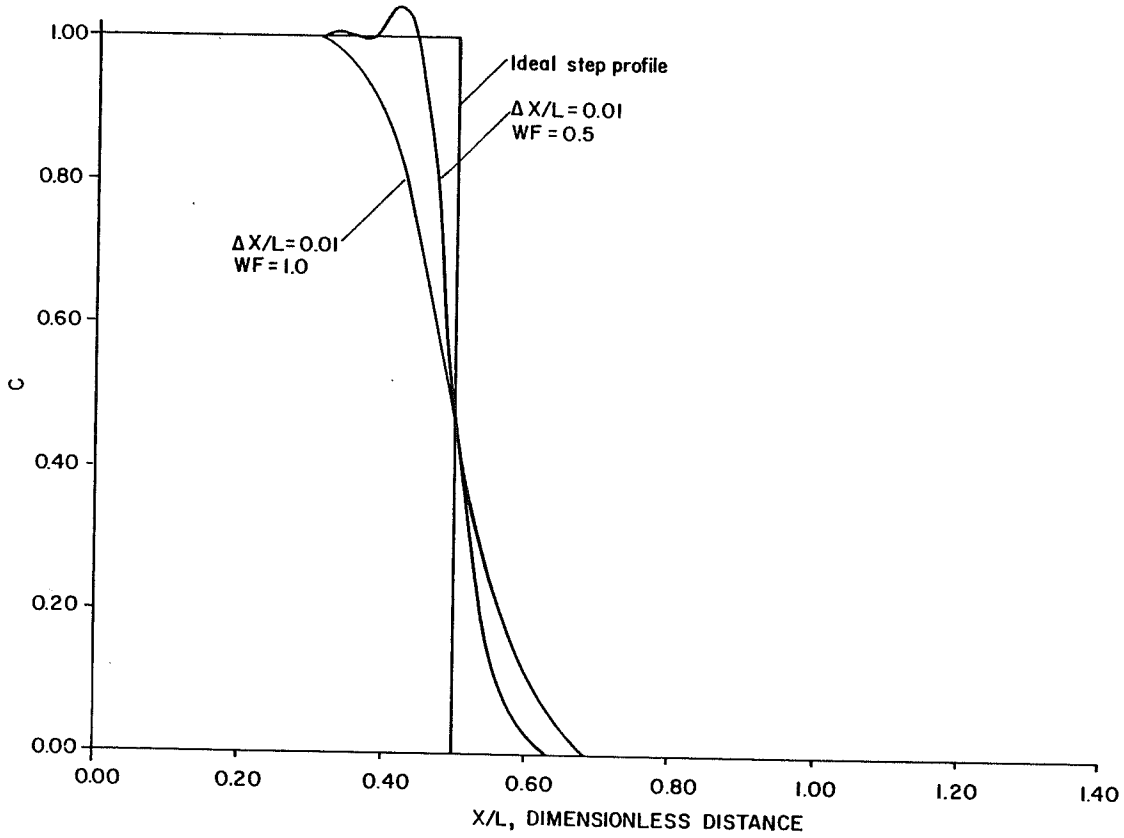

Figure 3-3. Profile showing effect of weighting factor for fixed grid simulation.

to truncation error in the vertical direction. The simulator was modified to solve the equation:

$$K_{yy} \frac{\partial^2 C}{\partial y^2} = \frac{\partial C}{\partial t} \qquad (3\text{-}1)$$

A concentration of 1.0 was input in the blocks at the top of the system (figure (3-4)) and the program was run for an adequate number of time steps to develop a vertical concentration profile. Provided the concentration at the bottom of the system is insignificant, this problem has a direct analogy to the heating of an infinite slab.(4) The analytic solution is given by:

$$C = 1 - \text{erf} \frac{y}{\sqrt{(4K_{yy})t}} \qquad (3\text{-}2)$$

Figure (3-5), a vertical profile of concentration versus dimensionless vertical distance, y/H, shows that truncation error is not very sensitive to grid block size in the y-direction. This is to be expected as the finite difference approximation to the dispersion term in equation (3-1) is second order correct.(22) Therefore, use of one grid block per layer for history matching should not introduce significant error.

3.1d Summary

Simulation by fixed grid finite difference methods is a fast process requiring relatively little computation time. However, to reduce truncation error, a large number of grid blocks have to be taken, pushing storage require-

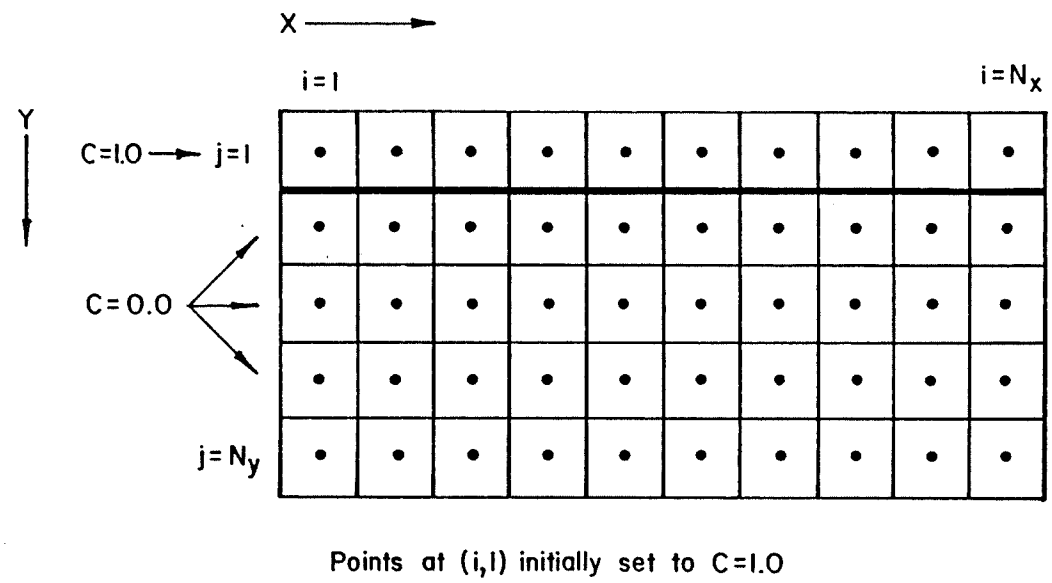

Figure 3-4. Fixed grid simulator adaptation for y-direction dispersion check.

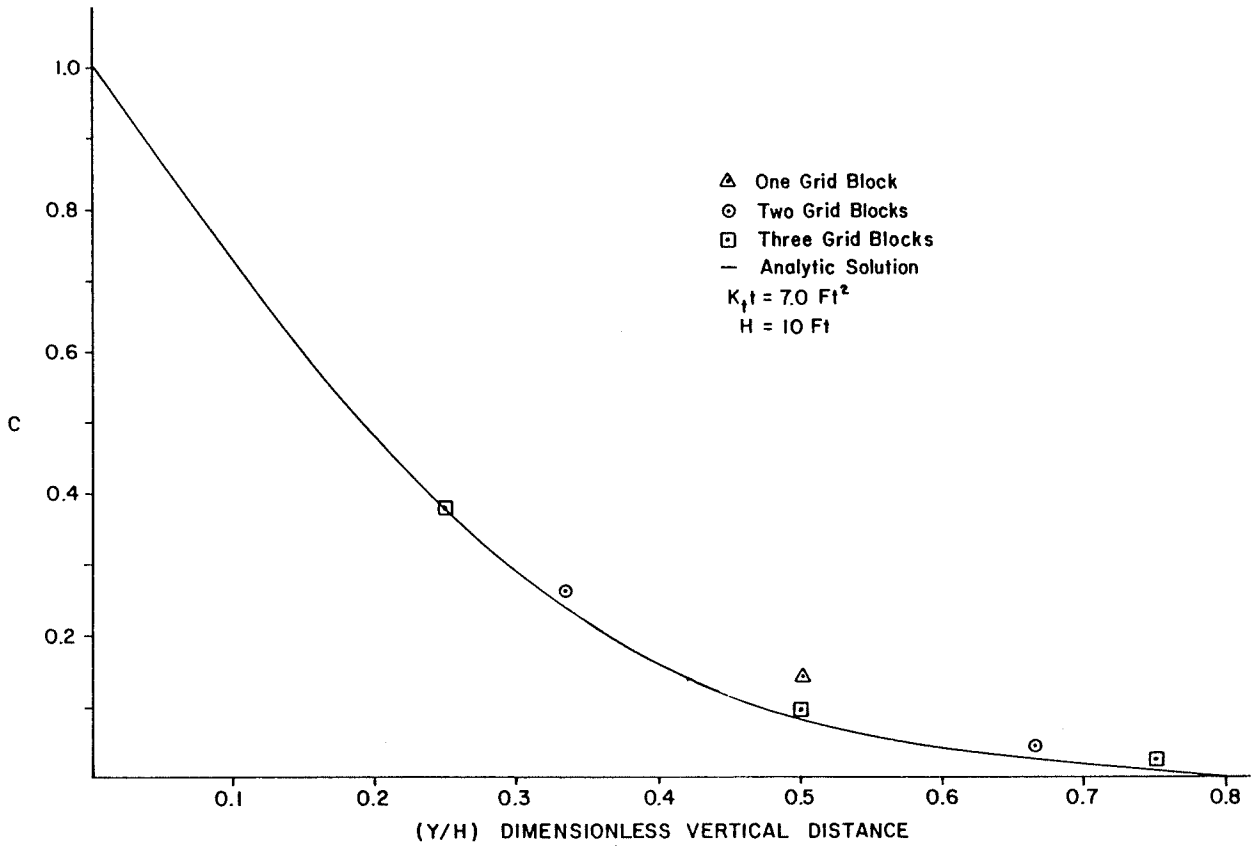

Figure 3-5. Transverse dispersion profile showing effect of the grid size in vertical direction for fixed grid simulation.

ments near the maximum allowable on most computers for models of moderate size. For example, simulation of the MP-131 well system (section 4.2b) uses a 17 by 90 grid block system requiring in excess of 200,000 octal words of storage. The normal maximum allowable storage on the University of Texas' CDC Dual Cyber 170/750 machine is 220,000 octal words. Modeling of the outer observer, MP-132, would need more than the maximum allowable storage. Even then, numerical dispersion is barely within acceptable limits. Because of this, attention was turned towards developing a simulator utilizing the moving point method.

3.2 Moving Point Simulation

The moving point method properly takes into account all levels of physical dispersion. This method requires substantially less computer storage than the fixed grid finite difference simulator, but does take more time for corresponding simulation runs of similar accuracies. Good agreement resulted with the analytic solution to the one dimensional homogeneous dispersion equation, in history plots of concentration versus pore volumes injected, for Peclet numbers ranging from ∞ to 8.78 (figures (3-6) to (3-9)). This equation is given by

$$K_{xx} \frac{\partial^2 C}{\partial x^2} - v_x \frac{\partial C}{\partial x} = \frac{\partial C}{\partial t} \qquad (3\text{-}3)$$

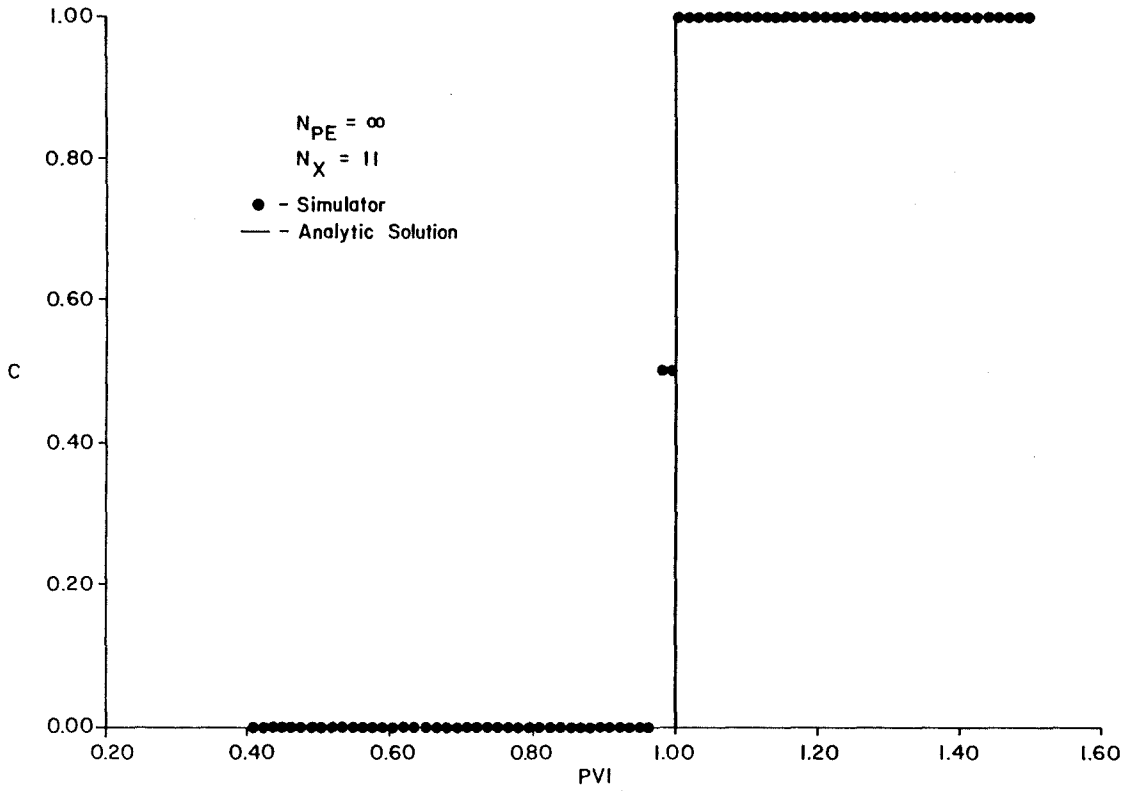

Figure 3-6. Moving point simulation history curve for $N_{PE} = \infty$.

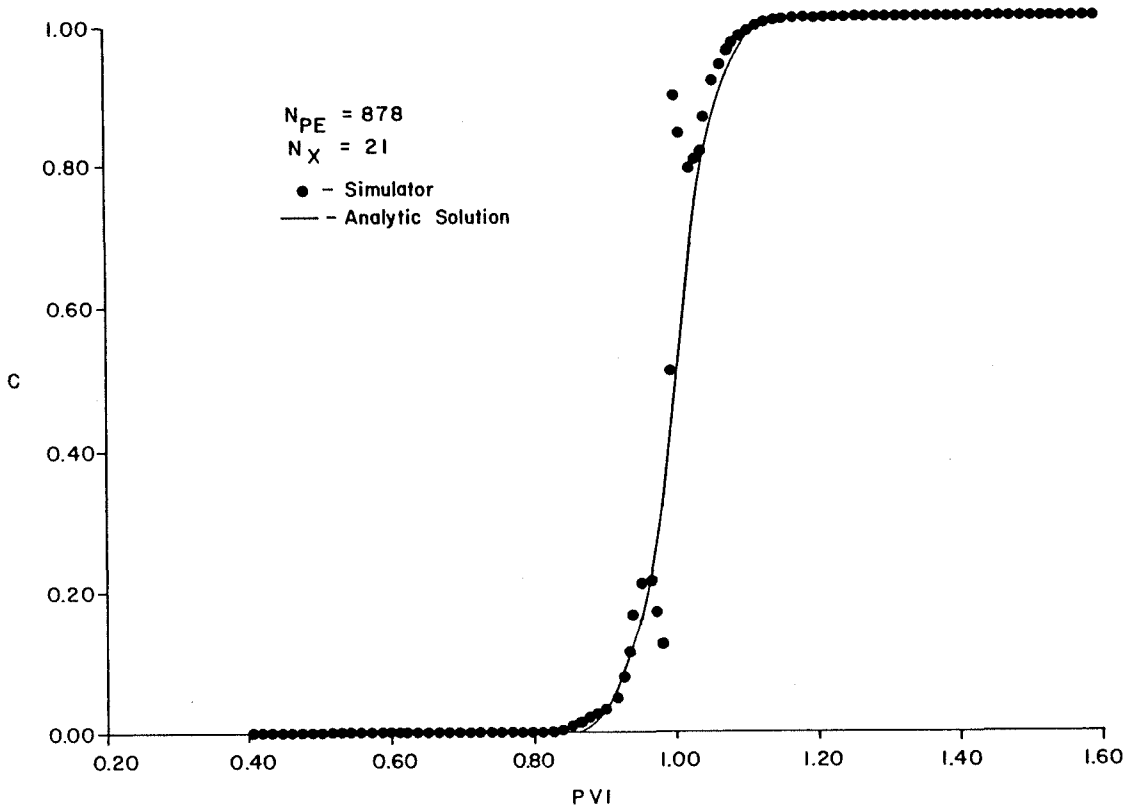

Figure 3-7. Moving point simulation history curve for N_{PE} = 878.

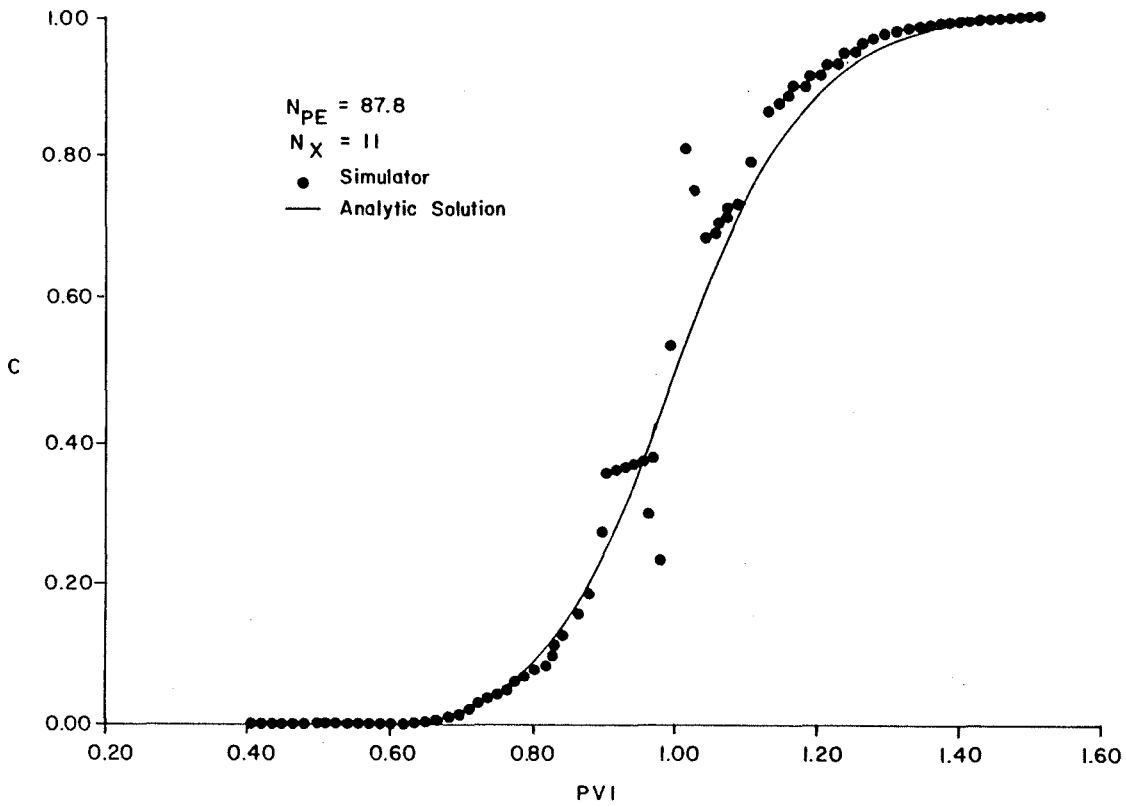

Figure 3-8, Moving point simulation history curve for N_{PE} = 87.8.

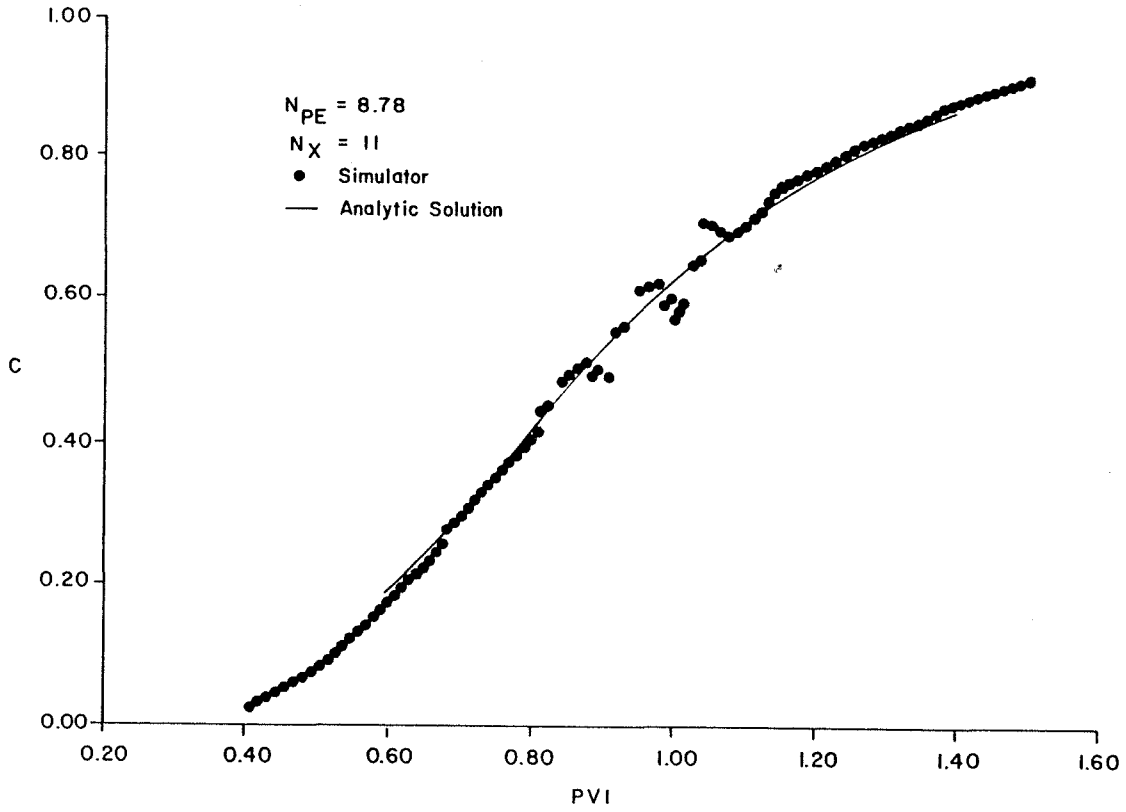

Figure 3-9. Moving point simulation history curve for $N_{PE} = 8.78$.

with the approximate analytic solution[16]

$$C/CI = \tfrac{1}{2}\left[1 - \operatorname{erf}\left(\frac{X/L - PVI}{2\sqrt{PVI/N_{PE}}}\right)\right] \qquad (3\text{-}4)$$

where

$N_{PE} \equiv$ Peclet number, for this special case $= L/\alpha_\ell$

At an infinite Peclet number, ideally a step function should result and as shown in figure (3-6), the simulator gives excellent results.

Oscillation develops around one pore volume injected at Peclet numbers of 878, 87.8, and 8.78. This oscillation, as will be discussed later, can be reduced by taking more grid blocks in the x-direction.

History plot oscillation is inherent to the moving point method when dispersion is introduced. Points immediately ahead of the displacing front with an initial concentration of zero will often fall within the same grid rectangle as points having an initial concentration of 1.0 behind the front as shown in figure (3-10). Dispersion calculations are performed using the average concentration of all points within the grid and therefore those rows ahead of the front will lose more concentration due to dispersion than would naturally occur and those rows of points behind the front will lose less concentration.

As an example, figure (3-10) shows three adjacent regions, (i-1,j), (i,j), and (i+1,j) having C^*'s of 1.0, 0.5, and 0.0, respectively at $t = t^0$. Let us assume

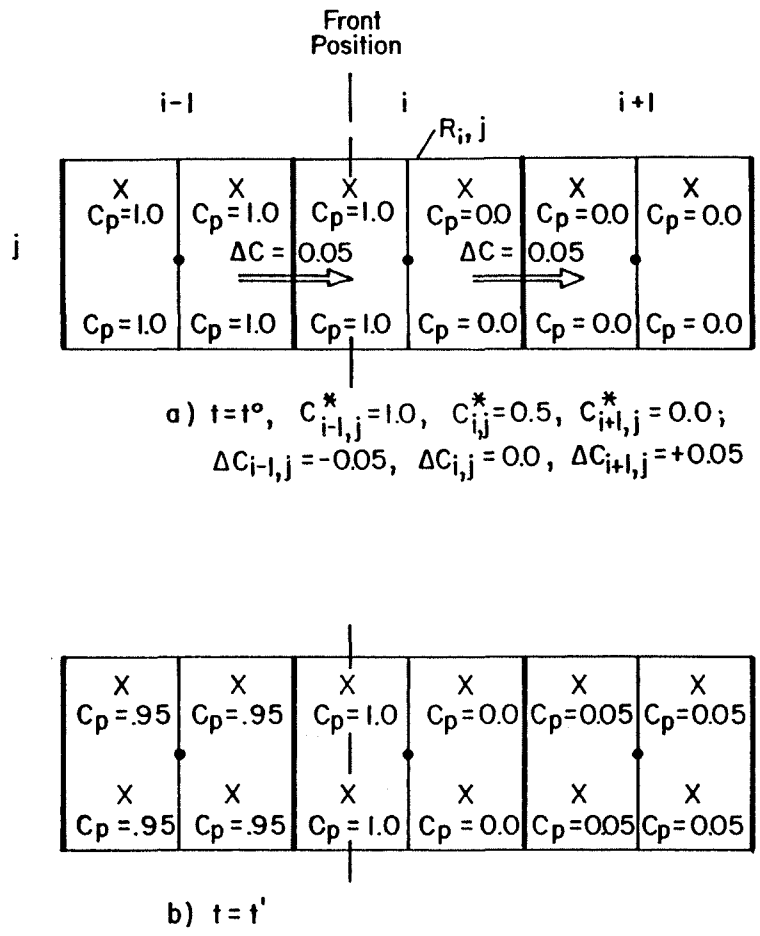

Figure 3-10. Illustration of origin of introduced oscillation in moving point simulation.

regions to the left of the (i-1,j) blocks have concentrations equal to 1.0 and blocks to the right of the (i+1,j) region have concentrations of 0.0. Let us further assume a concentration gradient of 0.5 between the two regions will cause a change in concentration, ΔC, of 0.05 due to dispersive flux to result during a given time step. Therefore, $\Delta C_{i-1,j} = -0.05$, $\Delta C_{i,j} = 0.0$, and $\Delta C_{i+1,j} = 0.05$, for the time step from $t = t^0$ to $t = t^1$. All points in region (i-1,j) initially had $C_p^0 = 1.0$ and therefore have $C_p^1 = 0.95$. Points in region (i+1,j) will all have $C_p^1 = 0.05$ since they were initially at zero concentration. The points in region (i,j) experience no change because equal amounts dispersed into and out of the region. The two points at the leading edge of the front remain at $C_p^1 = 1.0$ and the two directly ahead of the front at $C_p^1 = 0.0$. Thus, the individual rows of points within region (i,j) do not allow a smooth transition from C = 0.0 ahead of the front to C = 1.0 behind the front.

This effect is magnified by the outflow node concentrations, which are sampled for history curves, because they average only the points in the 1/2 grid spacing to the left of the nodes within the system. For our simple example using only two rows per entire grid, only one row at a time will be averaged as they pass through the last 1/2 grid region on the outflow end. The result is a history

curve oscillation at approximately one pore volume injected for homogeneous systems.

Concentration profiles do not exhibit the introduced oscillation as severely as history curves while the front is within the system, away from the first or last 1/2 node regions at the inflow and outflow ends, respectively. Using the same logic as the preceding discussion, profiles do not oscillate as much because the front is within the system and the nodal concentrations average the point concentrations within an entire grid spacing, thus dampening out any irregularities in concentrations between adjacent rows of points. Figure (3-11) shows a concentration profile at 1/2 pore volume injected. No oscillation is apparent for the Peclet number of 87.8 and this is very similar to the results obtained by Naiki.[23] Both Naiki's and our runs matched the analytical profile well and oscillation is not apparent.

3.2a Effect of boundary conditions and sampling on outflow end

Sampling of flow rate averaged nodal concentrations on the outflow end with reflective boundary conditions proved to be the best method of history plotting for our purposes. Naiki[23] pointed out in a previous work that the three point upstream weighting boundary condition exhibited less oscillation than the reflec-

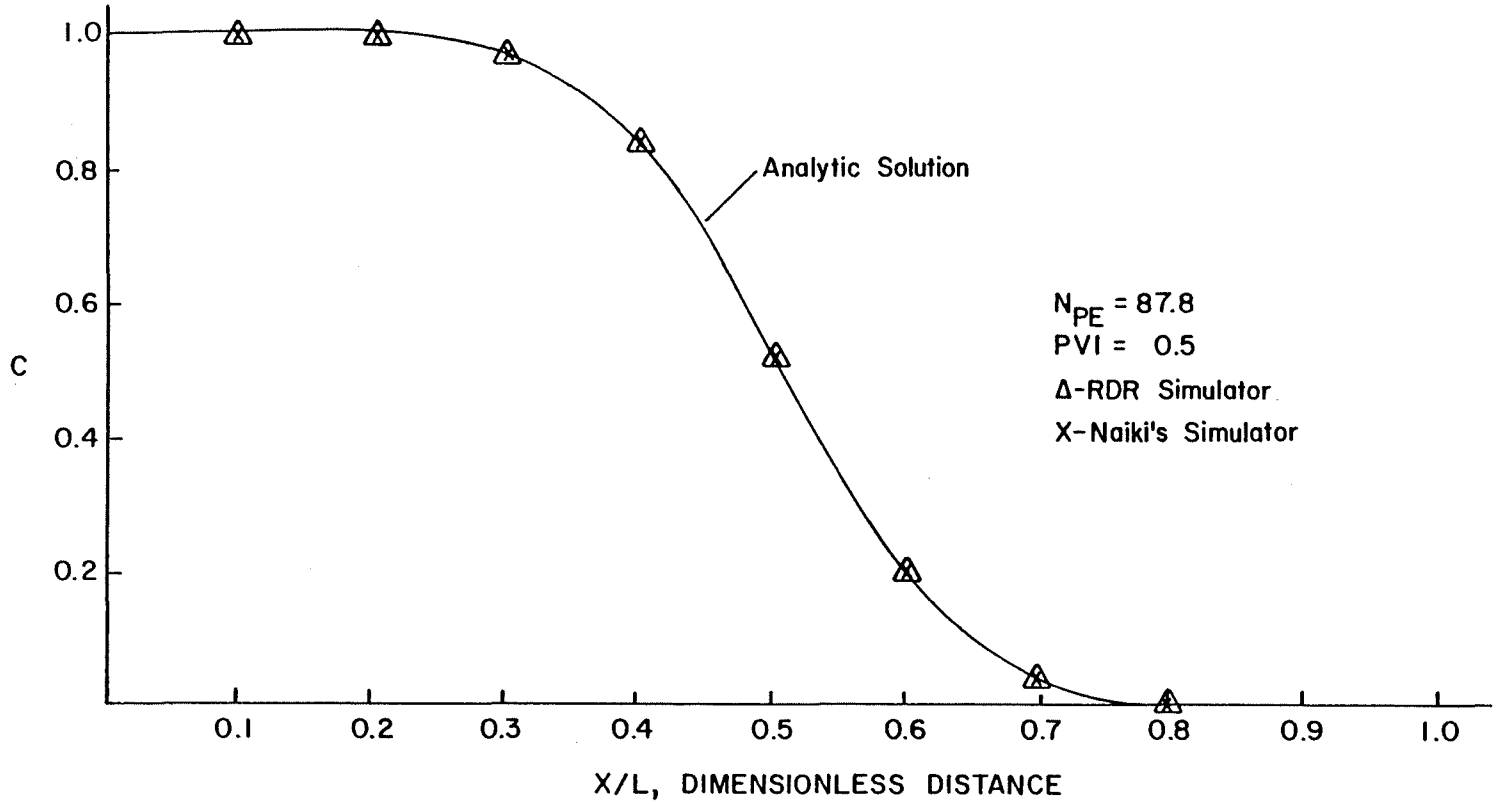

Figure 3-11. Moving point simulation profile of both Naiki's and our's compared to analytic solution.

tive condition. Our work agreed with the prior finding as shown in figure (3-12). However, the outlet node concentrations are calculated based upon the concentrations of the $C_{N_{x-1,j}}$ and $C_{N_{x-2,j}}$ nodes (equation 2-71). Considering the case of no physical dispersion, the outlet node will record the injected concentration as soon as the front passes through the $C_{N_{x-1,j}}$ region--before actually reaching the outflow end. This results in a history plot offset to the left. This "shifting" was found to occur even when physical dispersion is introduced as shown in figure (3-12) for $N_{PE} = 87.8$. Because we required accurate arrival times during the history matching phase of this work, reflection boundary conditions were judged better for our purposes. The greater oscillations experienced do not present any special problems as the general trend of dispersion is not disturbed.

As stated in Chapter 2, a point sampling technique was tried for outlet concentrations (figure (3-13)). Reflective boundary conditions were used at the outflow end, but instead of using node averaged concentration for history plots, individual points were sampled and averaged for each interval as they passed out of the system. It was hoped this approach would best describe the arrival time of the front, which is crucial for α_t determination. The arrival time was delayed as evidenced by the shifting of the history plot to the right, but even greater

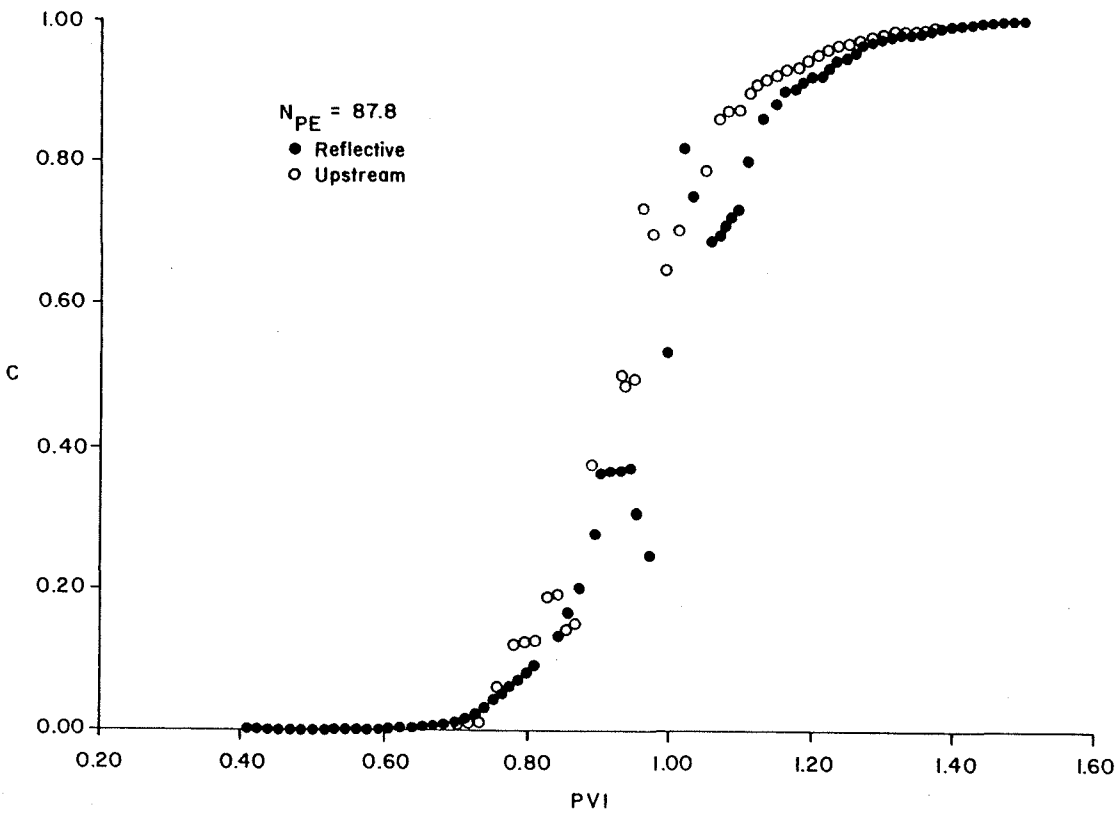

Figure 3-12. History curve comparison of reflective and 3-point upstream boundary conditions on outflow end for moving point simulation.

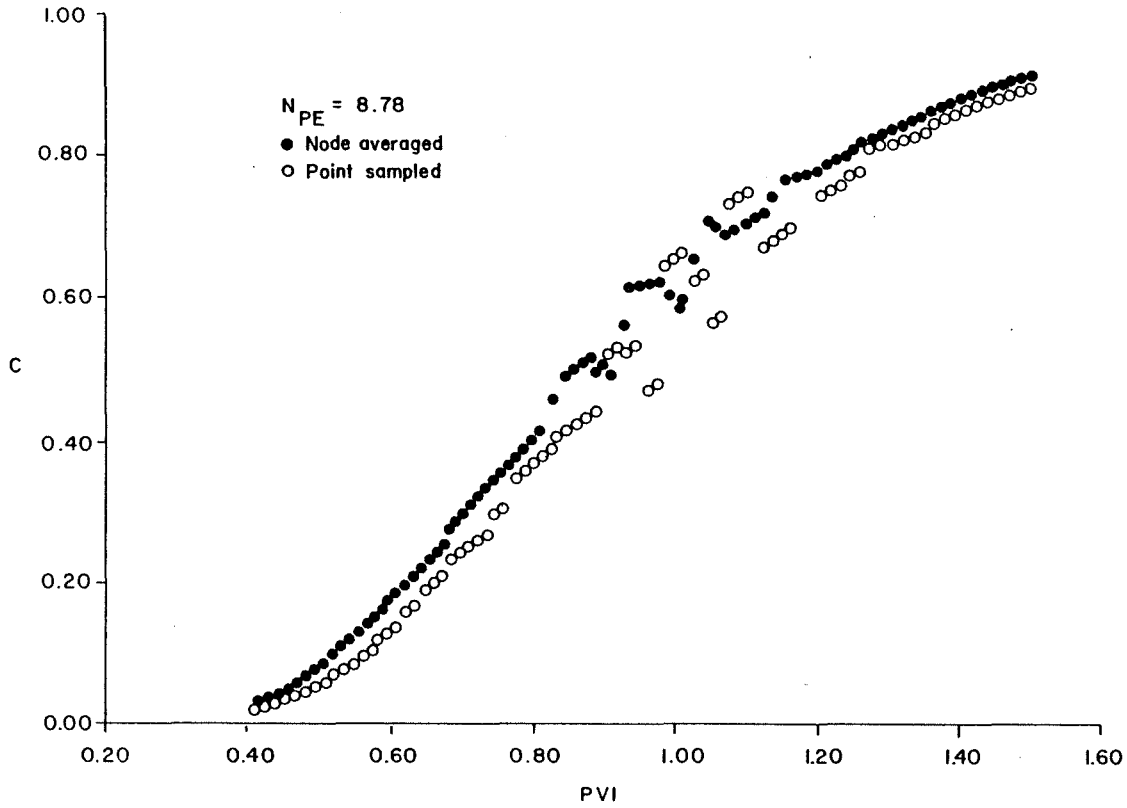

Figure 3-13. Comparison of node averaged and point sampled effluent histories for moving point simulation.

oscillation occurred. This method appears less desirable than using node averaged concentrations because the oscillations are more severe and the arrival time can be "artificially" adjusted by varying the starting position of the first row of points injected into the system (see section 3.2f).

3.2b Effect of grid size in x-direction

The number of grids required in the x-direction without loss of accuracy is greatly reduced by the moving point method as compared to the fixed grid finite difference technique discussed previously. Oscillations were reduced as the number of grid blocks increased from 5 to 21 (figure (3-14)). As the number of grid blocks increase, the already long computing times experienced by the moving point method severely increase.

Table (3-1) illustrates typical computation times for homogeneous systems with both the moving point and fixed grid simulators (performed on The University of Texas CDC Dual Cyber 170/750 machine). Notice that the computing times on a per grid block, per time step basis for the moving point runs increase from 3.01×10^{-3} sec/(grid block) (time step) to 5.21×10^{-3} sec/(grid block) (time step) as the system size increases from 4 by 5 grid blocks to 4 by 21 grid blocks, respectively. This is the result of the greater number of moving points

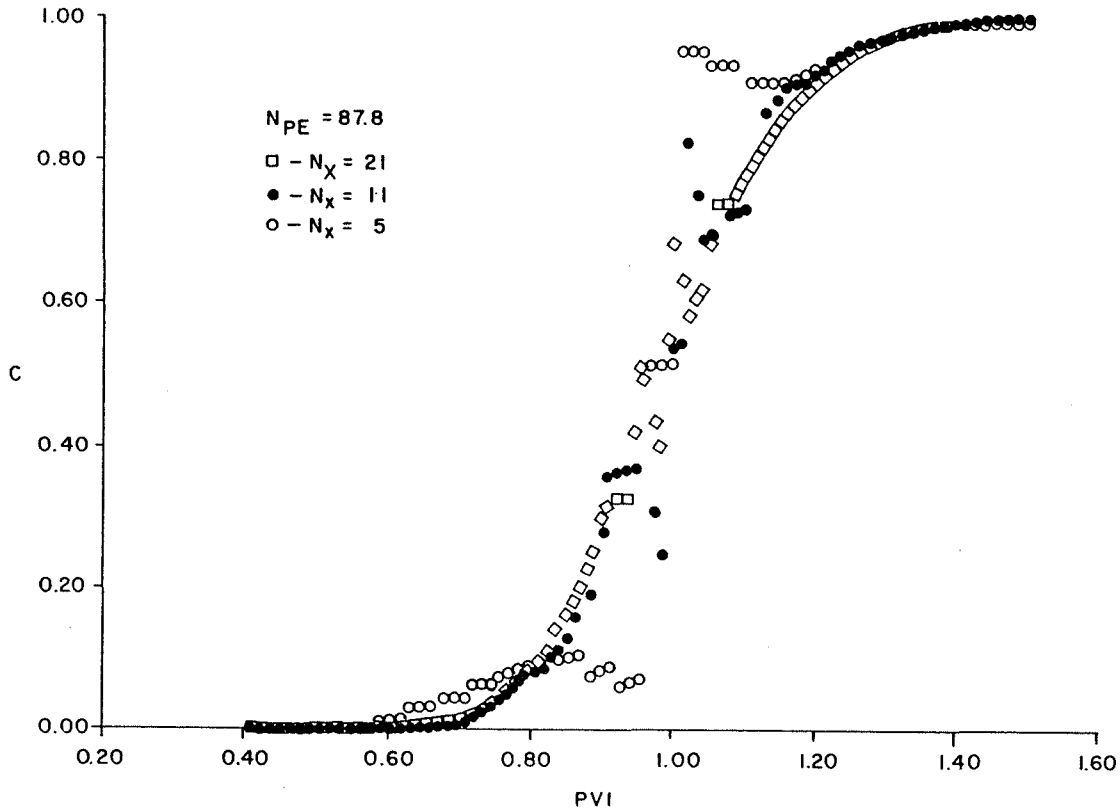

Figure 3-14. Effect of x-direction grid size on history curves for moving point simulator.

Table 3-1

Typical Computation Times
for the Simulator Runs

Simulator	System Size (N_y by N_x)	CPU sec / PVI	CPU sec / (grid block) (time step)	CPU sec / (grid block) (time step) (moving point)
Moving Point	4 X 5	12.5	3.01×10^{-3}	5.01×10^{-5}
	4 X 21	91.2	5.21×10^{-3}	2.06×10^{-5}
Fixed Grid	4 X 21	3.0	1.75×10^{-4}	----

needed as the number of grid blocks increase. The fixed grid simulator required approximately 1.75×10^{-4} CPU sec/(grid block) (time step), which is substantially less than the moving point method. Because of the relatively large computing times taken by moving point simulation, system sizes should be kept as small as possible without introducing large numerical error.

Even though use of fewer blocks increases oscillation, the general trend of the history curves remains the same for the model sizes discussed above. For our purposes, 11 nodes in the x-direction proved sufficient for most homogeneous systems.

In heterogeneous systems, no hard and fast rules can be drawn as to the proper number of nodes in the x-direction. As little as 5 nodes were used for history matching the field test data for the El Dorado field (see Chapter 4). The best procedure is to make a few trial runs with the desired system and input data, then observe the resulting history plots and other important indicators such as material balances and computation time. Only then can the grid block size be properly determined.

3.2c Grid size in transverse direction

As with the fixed grid finite difference simulator, only one grid block per layer is needed to assure an accurate description of transverse dispersion. The moving point simulator was modified in much the same way as pre-

viously discussed for the fixed grid system, solving equation (3-1). Figure (3-15) shows that the vertical spacing of grid blocks has little effect on numerical error. A good match resulted between the run of only one grid block through the ten foot homogeneous system and the analytic solution given by equation (3-2).

3.2d Effect of number of points per grid

Figure (3-16) shows that the use of three points per grid in both x and y directions is adequate for proper two dimensional calculations. Error was increased when only 2 points per grid were allotted, while 4 points/grid did not significantly increase accuracy and would unnecessarily add to computing time. Runs with no vertical flow could be made with 3 points per grid in the x-direction and 1 point/grid in the y-direction.

3.2e Time step sensitivity

The nature of the moving point method does not allow any simple formula for time step selection. As discussed earlier, the dispersion calculations were changed to an implicit procedure to allow greater time steps without causing instability. During the course of the research it became apparent that good results were obtained when the time step moved the points in the fastest layer $\frac{1}{2}$ their initial spacing per time step. This is no hard and fast rule. Different time steps can be

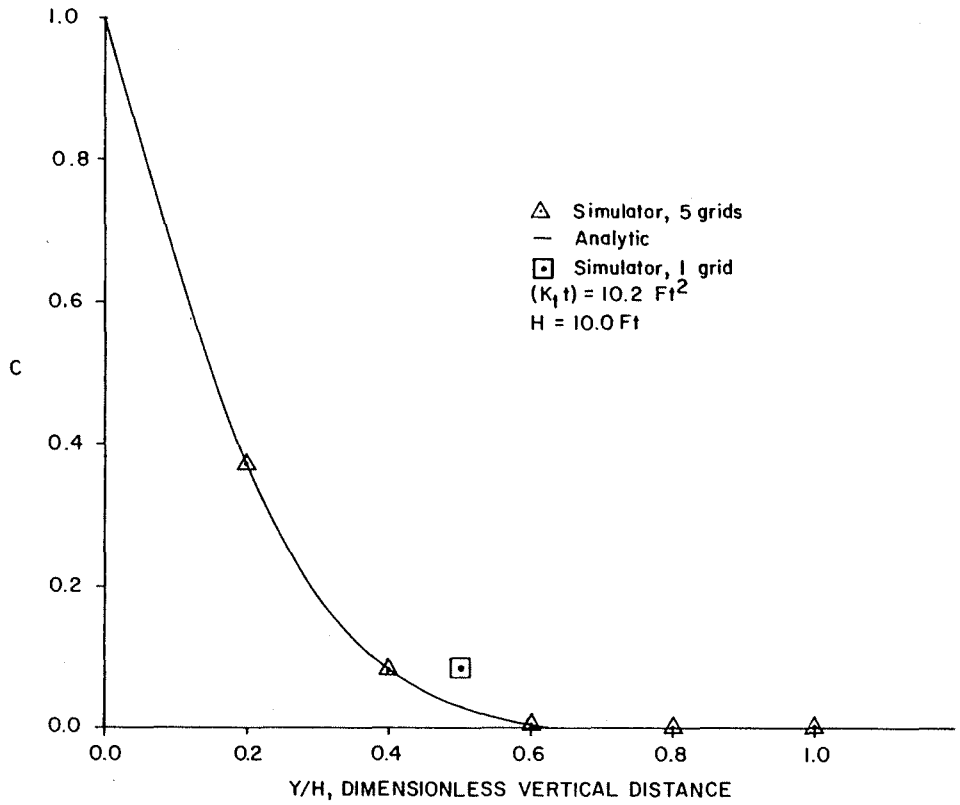

Figure 3-15. Transverse dispersion check profile for moving point simulator.

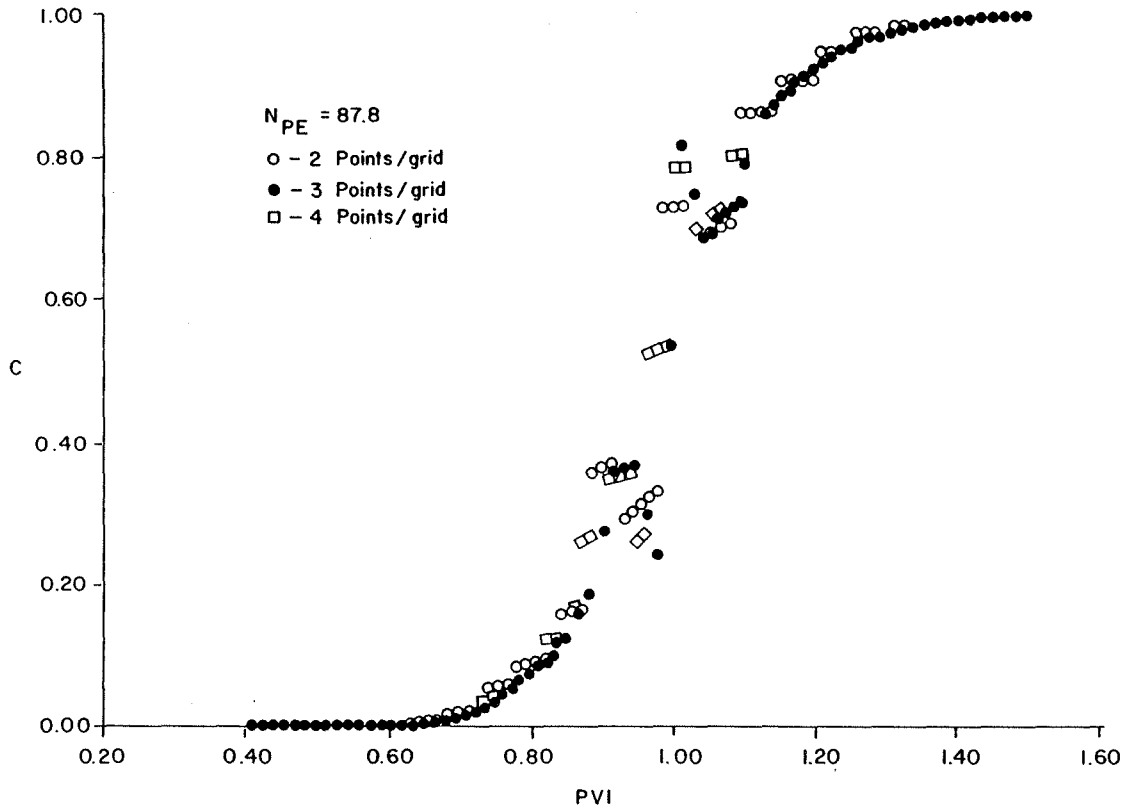

Figure 3-16. Effect of initial point spacing on history curves for moving point simulation.

selected (larger or smaller) and yield excellent results. The time step should not be so great, though, as to allow points to either overrun one another or to race past the inflow end creating a larger spacing than originally intended.

3.2f Effect of initial point position

The position, with regard to the x-direction, of the first row of points entering the system having the injection concentration, can significantly affect the breakthrough point of the history curves. Figure (3-17) illustrates 2 different initial positions of points at the start of calculations in an 11 node system and their resultant history plots. The plot having the desired breakthrough of C = 0.05 at one pore volume injected was created when the points were initially placed 1/3 the distance of the grid block to the left of the inflow boundary. When the points were started exactly on the inflow boundary, the history plot was incorrectly shifted to the left. Obviously, starting the points on the inflow boundary appears to be theoretically correct, but the plot is shifted to the left because the nodes at the outflow end are affected by points as they move into its boundary ½ grid spacing into the system. Therefore, placing the first row of points of the front out of the system to the

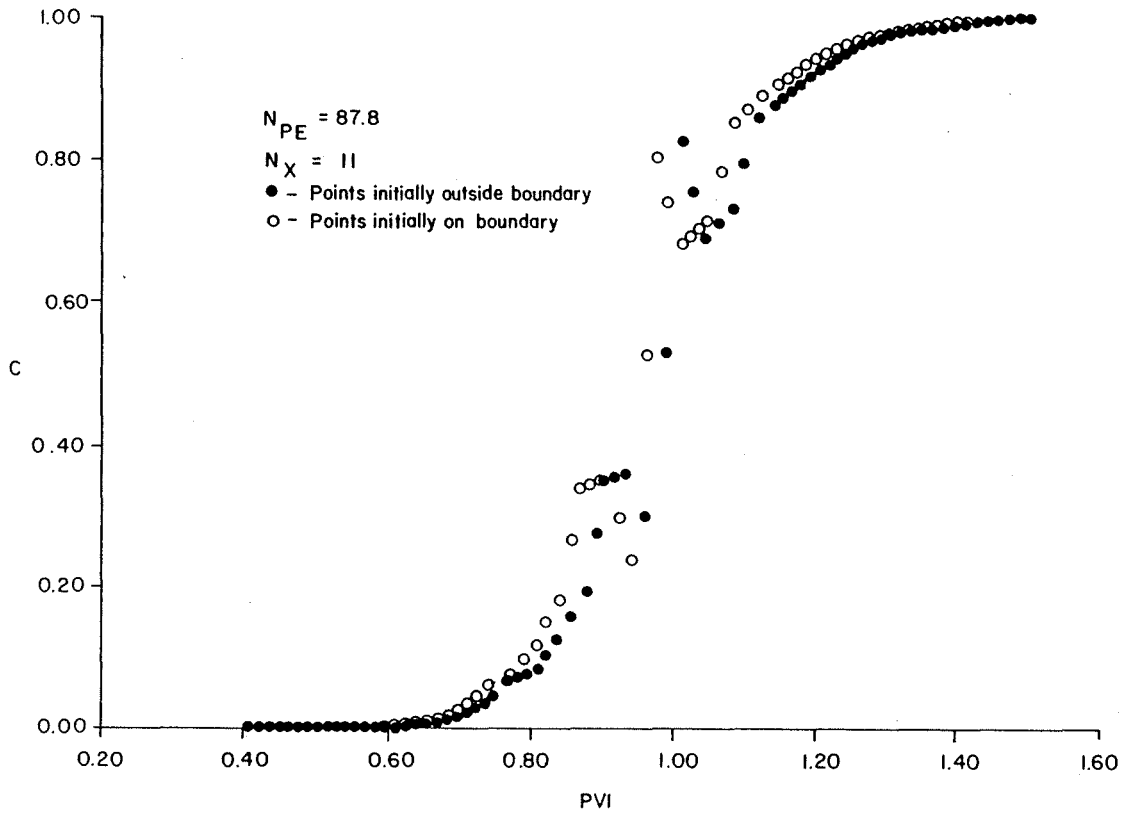

Figure 3-17. Effect of initial position of front points on history curve breakthrough.

left of the inflow boundary artificially corrects this problem without significantly affecting the curvature of the history plots.

CHAPTER 4. RESULTS

4.1 History Matching Field Data

The major focus of our research is to determine dispersivities (both α_ℓ and α_t) occuring on a field scale in actual heterogeneous reservoirs. This will be accomplished by matching effluent history curves produced by our simulator with data observed in miscible field displacements. The only data available to us was from the El Dorado field in Kansas where a fresh water solution was injected through a well (MP-118), displacing the formation salt water, and flow concentrations measured in two observation wells, MP-131 and MP-132, as illustrated in figure (4-1).(26)

The observation wells were not perforated through their entire pay zone, instead they were perforated through a one foot section (for more details see sections 4.2a and 4.3). The wells sampled fluid through the perforated section at low flow rates, on the order of 5 barrels per day compared to the injection of fluid which averaged approximately 150 barrels/day.(26) This low sampling rate was assumed to not significantly distort the flow streamlines through the reservoir in the vicinity of the observers. Also, the observation wells were posi-

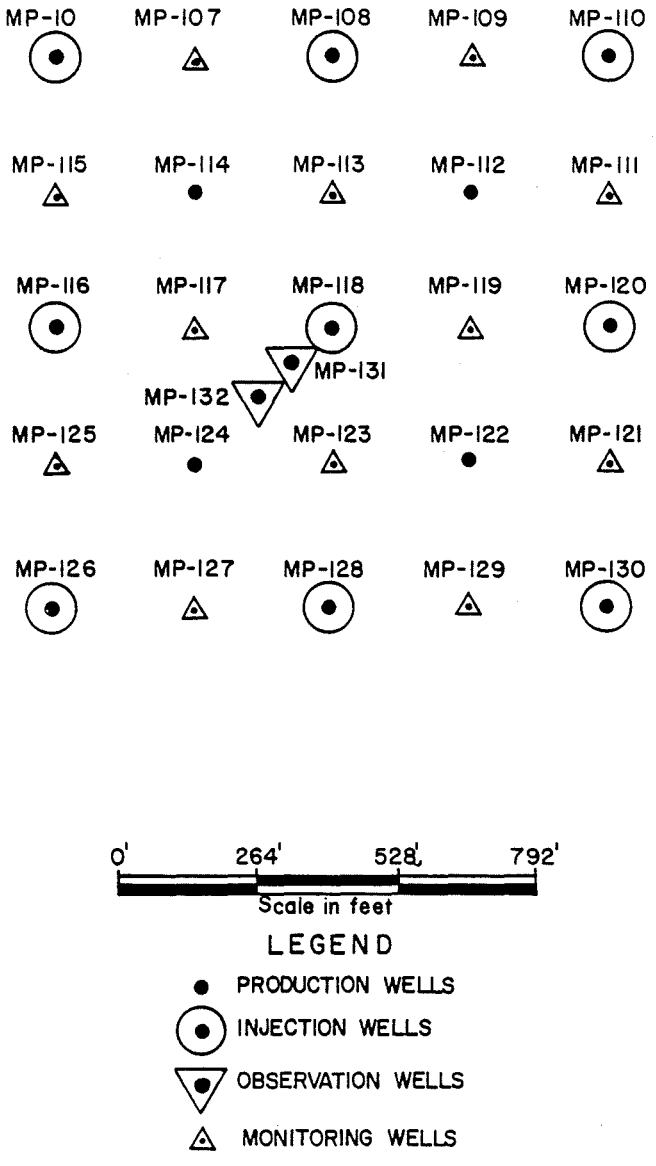

Figure 4-1. Project layout showing location of the observation wells.

tioned directly between the injection and production wells. Because of these factors, a linear simulator properly models flow from the injection well MP-118 to either of the two observation wells, MP-131 or MP-132.

For our initial purposes, no vertical flow was assumed, and the reservoir was modeled as being composed of individual layers given by the core data taken from the wells. These layers were assumed to have constant thickness, porosity, and permeability through their entire section and velocity independent of x. For these cases, the dispersion equation takes the form:

$$K_{xx} \frac{\partial^2 C}{\partial x^2} + \frac{1}{\phi} \frac{\partial}{\partial y}\left(\phi K_{yy} \frac{\partial C}{\partial y} \right) - v_x \frac{\partial C}{\partial x} = \frac{\partial C}{\partial t} \qquad (4\text{-}1)$$

where

$$K_{xx} = \frac{D_o}{F\phi} + \alpha_\ell v_x$$

$$K_{yy} = \frac{D_o}{F\phi} + \alpha_t v_x$$

The slopes and breakthrough times of history plots produced by the simulator are controlled by adjusting values of α_ℓ and α_t.

4.1a α_t Variation

The transverse dispersivity, α_t, has the effect of making multilayered media behave, for flow purposes, as a single homogeneous system with averaged flow properties.[16] Figure (4-2) shows history plots of hori-

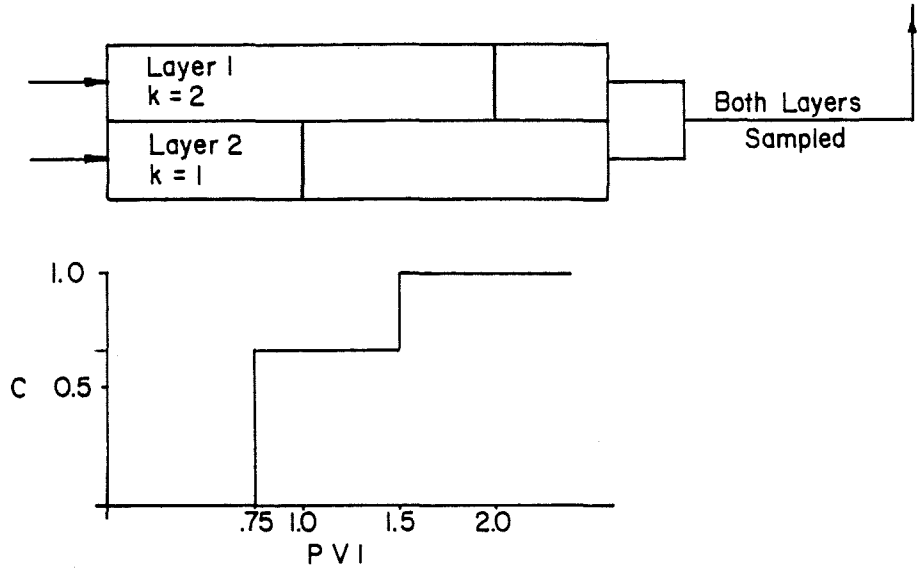

a.) $\alpha_t = 0$

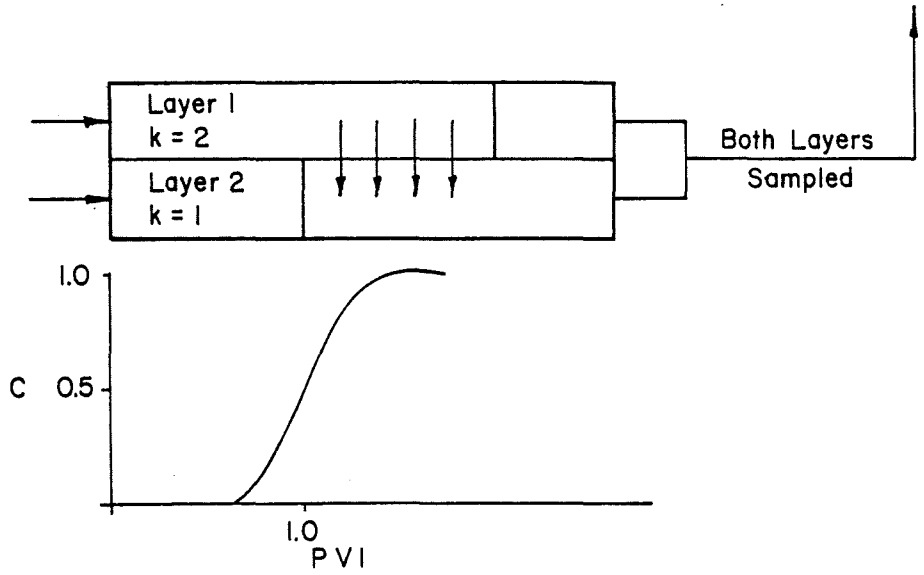

b.) $\alpha_t \gg 0$, Sufficient to cause apparent "one layer" flow

Figure 4-2. Effect of α_t on history curves in two layer system with 2:1 contrasting permeabilities.

zontal flow through a system of two layers in which one layer has a permeability throughout of exactly twice the other. All other properties of the layers are identical. When no transverse dispersion is input ($\alpha_t = 0$), the history plot has two plateaus corresponding to breakthroughs of each layer. At high levels of transverse dispersion, the resultant plot has a distinctly one layer characteristic with some rounding of the slope of the curve. The moving point simulator was run with the two layer system and produced curves exactly as described in the above discussion (figure (4-3)). For a $\alpha_t = 10$ ft through a total system height of 10 ft, one breakthrough point was observed indicating apparent "one-layer" flow.

For history matching our well data, concentrations from only one layer of the interval will be sampled as only one foot of the wellbore is perforated. We should expect to observe history curves having characteristics of one layer systems, whether or not transverse dispersion actually occurs. Our values for transverse dispersivities will be obtained by properly matching the breakthrough ($C = 0.5$) time of the history plots. Three situations can occur assuming D'arcy's Law is valid and no vertical flow:

1. The (k/ϕ) term of the sampling interval is less than the average (k/ϕ) for the entire system.
2. The (k/ϕ) term of the sampling interval is greater than the average (k/ϕ) for the entire system.

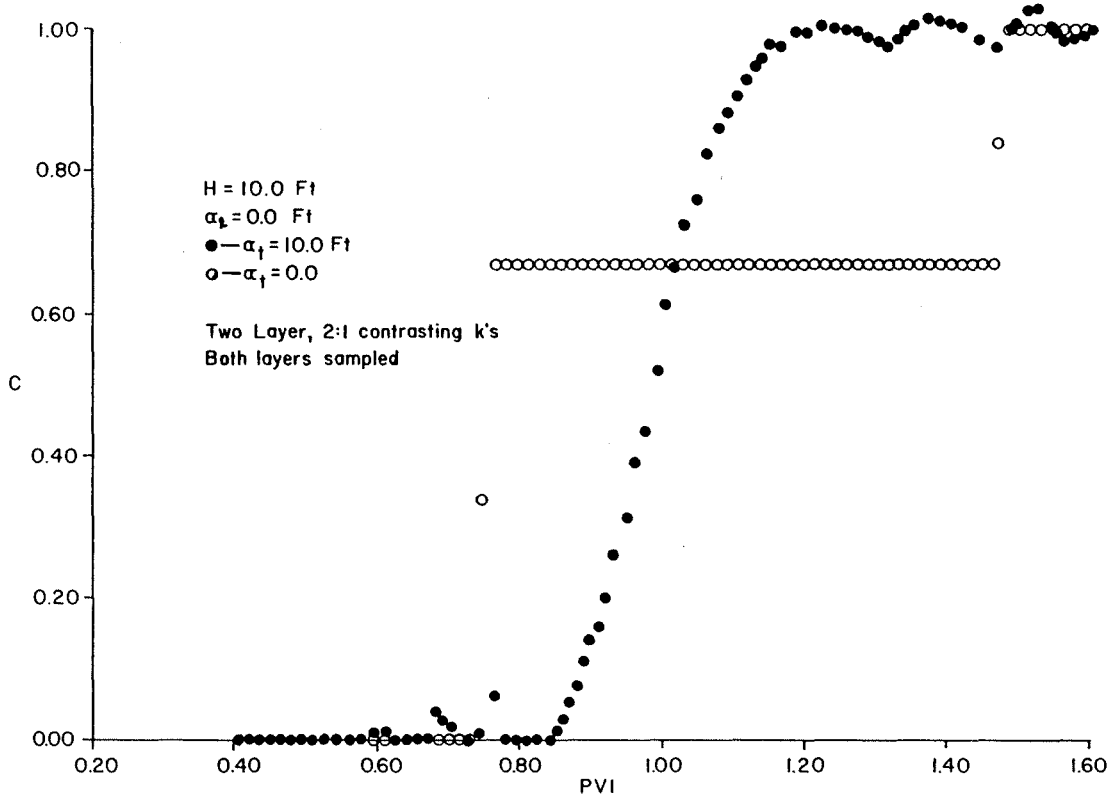

Figure 4-3. Moving point simulation showing effect of α_t on history plot of two layer system with 2:1 contrasting permeabilities.

3. The (k/ϕ) term of the sampling interval is equal to the average (k/ϕ) for the entire system.

To illustrate the three situations, let us again turn our attention to the two layer system with 2 to 1 contrasting permeabilities as described above. When α_t is large enough, the resulting history plot breaks through (C = 0.5) at one pore volume injected when only the slow layer is sampled as shown in figure (4-4). When α_t is set to zero the curve, sampled in the same manner, breaks through at 1.5 pore volume injected. Figure (4-5) shows history plots produced from the moving point simulator for the same α_t variation described above. Increasing the α_t shifts the curve to the left. Values of α_t between zero and those causing "one layer" flow (breakthrough at one pore volume injected) will result in a curve breaking between the two extremes. The α_t can be uniquely determined in such cases solely by matching the C = 0.5 points of the simulated and experimental curves by varying α_t.

The same logic applies to intervals sampled having (k/ϕ) terms greater than the average (figure (4-6)). When no α_t is input for this case, the curve now breaks out at 0.75 pore volumes injected. As α_t is increased, the curves will shift to the right--uniquely determining α_t by matching the C = 0.5 points. The moving point simulator was run with the above system and produced history

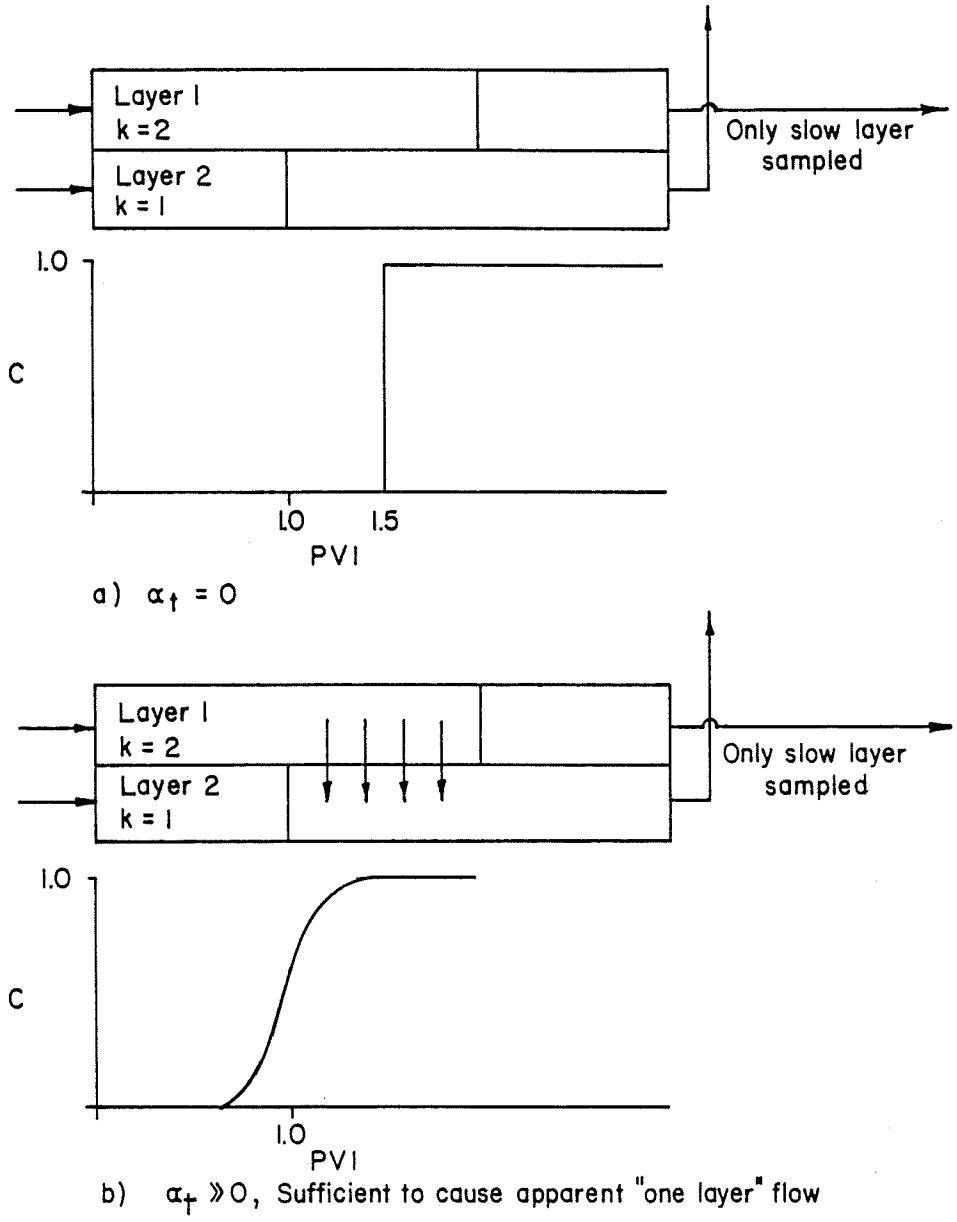

Figure 4-4. Effect of α_t on history curves of a two layer system with 2:1 contrasting permeabilities when only slow layer is sampled.

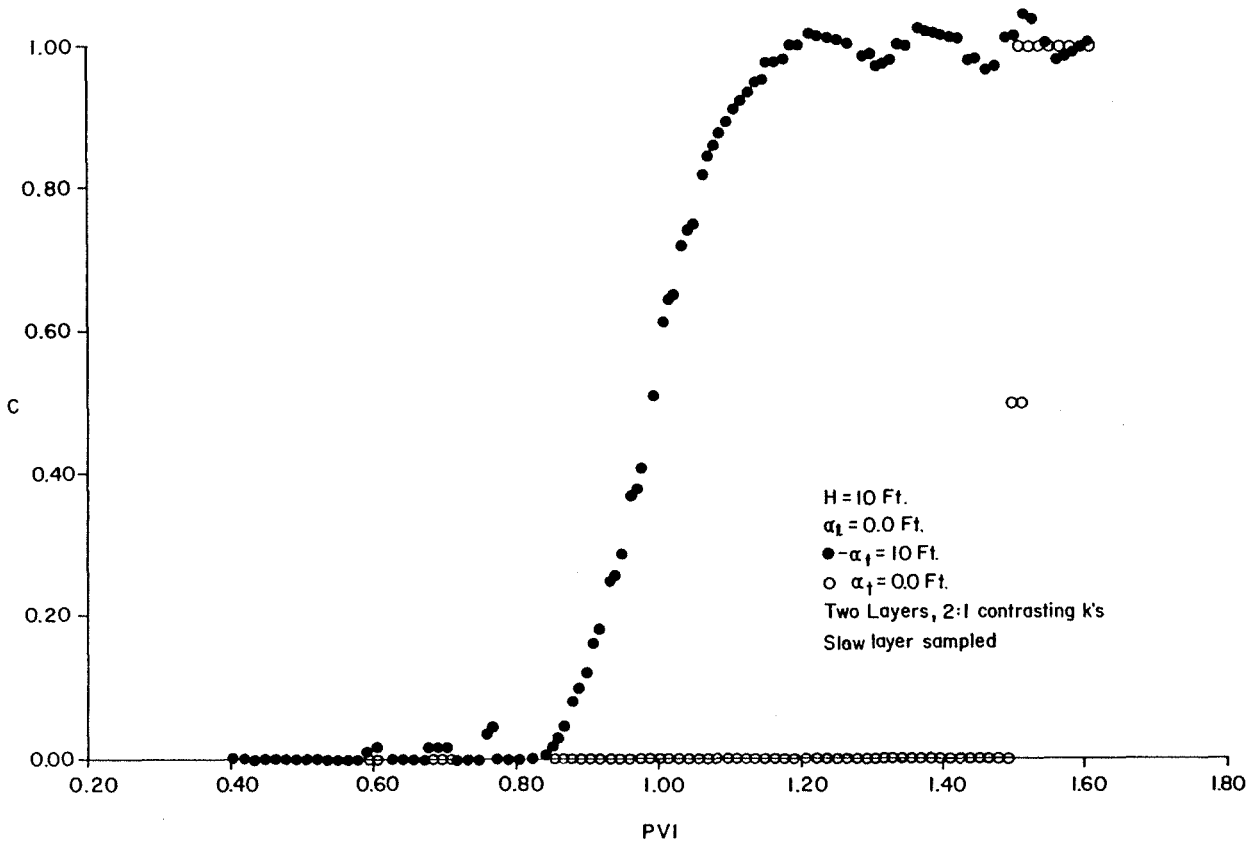

Figure 4-5. Moving point simulation showing effect of α_t on history curves for a two layer system with 2:1 contrasting permeabilities when only slow layer is sampled.

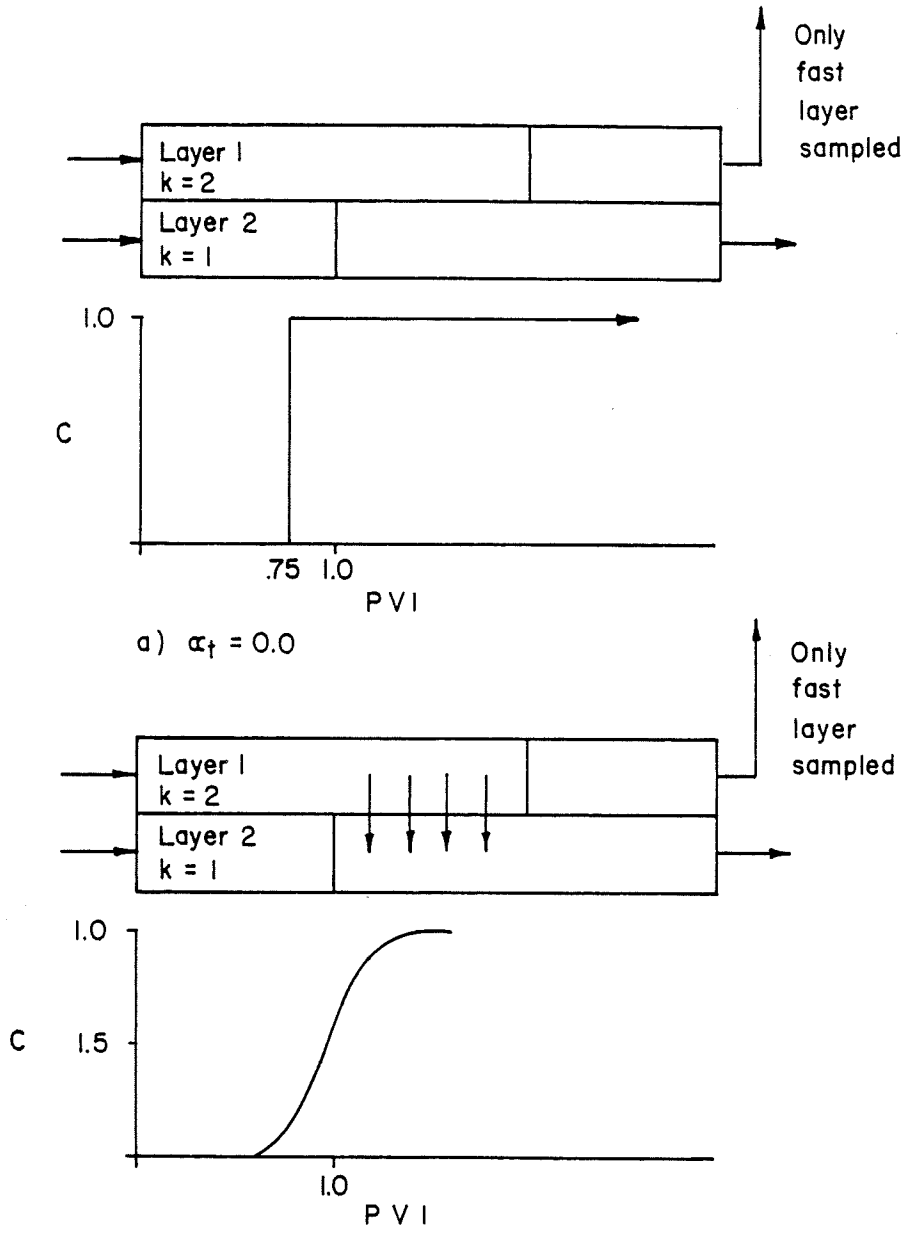

Figure 4-6. Effect of α_t on history curves of a two layer system with 2:1 contrasting permeabilities when only the fast layer is sampled.

curves indicating the same general trend as those in figure (4-6) (figure (4-7)).

When (k/ϕ) for the interval sampled is equal to the average for the system, α_t cannot be determined. Such a case would result in fluid breakthrough at one pore volume injected, no matter the value of α_t input. Of course, higher values of α_t will round the curve, but not in such a way to differentiate between the spreading caused by α_t or by α_ℓ.

4.1b α_ℓ Variation

Varying α_ℓ affects the degree of spreading of history curves. The midpoint (C = 0.5) is not significantly changed by α_ℓ. Figure (4-8) shows how spreading increases when α_ℓ is changed an order of magnitude for a homogeneous system.

4.1c Process of history matching

The preceding discussion lends itself to a generalized technique for history matching field data of miscible displacements sampled from a limited interval.

1. Vary α_t until the midpoint (C = 0.5) of the history plot corresponds to that of observed field data.
2. Vary α_ℓ to change slope as needed to match field data.

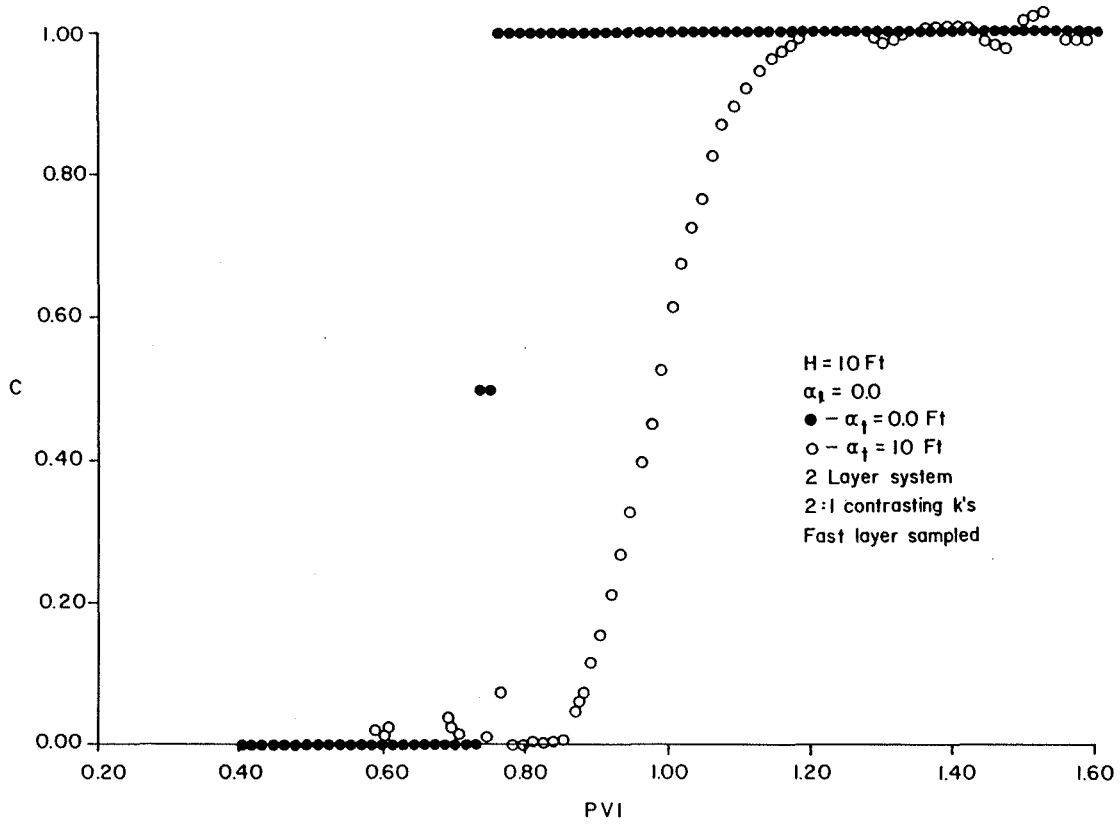

Figure 4-7. Moving point simulation showing effect of α_t on history curves for 2:1 contrasting permeability, two layer system when only the fast layer is sampled.

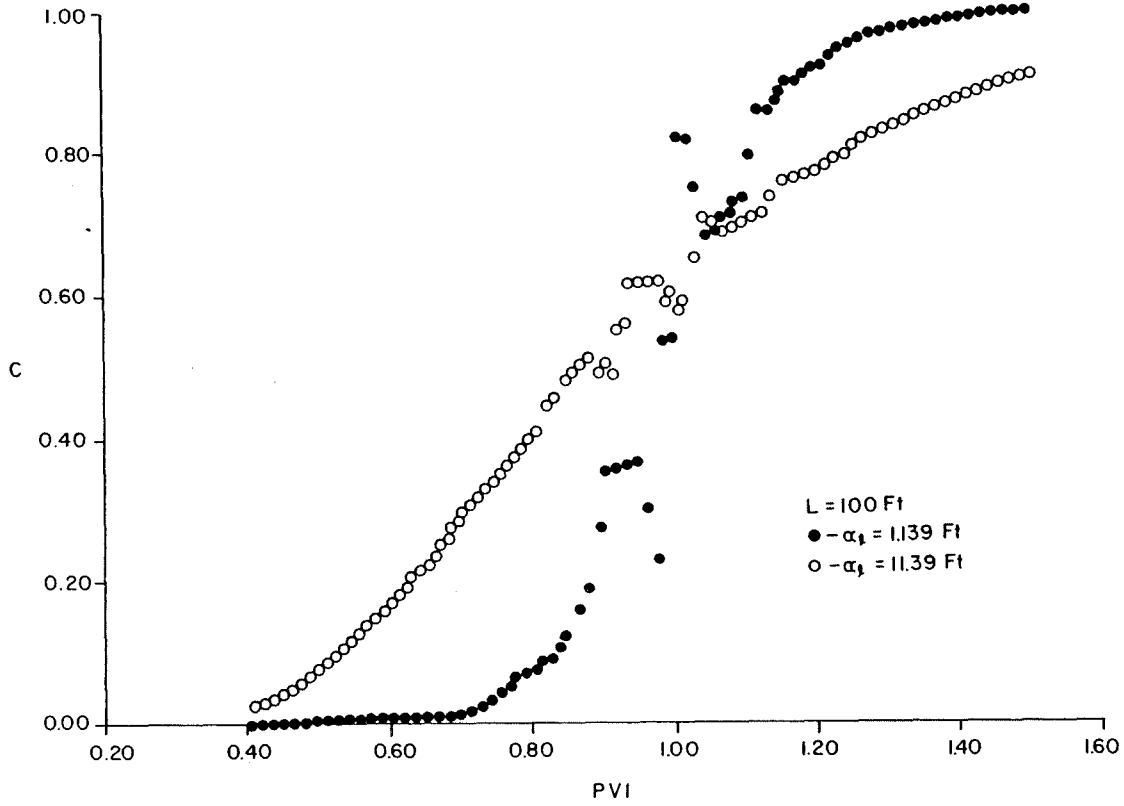

Figure 4-8. Moving point simulation showing effect of α_ℓ variation.

This process has proven to be effective in reducing the number of trial runs needed to completely match field data.

4.2 History Matching MP-131 Field Data

Observation well MP-131 is located 90 feet away from injection well MP-118 in the El Dorado field (figure (4-1)). Samples of fluid have been taken at various times during the injection of fresh water in MP-118 and have been plotted as concentration versus pore volumes injected (figure (4-9)). Significant spreading of the data is apparent, suggesting that physical dispersion is a factor upon fluid flow in the reservoir.

4.2a Core data

Cores have been taken from the pay sections of MP-131, MP-132, and the injector MP-118, and permeabilities and porosities of one foot intervals along their length measured and plotted in figure (4-10) as h versus log (k). None of the cores covered the entire pay section that is indicated from well logs to be approximately from 636 ft to 658 ft.

MP-131 was perforated through a 1-foot interval from 646 ft to 647 ft.[26] The permeability of that section is 614 md as measured from the MP-131 core and 448 md from the MP-118 core. Both permeabilities indicated for the perforated interval are greater than the average per-

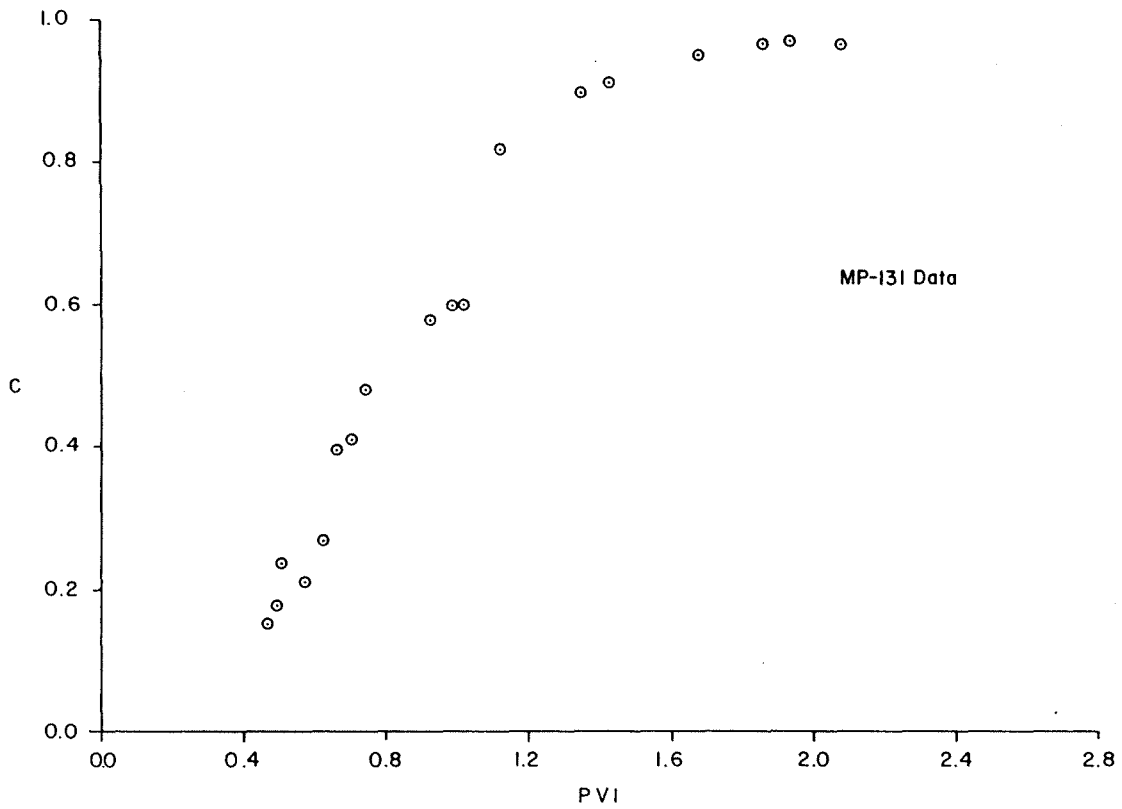

Figure 4-9. Field test data from well MP-131 plotted as C versus pore volume injected.

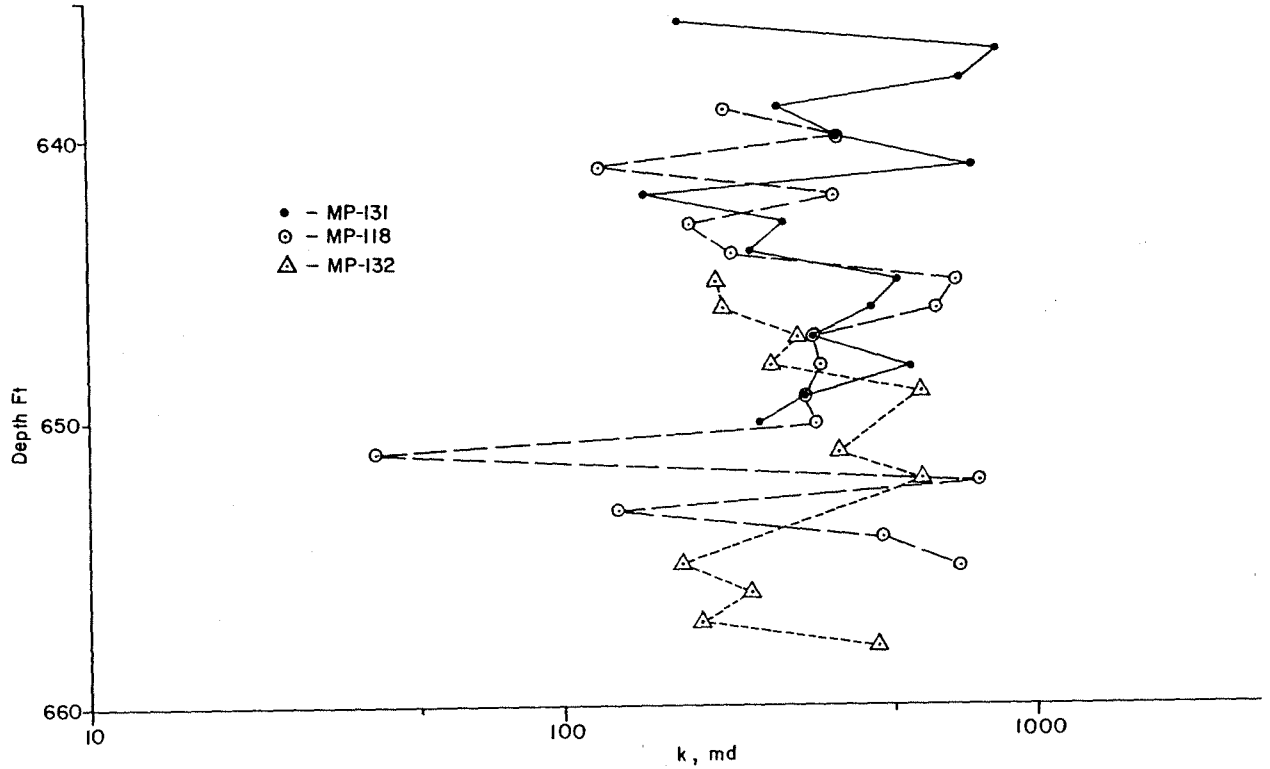

Figure 4-10. h vs log k plots for wells MP-118, MP-131, and MP-132.

meabilities of the entire cores of MP-131 and MP-118 which are 369 md and 419 md, respectively. This fact made α_t determination possible as discussed earlier.

4.2b Fixed grid finite difference model

The fixed grid history match was based on the MP-131 core which consisted of 17, 1-foot thick layers. As shown in Chapter 3, one grid per layer is sufficient in the vertical direction while approximately one grid per foot in the x-direction is required to keep numerical error to a minimum. This results in a 17 by 90 block centered system arranged in the same manner as in figure (2-4), being block centered with respect to both x and y directions. Midpoint weighting of the first derivative term was used. The value of the molecular diffusion coefficient, D_o, was found to be 0.0014 ft^2/day,[28] which is negligible compared to α_ℓ and α_t values needed to match observed field data.

The simulator was run with only the concentrations of the 614 md interval recorded for the history plots. Values of 6.2 ft and 0.031 ft for α_ℓ and α_t, respectively, matched the field data extremely well as shown in figure (4-11).

4.2c Moving point model

As discussed in Chapter 3, one grid block per layer needs to be used in the vertical direction, but only 5 to

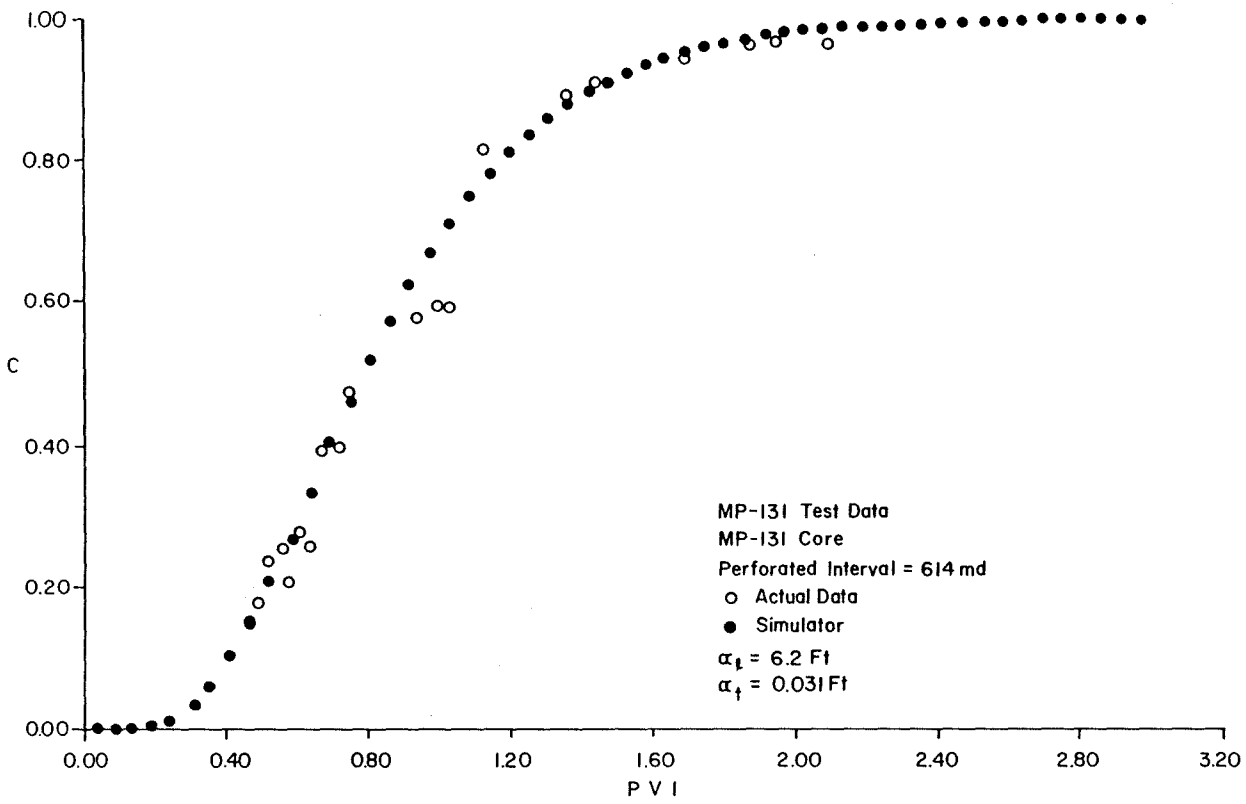

Figure 4-11. History plot of fixed grid simulation matching test data from MP-131.

11 grids are required in the x-direction. To save computing time, 5 grids were chosen for most runs and satisfactory results were obtained without severe oscillation. The 17 by 5 system utilizing the MP-131 core data is node centered in the x-direction and block centered in the y-direction in the same arrangement illustrated shown in figure (2-5).

Sensitivity runs were made changing the permeability of the perforated interval from the 614 md measured in the MP-131 core down to approximately the permeability observed in the injection well at the same depth of 448 md. For k = 614 md, and α_ℓ and α_t of 12 ft and 0.06 ft, respectively, the resulting history plot matched the field data very well (figure (4-12)). When the permeability of the interval was decreased to 550 md, an α_ℓ of 15 ft and an α_t of 0.05 ft resulted in a good match (figure (4-13)). Input values of 15 ft for α_ℓ and 0.04 ft for α_t matched the observed data when k was 500 md for the sampling interval (figure (4-14)) and values of 20 ft for α_ℓ and 0.0 ft for α_t matched the field data when k was reduced to 450 md (figure (4-15)).

4.2d Summary

Table (4-1) summarizes the results for the various moving point and fixed grid simulator runs. In general, as the permeability of the sampling interval was reduced,

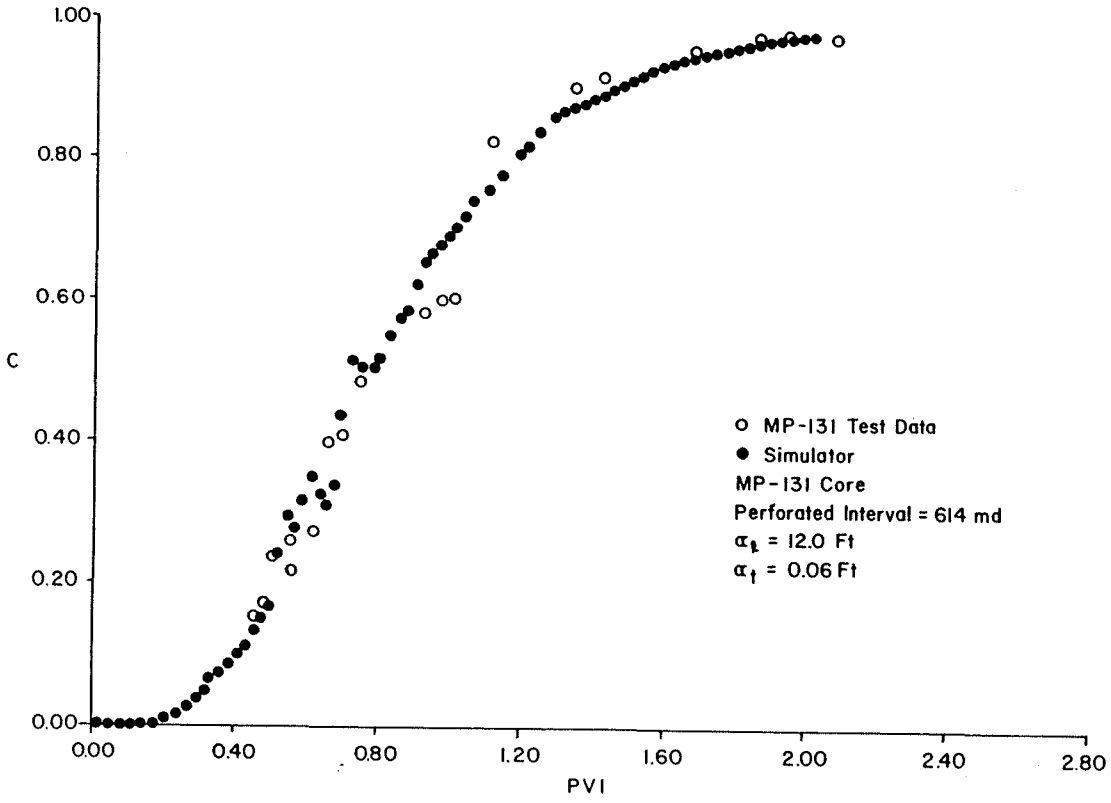

Figure 4-12. History plot of moving point simulator matching test data from MP-131.

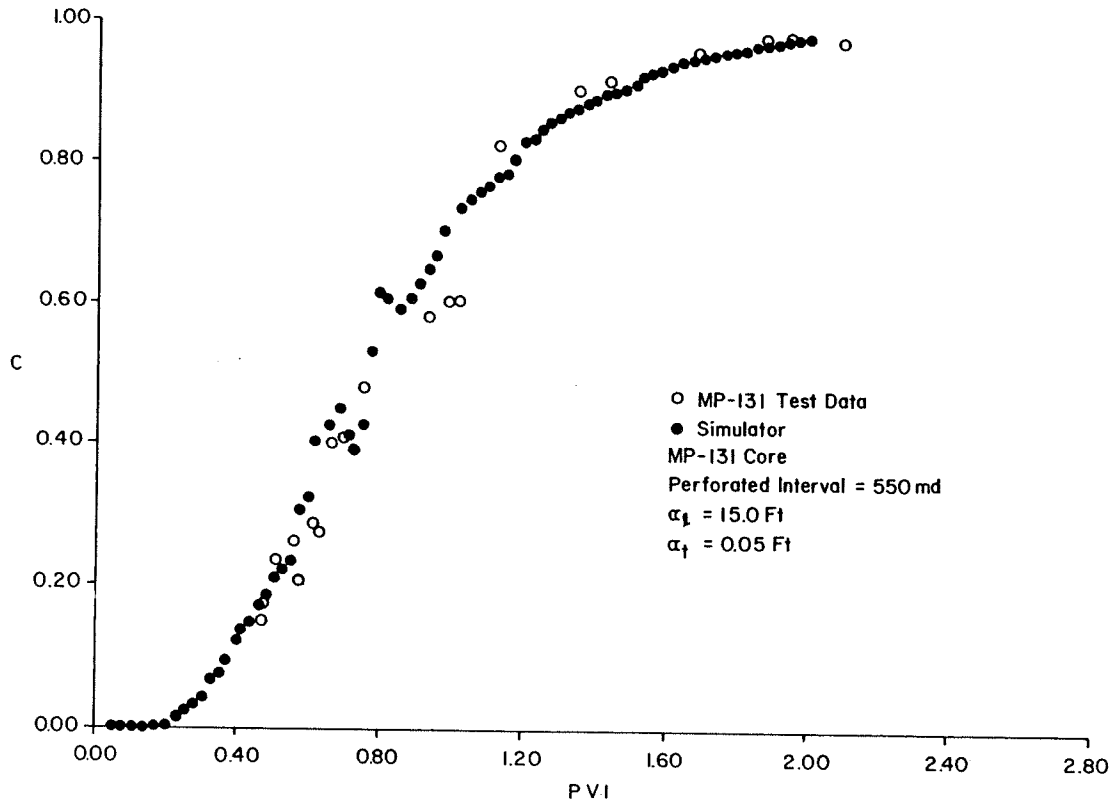

Figure 4-13. Moving point simulation history match of MP-131 test data with perforated interval input as 550 md.

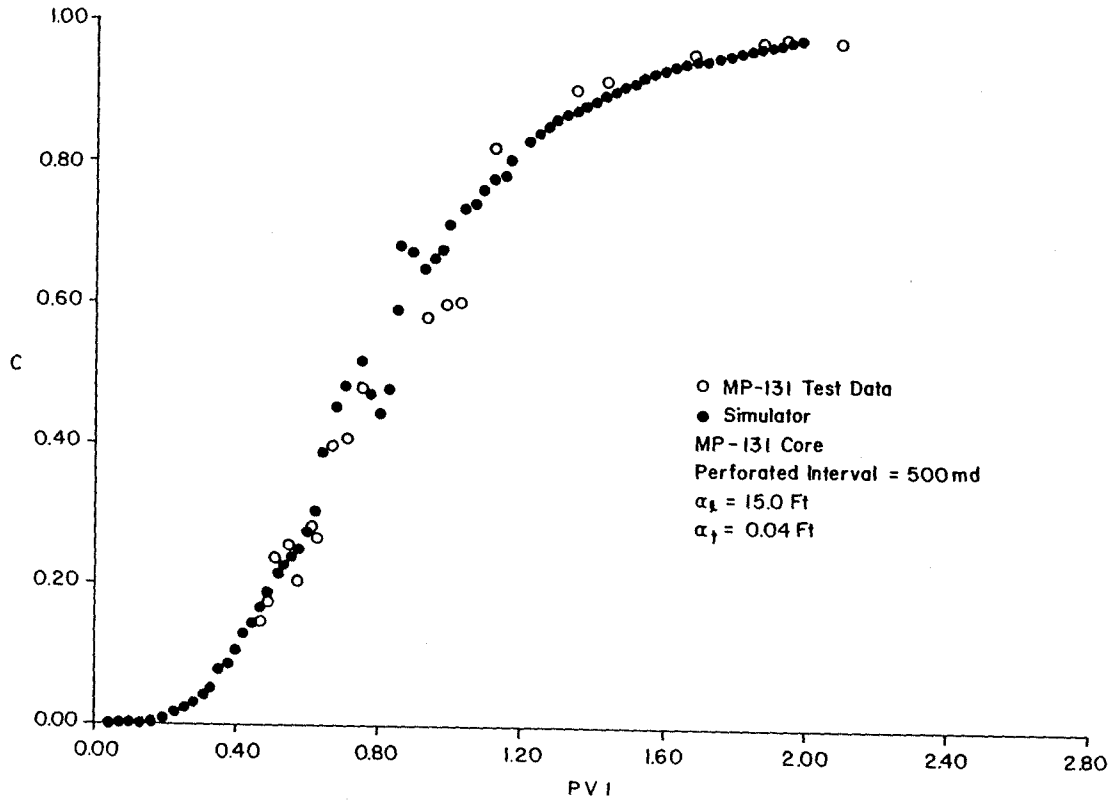

Figure 4-14. Moving point simulation history match of MP-131 test data with perforated interval input as 500 md.

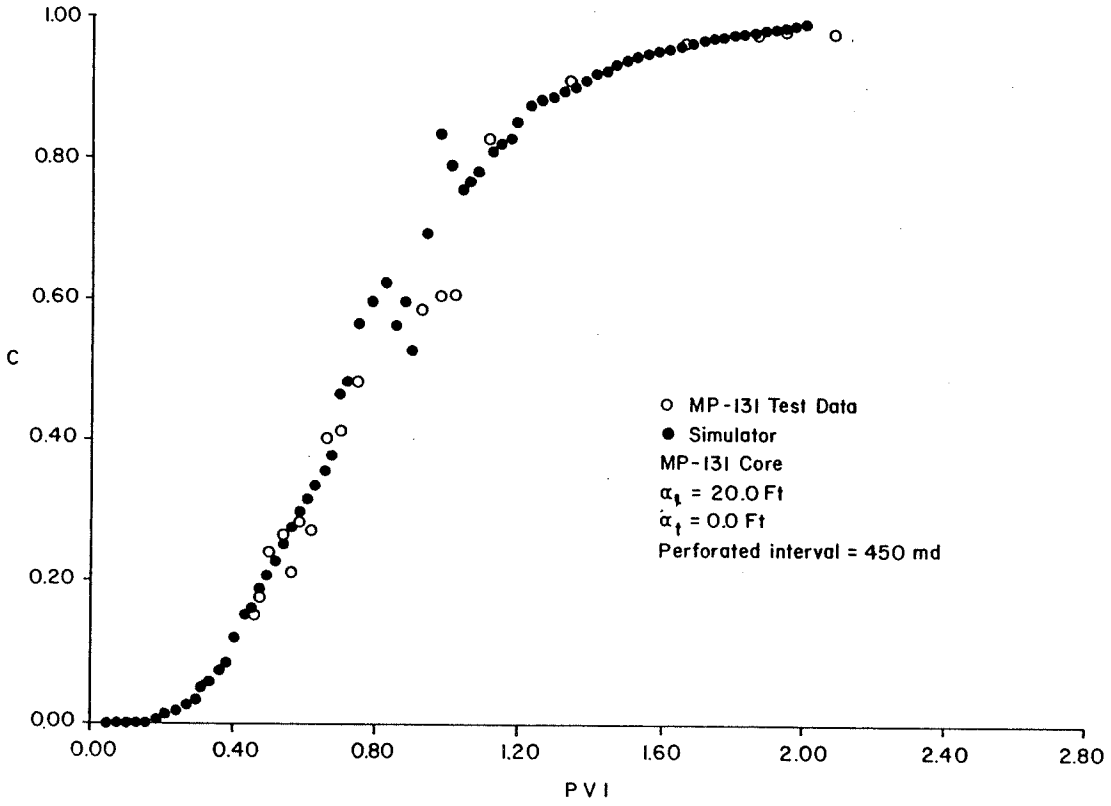

Figure 4-15. Moving point simulation history match of MP-131 test data with perforated interval input as 450 md.

Table 4-1. Values of α_ℓ and α_t matching observed field data from MP-131 by simulation of MP-131 core data with various permeabilities input for the perforated interval.

Simulation	$k_{(\text{perforated interval})}$ (md)	α_ℓ (ft)	α_t (ft)
Moving Point	614	12.0	0.06
	550	15.0	0.05
	500	15.0	0.04
	450	20.0	0.0
Fixed Grid	614	6.2	0.031

α_ℓ increased and α_t decreased to match the observed field data.

This is to be expected because all permeabilities input for the sampling interval were greater than the average for the entire section. As discussed previously in this chapter, increasing α_t when the permeability of the sampled interval is greater than the average shifts the history curve to the right. However, decreasing the permeability input for the sampling interval also shifts the curve to the right, everything else held constant. Therefore, as the permeability input is decreased for a layer, but still remains greater than the average for the entire section, the α_t must decrease to keep the breakthrough of the history plot at the same point of pore volumes injected. The decrease in α_t reduces the spreading of the curve somewhat and this must be offset by an increase in α_ℓ.

The fixed grid simulator was run with the perforated interval input as 614 md and matched the field data with an α_ℓ of 6 ft and an α_t of 0.031 ft. The values of both α_ℓ and α_t are roughly $\frac{1}{2}$ of that matching the field data with the moving point simulator. The major reason for the difference in the two simulators is the greater numerical error introduced by the fixed grid finite difference techniques. Although the fixed grid simulator was instructive and produced results requiring

little computation time, the moving point simulator has a higher degree of accuracy and its results are more conclusive.

4.3 History Matching MP-131 Field Data With MP-118 Core

The moving point simulator was run with the core data from well MP-118. The grid system was 15 x 5 since only 15 feet of core was measured. The perforated interval of 646 ft in MP-131 corresponds to a permeability of 448 md at the same depth in MP-118. This was changed to 614 md and α_ℓ and α_t were input as 12 ft and 0.06 ft, respectively, the same values matching field data with MP-131 core data. Figure (4-16) illustrates the resulting history plot. The curve has much the same characteristics as the similar run with MP-131 data, but it is slightly displaced to the right. This is due to the higher average permeability of the MP-118 core data as compared to the MP-131 data.

4.4 History Matching MP-132 Field Data

Observation well MP-132 is located 187 feet away from the injector well MP-118 (figure (4-1)). Fluid samples were taken during the same injection test as described for MP-131. A plot of concentration versus pore volume injected is shown in figure (4-17). It is apparent that the testing was not continued long enough for con-

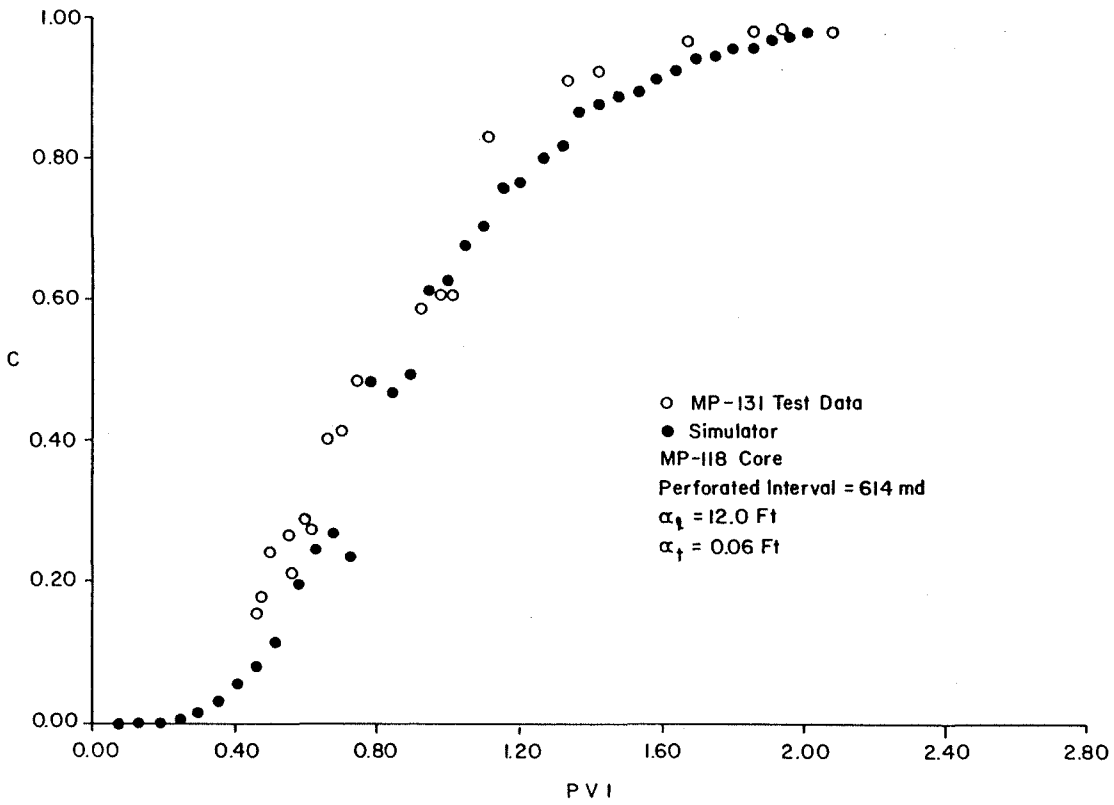

Figure 4-16. Moving point simulation of core data from MP-118 with perforated interval input as 614 md.

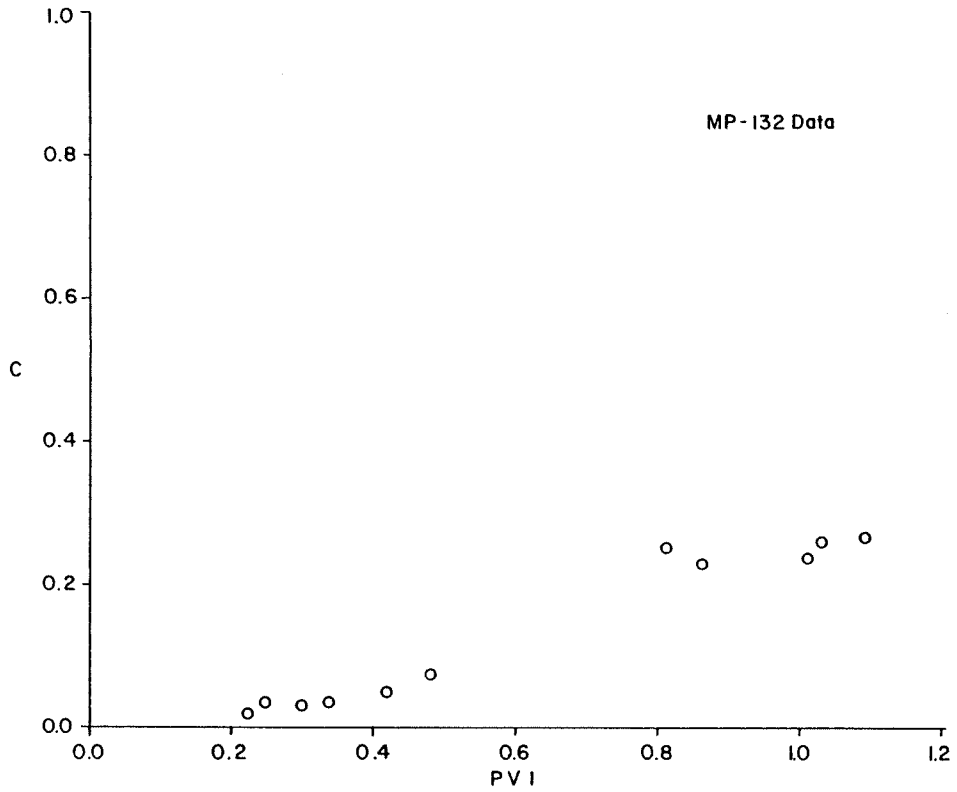

Figure 4-17. Field test data from MP-132 plotted as C versus pore volume injected.

centrations to reach values high enough for adequate and α_t determination.

Core data was taken through the pay section from 645 to 658 feet and is shown in figure (4-10) plotted as h versus log k. The permeability of the perforated interval at 647 feet was measured to be 319 md.

The moving point model was run for a 12 x 5 grid system using the core data from MP-132. The perforated interval was sampled and values for α_ℓ and α_t were input as 12 ft and 0.06 ft, respectively. As can be seen in figure (4-18), it appears this does not even closely match the data, being much sharper (steeper slope) at the breakthrough. However, the lack of data at high concentrations prevents any conclusions to be drawn as to the actual dispersivity values.

4.5 Comparison of the Lake and Hirasaki and the Fried Combarnous Methods for Calculating α_{EFF} for Multilayered Media

As discussed in Chapter 1, two approaches were studied for calculation of equivalent one dimensional dispersion coefficients of multilayered heterogeneous systems in the asymptotic regime. The L&H method was discussed in Chapter 1, and Appendix B details the F&C procedure which takes the form:

$$\alpha_{EFF} = \sum_{j=1}^{M} \left[\frac{\alpha_\ell \; v_{x_m} \; \phi_m}{\bar{v}_x \; \bar{\phi} \; H} h_m + \frac{\phi_m^2}{\alpha_t \; \bar{k} \; k_m \; H} \left(\frac{k_m}{\phi_m} - \frac{\bar{k}}{\bar{\phi}} \right)^2 \frac{1}{3} h_m^3 \right] \quad (4\text{-}2)$$

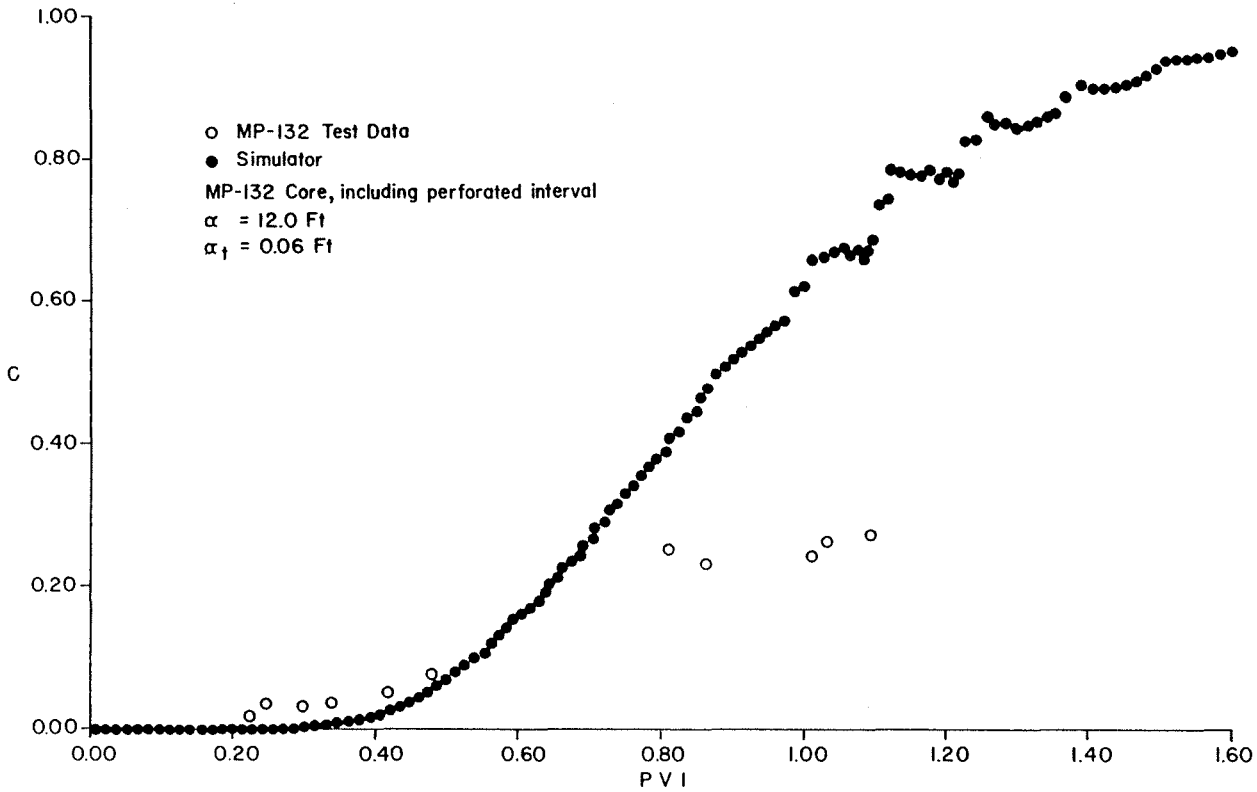

Figure 4-18. Moving point simulation history plot with MP-132 core with α_ℓ = 12 ft and α_t = 0.06 ft.

A program, TDISP, has been written by L. W. Lake[24] for computing the L&H coefficient for multilayered systems and was modified to also calculate the F&C effective dispersivity by equation (4-2).

Two simple systems of four layers were devised to check the relative accuracy of the two methods with the resulting history plots from the moving point simulator (figure (4-19)). In one system, the layers were arranged in a 4411 permeability sequence and in the other system the layers were arranged in a 4141 permeability ordering. By that we mean two permeabilities--different by a factor of 4--were used. All other properties of the layers were constant. The 4411 system was constructed with two identical high permeability layers above two identical low permeability layers (different by a factor of 4). The 4141 system had alternate layers of high permeability and low permeability.

4.5a 4141 system ordering results

The 4141 system was composed of four, 1 foot thick layers and an α_ℓ and α_t of 0.5 ft and 0.0167, respectively, were input for a system length of 1500 ft. The α_{EFF} calculated by the L&H and F&C methods were identical and given as 11.73 ft. The moving point simulator was run with the input data and permeability ordering given above and the resulting history plot is shown in figure (4-20).

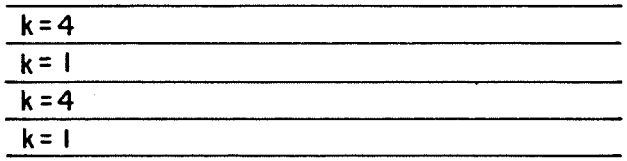

a) 4141 System

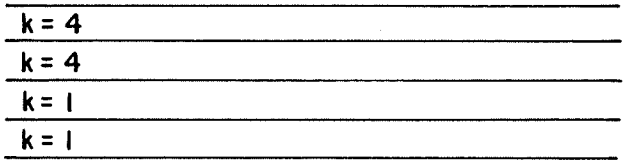

b) 4411 System

Figure 4-19. Systems used to compare L&H and F&C methods for determining α_{EFF}'s.

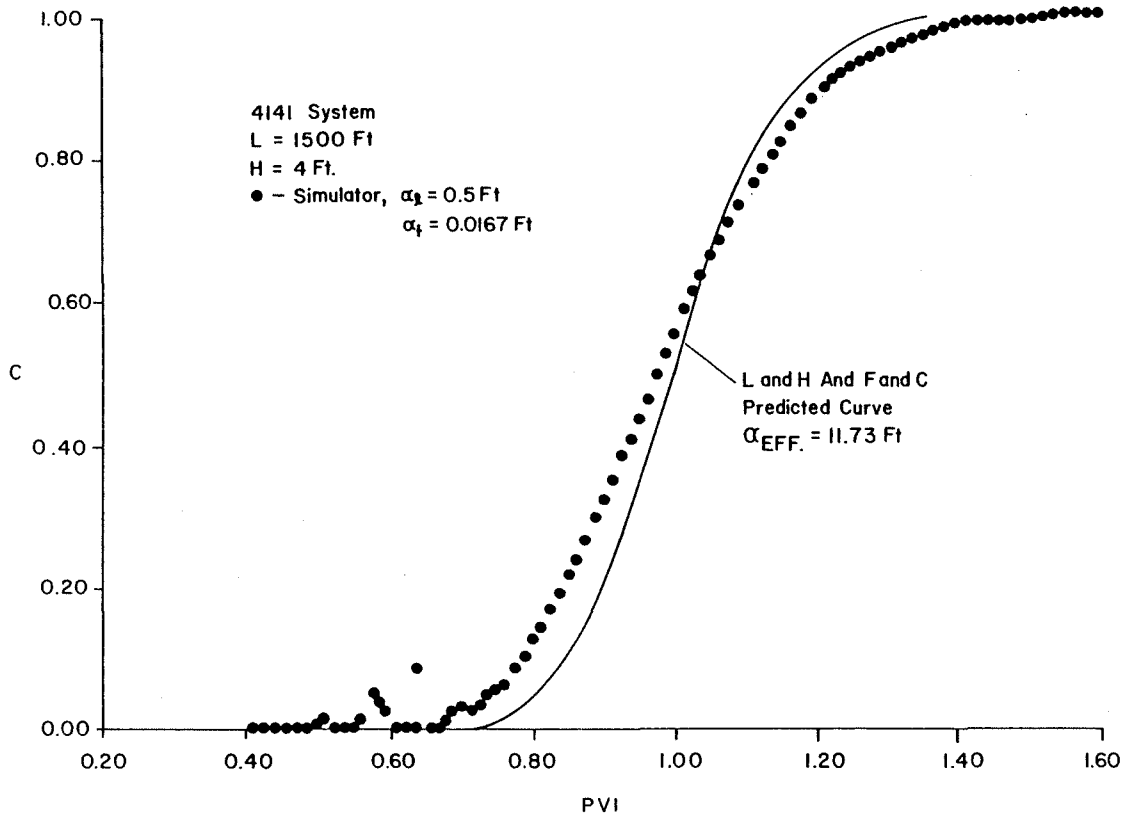

Figure 4-20. Comparison of L&H and F&C calculated α_{EFF}'s to corresponding heterogeneous moving point simulation for the 4141 system.

Also included in figure (4-20) is the history plot of the equivalent homogeneous system with averaged properties and an α_{EFF} of 11.73 ft as indicated by both methods. The simulator run exhibited more dispersion than calculated analytically by both methods and was estimated to be $\alpha_{EFF} \cong 21.6$ ft by the graphical method given by Perkins and Johnson.(3)

4.5b 4411 system ordering results

The same data was again input as for the previous system except the ordering of the layers was changed to 4411. The L&H procedure computed an α_{EFF} of 45.4 ft while the F&C method calculated α_{EFF} to again be 11.73 ft. The simulator run is shown in figure (4-21) and produced a history plot with an effective longitudinal dispersivity of approximately 59 ft.

4.5c Actual core data results

In addition to the two proposed system described above, actual data from a well core in the Gas Draw Field located in Wyoming was tested. An analysis of a height versus log (k) plot (figure (4-22)) of the 20 foot pay zone shows that the reservoir contains a high perm streak in the middle, bounded above and below by layers of low permeability. For a system length of 10,000 ft and a α_ℓ and α_t of 12 ft and 0.5 ft, respectively, the F&C coefficient was 16.7 ft, while the L&H coefficient was signi-

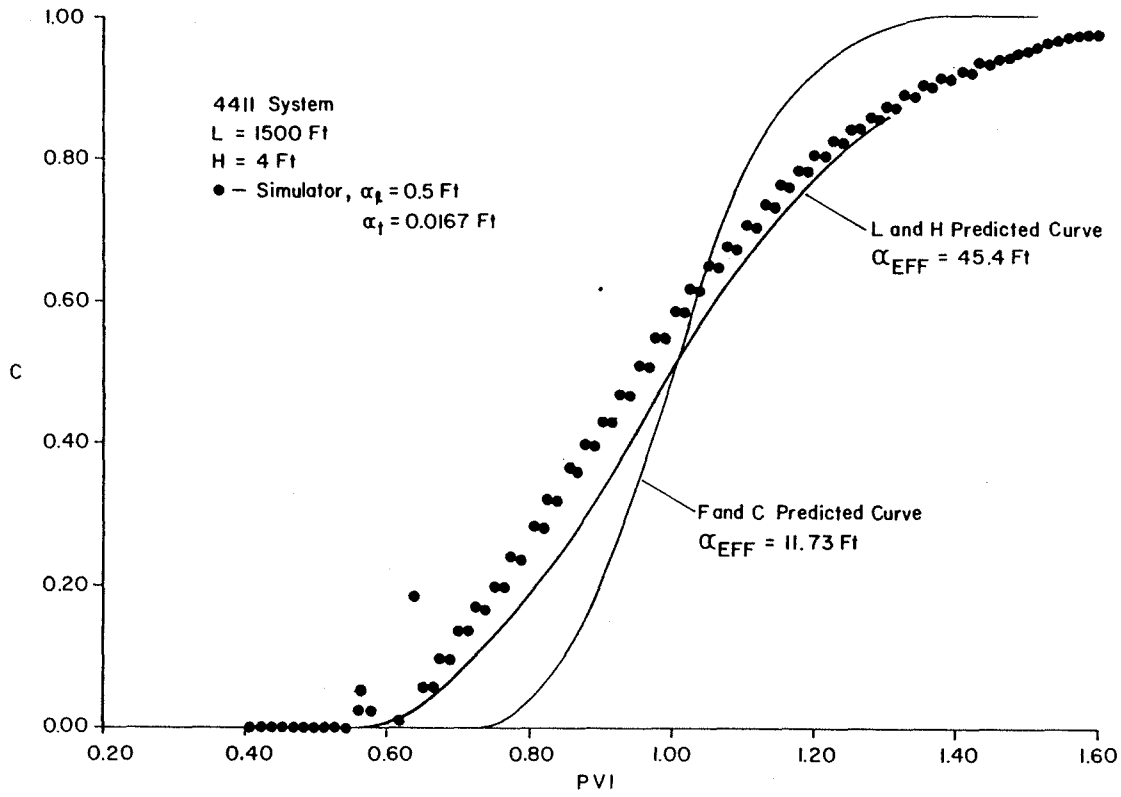

Figure 4-21. Comparison of L&H and F&C calculated α_{EFF}'s to corresponding heterogeneous moving point simulation for the 4411 system.

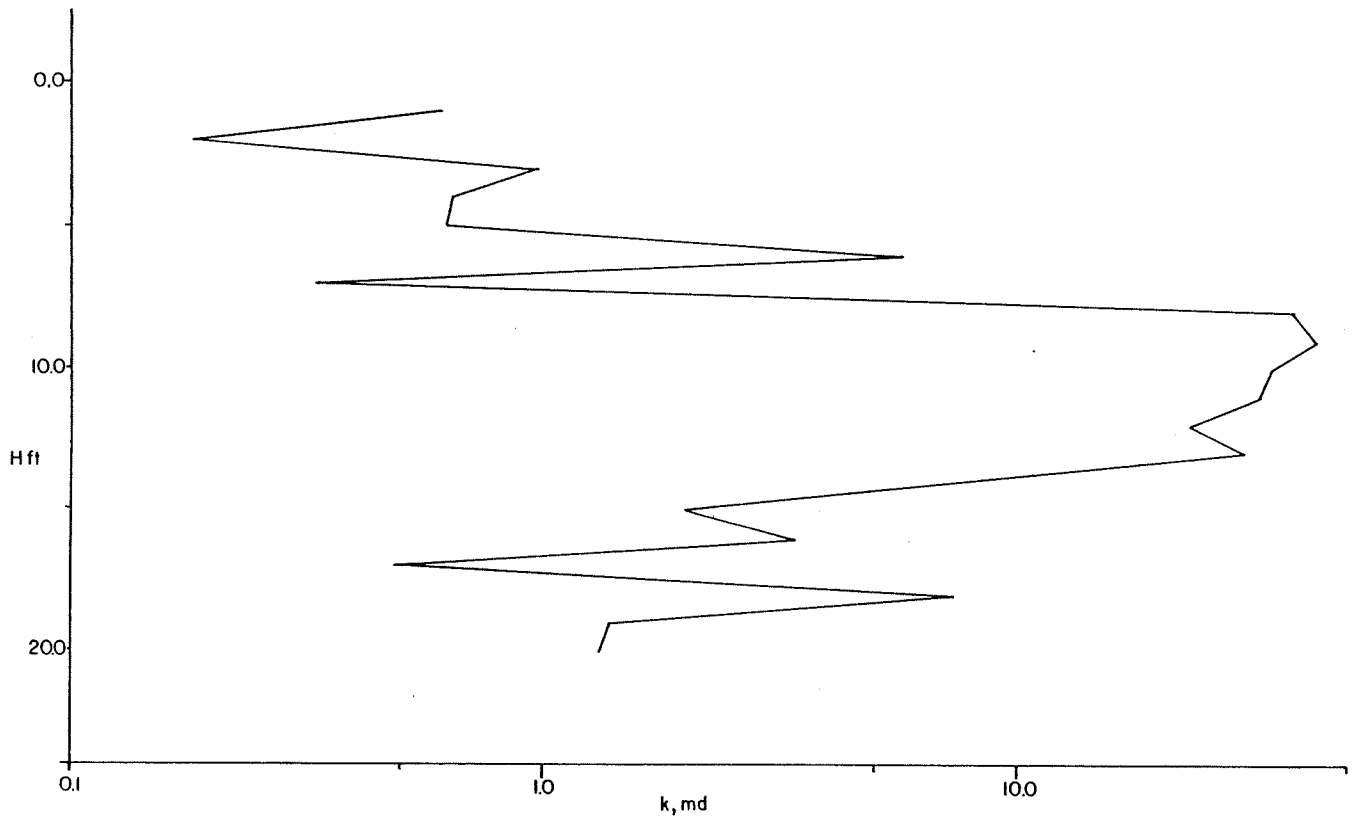

Figure 4-22. Plot of h vs log k of core data from the Gas Draw field.

ficantly greater at 260 ft. The moving point simulator was run with the heterogeneous core and input data given above. The history plot (figure (4-23)) displayed "one layer" characteristics with one smooth curve and the α_{EFF} of the plot was calculated to be 550 ft.

4.5d Summary

Table (4-2) summarizes the results from the various runs described above. As is evident from inspection of equation (4-2), the F&C method does not consider the spatial ordering of the various layers. However, simulator runs of heterogeneous multilayered systems exhibited a pronounced change as shown by the increase in α_{EFF} from 21.6 ft to 59 ft as the permeability ordering changed from 4141 to 4411, respectively, in the systems described in 4.5a and 4.5b. When actual core data was tested, even larger discrepancies between the two methods resulted. The F&C calculated α_{EFF} of the core data from the Gas Draw Field was approximately a factor of 1/34 less than the α_{EFF} produced by moving point simulation, while the L&H method computed an α_{EFF} of $\frac{1}{2}$ less than actual.

In general, the L&H method estimated simulator produced α_{EFF}'s far better than the F&C method, the F&C method being more accurate for small permeability

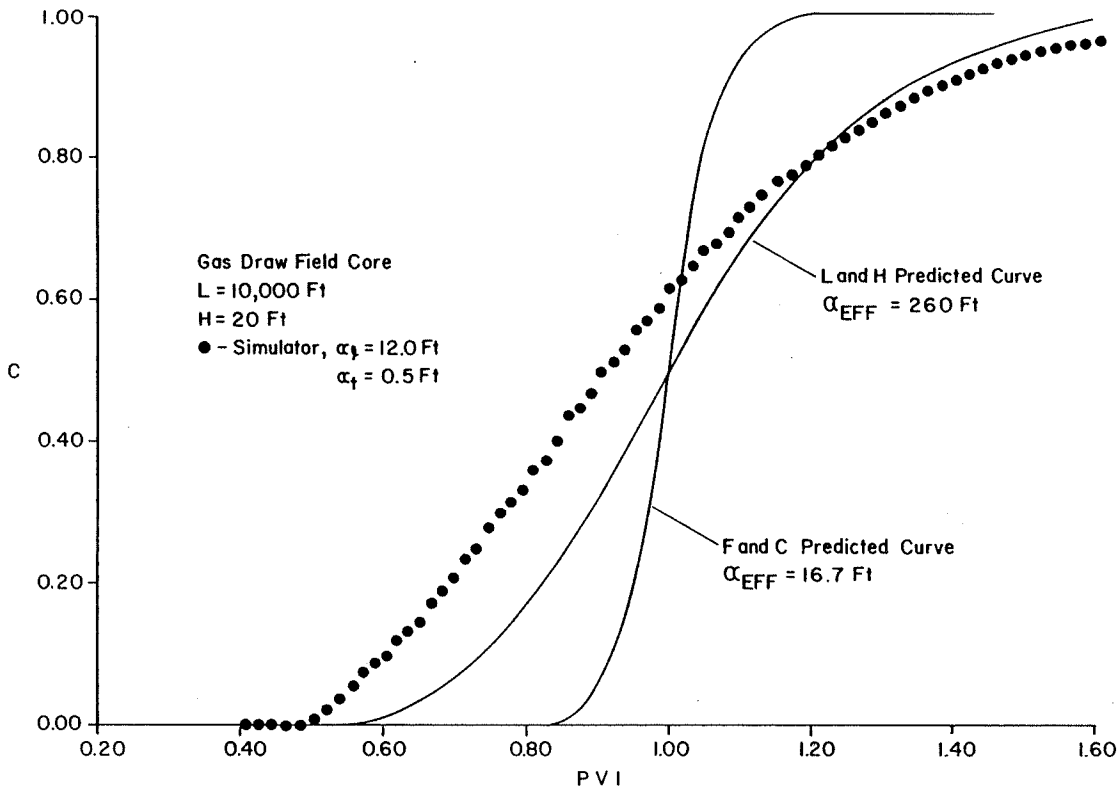

Figure 4-23. History plot comparison of L&H and F&C α_{EFF}'s to corresponding heterogeneous moving point simulation of core data from the Gas Draw field.

Table 4-2. Comparison of L&H and F&C

Calculated α_{EFF} with Corresponding Simulator Runs

	α_{EFF} (ft)		
System	F&C	L&H	Simulator
4141	11.73	11.73	21.6
4411	11.73	45.4	59
Gas Draw Field Well Core	16.7	260	550

variations. The major reason the L&H method is superior is because it takes into account the spatial sequence of heterogeneous layers.

4.6 Ideal Sampling Procedure

From the results of this study, generalizations can be made as to the ideal sampling scheme for α_ℓ and α_t determination occurring within a reservoir. These are summarized below:

1. The observation well should be positioned directly between the injector and producer wells. This arrangement insures that sampled flow streamlines are linear through the modeled system, allowing accurate determination of flow length paths.
2. The observation well should be perforated only through a limited, small interval compared to the entire thickness of the pay zone. The observer should disrupt the streamlines as little as possible allowing accurate computation of α_ℓ and α_t. Perforating the entire pay zone would, in effect, make the observer a production well if fluid is sampled at rates equal to flow through the reservoir. This would distort streamlines significantly introducing an apparent dispersion which can not be separated from actual dispersion through history matching techniques.

3. As a continuation of the above discussion, fluid should be sampled from the perforated interval as close as possible to the actual flow rate through the zone in the field. This prevents flow from adjacent layers which would increase apparent dispersion.
4. The reservoir should be vertically heterogeneous, with k varying significantly with height, but horizontal layers should be consistent with respect to k from injector to observer. The observer should be perforated through an interval where the (k/ϕ) term is significantly greater than the average through the entire system height. A range of α_t values can then be determined as discussed earlier in this paper. α_t can also be determined if the perforated interval has a (k/ϕ) term less than the average. However, this is not preferred[24] as transverse flow will cause fluid to enter from layers above and below, probably increasing the apparent transition zone more than the due just to α_t and α_ℓ.

4.7 Effect of Fluid Withdrawal Rates from Limited Perforated Intervals

A study was peformed to determine if the rate of fluid withdrawal from limited perforated zones would

significantly affect effluent history data. A homogeneous model was used, dimensioned as the MP-131 well test system, 90 ft long and 17 ft thick. Seventeen grid nodes were used in the y-direction and 10 in the x-direction, with effluent sampling of the eighth layer from the top, corresponding to the height of the MP-131 perforated interval. The same dispersivities were used as those matching the MP-131 test data with the 614 md perforated interval, 12 ft for α_ℓ and 0.06 ft for α_t. Since vertical flow is introduced when withdrawal rates differ from flow rates given by equation (2-11), which assumes flow according to D'arcy's Law and injection into individual layers according to their (kh) product compared to the (kh) sum over all the layers, permeabilities in the y-direction, k_y, need to be specified and were input as 1/10 (0.1) of the horizontal permeability, k_x.

A run was first made with the fraction produced through the perforated interval, f_p, equal to that given by equation (2-11), introducing no vertical flow in the system. Since the model is homogeneous and consists of seventeen layers of equal height, f_p equals 1/17. The resulting moving point simulator history plot is shown in figure (4-24). Another run was then performed whereby the model is identical to the one described above, except f_p was increased to 0.5, causing vertical flow near the perforated interval. This history plot is also shown on

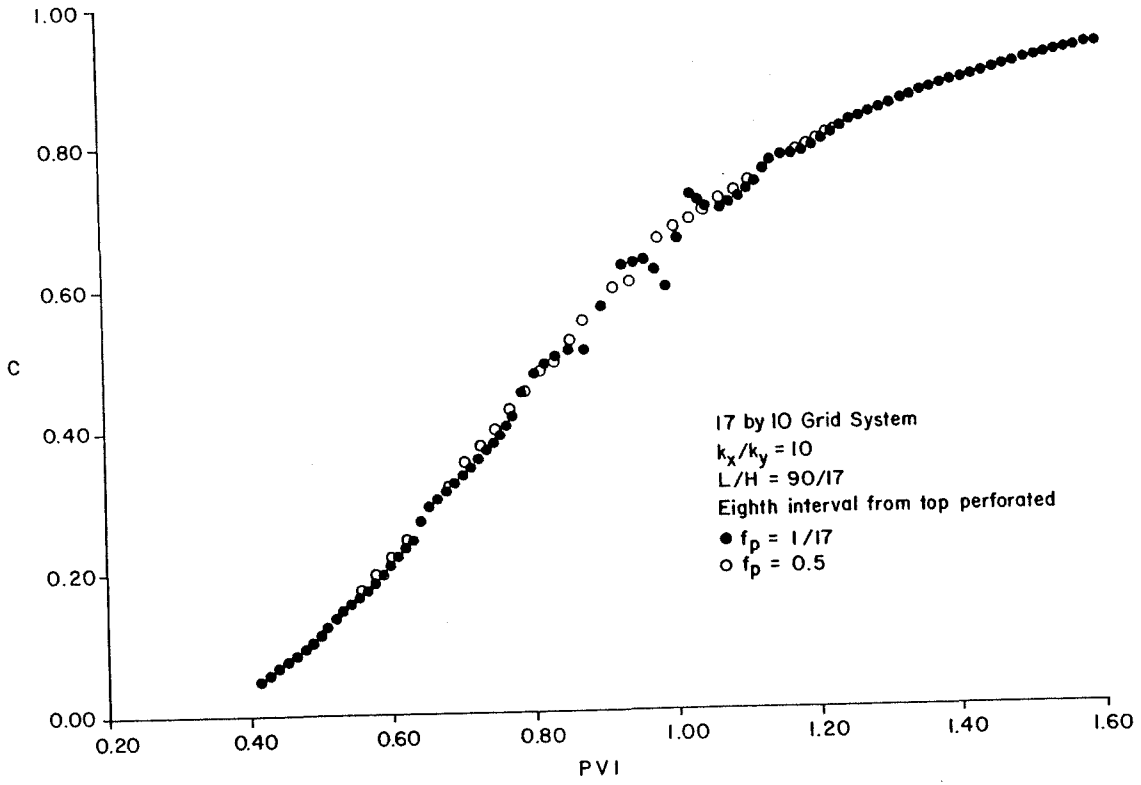

Figure 4-24. Effect of f_p from limited perforated interval on history plots.

figure (4-19) and there is no noticeable difference between the $f_p = 1/17$ and $f_p = 0.5$ plots, with regard to slope or arrival times.

Since the case of producing ½ of the fluid flow rate through an interval only 1/17 as thick as the entire homogeneous pay zone is greater than would probably occur under observation well sampling if at least some attention is paid to injection rates in the field, we can conclude that withdrawal rates will not affect homogeneous system history data. This should be true for systems having L/H (total length/total height) ratios as least as large as the MP-131 system L/H of over 5. As the L/H ratio for the system decreases, vertical flow rates increase for the same f_p, and distortion of history data can be expected to occur at lower variations of f_p from that creating no vertical flow.

As discussed previously, heterogeneous systems, under certain conditions, will behave as homogeneous systems for flow purposes. Accordingly, we should expect that withdrawal rates should not affect history data for heterogeneous systems of L/H greater than 5, provided such systems can be replaced by equivalent, one-dimensional, homogeneous models.

CHAPTER 5. CONCLUSIONS

As a result of this study, the following conclusions can be drawn:

1. The moving point method as described by Garder, Peaceman et al.,[25] effectively represents all levels of two dimensionsal physical dispersion without introducing significant numerical error.
2. The L&H method of computing effective one-dimensionsal dispersion coefficients of multi-layered, heterogeneous systems in the asymptotic regime, although indicating somewhat less spreading than exhibited by corresponding heterogeneous simulator runs, proved to be much more accurate than the F&C method. The major cause of error in the F&C computation is neglection of the often times significant effect of the relative spatial configuration of the various heterogeneous layers.
3. Unique determination of α_t and α_ℓ values can be made through history matching experimental data, provided the sampling interval has a (k/ϕ) term different than the average for the entire system of layers. When the (k/ϕ) term for the sampling

interval cannot be determined precisely, at best only a range of α_ℓ and α_t values can be determined.

4. Moving point simulation with the core data from well MP-131 from the El Dorado field history matched experimental test data sampled from the same well with values input for α_ℓ ranging from 12 ft to 20 ft and α_t values ranging from 0.0 ft to 0.06 ft. These ratios of α_ℓ to α_t are over an order of magnitude greater than those found by laboratory measurements of approximately 30.(3) This can be attributed to inhomogeneities occurring within the reservoir, such as shale streaks, reducing the transverse components of dispersion relative to the longitudinal components.
5. The "ideal" situation for sampling fluid for determination of field wide dispersivities would be:
   a. Observation well positioned directly between injector and producer wells.
   b. Observation well perforated through a small interval compared to entire "pay" zone.
   c. Fluid sampling rate as close as possible to actual flow rate through the zone in the field.
   d. Perforated interval is in zone of significantly greater (k/ϕ) than the average for the entire pay section and the (k/ϕ) for the zone is

uniform throughout system from the injector to the observer well.

6. Reasonable fluid withdrawal rates from limited perforated intervals, within an order of magnitude of rates causing no vertical flow within the system, should not distort the history data of homogeneous systems of L/H greater than 5. We can expect the same for heterogeneous systems that can be modeled, for flow purposes, by equivalent homogeneous systems.

CHAPTER 6. RECOMMENDATIONS FOR FUTURE WORK

To better understand field scale dispersion, it is recommended that:

1. More field test dispersion data should be obtained from various reservoirs so that possible generalizations can be made as to the effects of system size and reservoir heterogeneities on observed dispersivities.
2. Because of the long computing times experienced by the moving point simulator, the computer coding should be scrutinized to make sure computations are performed in the most efficient manner.
3. More comparisons should be performed between history plots of the L&H grouped systems and the corresponding original heterogeneous systems to determine if any refinements of the L&H method are warranted.
4. The moving point simulator could be adapted to model reservoir heterogeneities other than only as a series of layers. The effects of different heterogeneous models on history plots could be studied in detail.

5. Off-diagonal dispersion terms were neglected in our analysis. Detailed studies could be performed to determine under what conditions their ommission will cause unacceptable distortion of history plots.
6. Further investigations should be made of the effects of fluid withdrawal rates from limited perforated intervals on vertical flow within the reservoir and on the subsequent effluent histories.
7. This work should be extended to include pattern displacements.

TABLE OF NOMENCLATURE

a	Capillary tube radius, L
A	Cross sectional area, L^2
C	Concentration of dispersing component in fluid, M/L^3
C_s	Concentration of dispersing component in rock, M/L^3
$\overline{C}$	Flow rate averaged concentration of dispersing component in fluid, M/L^3
CI	Injected fluid concentration of dispersing component, M/L^3
d_p	Particle diameter, L
D_o	Molecular diffusion coefficient, L^2/t
erf	Error function, $\text{erf}(x) = \frac{2}{\sqrt{\pi}} \int_o^x e^{-t^2}\, dt$
f_I	Fraction of total volumetric flow rate injected into the perforated interval
f_P	Fraction of total volumetric flow rate produced out of perforated interval
F	Formation electrical resistivity factor, dimensionless
h	Reservoir layer height, L
H	Total system height, L
k	Permeability, L^2
$\overline{k}$	Thickness weighted average permeability, L^2

K	Dispersion coefficient, L^2/t
$\overline{K}$	Thickness weighted average dispersion coefficient, L^2/t
K_{EFF}	Effective Longitudinal Dispersion Coefficient, L^2/t
L	System length, L
M	Total number of reservoir layers
N	Mass flux, $M/L^2.t$
N_x	Number of grid blocks in x-direction
N_y	Number of grid blocks in y-direction
$N_{G/L}$	Number of grid blocks per reservoir layer
N_{PE}	Peclet number, dimensionless
N_{TD}	Transverse dispersion number, dimensionless
P	Pressure F/L^2
PIB	Bottom layer of injection perforated interval
PIT	Top layer of injection perforated interval
PPB	Bottom layer of production perforated interval
PPT	Top layer of production perforated interval
PVI	Pore volumes of injected fluid, dimensionless
q	Volumetric flowrate into finite difference grid block, L^3/t
Q	Total volumetric flowrate injected into all layers, L^3/t
r	Kinetic reaction rate of dispersing component in fluid, $M/L^3.t$

r_s	Kinetic reaction rate of dispersing component on rock surface, $M/L^3.t$
R	Total reaction rate, $M/L^3.t$
t	Time, t
T	Fluid transmissibility, $(L^3/t)(lb_f/L^2)$ $T = kA/\mu$
u	Superficial fluid velocity, L/t
v	Interstitial fluid velocity, L/t
v_{max}	Maximum velocity in capillary tube, L/t
$\lvert \vec{v} \rvert$	Magnitude of interstitial fluid velocity, L/t
$\overline{v}$	Height weighted average interstitial velocity, L/t
w	System width, L
W	Accumulation term, M/L^3
WF	Finite difference first spatial derivative weighting factor, dimensionless
x	Position with regard to the horizontal direction, L
y	Position with regard to the vertical direction, L

GREEK SYMBOLS

α	Dispersivity, L
α_{EFF}	Effective longitudinal dispersivity, L
β	Aris' constant, dimensionless
Δ	Small increment
∇	Gradient operator, 1/L
λ	$\frac{PVI - 1}{\sqrt{PVI}}$

Φ	$\int_{y_m}^{Y} \phi_m(v_{x_m} - \bar{v}_x)\, dy$
ϕ	Porosity, fraction
$\bar{\phi}$	Thickness weighted average porosity
ρ	Fluid density, M/L^3
ρ_s	Rock density, M/L^3
σ	Measure of inhomogeneity in porous media, dimensionless
μ	Fluid viscosity, M/Lt

SUPERSCRIPTS

n	Time step index
—	Thickness weighted average (except for C where it is flow rate averaged)
η	Aris' moment number

SUBSCRIPTS

A	Component A
i	Grid block index in x-direction
I	Injected
j	Grid block index in y-direction
ℓ	Longitudinal direction
m	Reservoir layer index
p	Referring to moving point
P	Produced
s	Pertaining to rock
t	Transverse direction

x	Horizontal direction
y	Vertical direction
xx, xy, yx, yy	Indices on dispersion coefficients indicating relative position in tensor
1	Pertaining to fast layer with respect to v, in a two layer system
2	Pertaining to slow layer with respect to v, in a two layer system

APPENDICES

APPENDIX A--Derivation of the Finite Difference Form of the Pressure Equation

The pressure equation for flow through porous media assuming D'arcy's Law is valid and no gravity effects are present, takes the form in two dimensions:

$$T_x \frac{\partial^2 P}{\partial x^2} + T_y \frac{\partial^2 P}{\partial y^2} - Q = 0 \qquad \text{(A-1)}$$

where

$P \equiv$ pressure

$T_x \equiv$ x-direction fluid transmissibility

$T_y \equiv$ y-direction fluid transmissibility

$Q \equiv$ source or sink term

The second derivative terms are best approximated in finite difference form[24] as:

$$\frac{\partial^2 P}{\partial x^2} \cong \frac{P_{i+1,j} - 2P_{i,j} + P_{i-1,j}}{(\Delta x)^2} \qquad \text{(A-2)}$$

$$\frac{\partial^2 P}{\partial y^2} \cong \frac{P_{i,j+1} - 2P_{i,j} - P_{i,j-1}}{(\Delta y)^2} \qquad \text{(A-3)}$$

Equation (A-1), written in finite difference form becomes:

$$T_{x_{i+1/2,j}} P_{i+1,j} + T_{y_{i,j+1/2}} P_{i,j+1} - (T_{x_{i+1/2,j}} + T_{y_{i,j+1/2}} + T_{x_{i-1/2,j}} + T_{y_{i,j-1/2}}) P_{i,j} + T_{x_{i-1/2,j}} P_{i-1,j} + T_{y_{i,j-1/2}} P_{i,j-1} - q_{i,j} = 0 \qquad \text{(A-4)}$$

where

$q_{i,j} \equiv$ source or sink volumetric flow rate in grid (i,j)

The transmissibility at the ½ grid spacing are the geometric average of the two adjacent grid block transmissibilities.

For example,

$$T_{x_{i+1/2,j}} = 2.0 \frac{T_{x_{i+1,j}} \cdot T_{x_{i,j}}}{T_{x_{i+1,j}} + T_{x_{i,j}}}$$

Boundary Conditions

Reflective (no-flow) boundary conditions are used for the system, which is the same system as for the moving point method (figure (2-5)), at all four boundaries. Injection and production of fluid at $i = 1$ and $i = N_x$, respectively, are accomplished through the use of the source and sink terms, $q_{i,j}$.

At $j = 1/2$

$$\left(\frac{\partial P}{\partial y}\right)_{i,1/2} \cong \frac{P_{i,1} - P_{i,0}}{\Delta y} = 0 \qquad \text{(A-5)}$$

$$P_{i,1} = P_{i,0} \qquad \text{(A-6)}$$

At $j = N_y + 1/2$

$$\left(\frac{\partial P}{\partial y}\right)_{i,N_y+1/2} \cong \frac{P_{i,N_y+1} - P_{i,N_y}}{\Delta y} = 0 \qquad \text{(A-7)}$$

$$P_{i,N_y+1} = P_{i,N_y} \qquad \text{(A-8)}$$

The nodes are face centered in the x-direction. No flow conditions are accomplished in the following manner:

At $i = 1$

$$\left(\frac{\partial P}{\partial x}\right)_{1,j} \cong \frac{P_{2,j} - P_{0,j}}{\Delta x} = 0 \qquad \text{(A-9)}$$

$$P_{2,j} = P_{0,j} \qquad \text{(A-10)}$$

At $i = N_x$

$$\left(\frac{\partial P}{\partial x}\right)_{N_x,j} \cong \frac{P_{N_x+1,j} - P_{N_x-1,j}}{\Delta x} = 0 \qquad \text{(A-11)}$$

$$P_{N_x+1,j} = P_{N_x-1,j} \qquad \text{(A-12)}$$

APPENDIX B--Derivation of F&C approach to a multilayered, heterogeneous system

As discussed in Chapter 1, F&C derived a method for determining an equivalent one dimensional dispersion coefficient for a multilayered system at the asymptotic regime (long time):

$$K_{EFF} = \frac{1}{\phi H} \int_o^H K_\ell \phi dy + \int_o^H \frac{\Phi^2}{K_t \phi} dy \qquad (B\text{-}1)$$

Assume a system of M layers with K_ℓ, K_t, k, h, and ϕ constant throughout each layer.

K_t integral

$$\int_o^H \frac{\Phi^2}{K_t \phi} dy = \int_{y1}^{y2} \frac{\Phi^2}{K_t \phi} dy + \int_{y2}^{y3} \frac{\Phi^2}{K_t \phi} dy + \ldots \int_{yM}^{yM+1} \frac{\Phi^2}{K_t \phi} dy \qquad (B\text{-}2)$$

where subscripts (1, 2, 3, . . . etc.) denote y position of the top of each respective layer.

For each layer,

$$\begin{aligned} \Phi_m &= \int_{y_m}^{y} \phi_m (v_{x_m} - \bar{v}_x) dy \\ &= \phi_m (v_{x_m} - \bar{v}_x) \int_{y_m}^{y} dy \\ &= \phi_m (v_{x_m} - \bar{v}_x) (y - y_m) \end{aligned} \qquad (B\text{-}4)$$

Substituting,

$$\int_{y_m}^{y_{m+1}} \frac{\Phi^2}{K_t \phi} dy = \int_{y_m}^{y_{m+1}} \frac{\phi_m^2 (v_{x_m} - \bar{v}_x)^2 (y - y_m)^2}{K_{t_m} \phi_m} dy$$

$$= \frac{\phi_m^2 (v_{x_m} - \bar{v}_x)^2}{K_{t_m} \phi_m} \frac{1}{3} (y_{m+1} - y_m)^3 \qquad (B\text{-}5)$$

Given the following,[24] (assuming D'arcy's Law is valid)

$$v_{x_m} = \frac{k_m}{\bar{k}} \frac{\bar{\phi}}{\phi_m} \bar{v}_x \tag{B-6}$$

and

$$K_{t_m} \cong \alpha_t \, v_{x_m} \tag{B-7}$$

$$\int_{y_m}^{y_{m+1}} \frac{\phi_m^2}{K_{t_m} \phi_m} \, dy = \frac{\phi_m^2 \left(\frac{k_m}{\bar{k}} \frac{\bar{\phi}}{\phi_m} \bar{v}_x - \bar{v}_x \right)^2}{\alpha_t \, v_{x_m} \, \phi_m} \frac{1}{3} (y_{m+1} - y_m)^3$$

$$= \frac{\phi_m^2 \, \bar{v}_x \, \bar{\phi}}{\alpha_t \, \bar{k} \, k_m} \left(\frac{k_m}{\phi_m} - \frac{\bar{k}}{\bar{\phi}} \right)^2 \frac{1}{3} (y_{m+1} - y_m)^3 \tag{B-8}$$

<u>K_ℓ integral</u>

Again handling each layer separately,

$$\int_{y_m}^{y_{m+1}} K_{\ell_m} \, \phi_m \, dy = \alpha_\ell \, v_{x_m} \, \phi_m \, (y_{m+1} - y_m) \tag{B-9}$$

Therefore for one layer of the system we have:

$$\alpha_{EFF} = \frac{1}{\bar{v}_x \, \bar{\phi} \, H} \left[\alpha_\ell \, v_{x_m} \, \phi_m \, (y_{m+1} - y_m) + \right.$$

$$\left. \frac{\phi_m^2 \, \bar{v}_x \, \bar{\phi}}{\alpha_t \, \bar{k} \, k_m} \left(\frac{k_m}{\phi_m} - \frac{\bar{k}}{\bar{\phi}} \right)^2 \frac{1}{3} (y_{m+1} - y_m)^3 \right]$$

$$= \frac{\alpha_\ell \, v_{x_m} \, \phi_m}{\bar{v}_x \, \bar{\phi} \, H} (y_{m+1} - y_m) + \frac{\phi_m^2}{\alpha_t \, \bar{k} \, k_m \, H} \left(\frac{k_m}{\phi_m} - \frac{\bar{k}}{\bar{\phi}} \right)^2$$

$$\cdot \frac{1}{3} (y_{m+1} - y_m)^3 \tag{B-10}$$

Extending to M layers, we have

$$\alpha_{EFF} = \sum_{m=1}^{M} \left[\frac{\alpha_\ell \; v_{x_m} \; \phi_m}{\bar{v}_x \; \bar{\phi} \; H} h_m + \frac{\phi_m^2}{\alpha_t \; \bar{k} \; k_m \; H} \left(\frac{k_m}{\phi_m} - \frac{\bar{k}}{\bar{\phi}} \right)^2 \cdot \frac{1}{3} h_m^3 \right] \qquad \text{(B-12)}$$

where

$$h_m = Y_{m+1} - Y_m$$

APPENDIX C

Fortran Listing of the Moving Point Simulator

```
      PROGRAM RDR57(INPUT,OUTPUT,TAPE6=OUTPUT,PLOTR)
C*************************************
C
C       TWO DIMENSIONAL MOVING POINT SIMULATOR
C
C        DATA SHOULD BE INPUT AS FOLLOWS:
C
C*********FIRST LINE
C
C      M,N,DELT,CT,VIS,PI,PVC
C
C WHERE:
C
C     M         NUMBER OF GRID BLOCKS IN Y-DIRECTION
C
C     N         NUMBER OF GRID BLOCKS IN X-DIRECTION
C
C     DELT      TIME STEP, DAYS
C
C     CT        TOTAL COMPRESSIBILITY, 1/PSI
C
C     VIS       FLUID VISCOSITY, CENTIPOISE
C
C     PI        INITIAL PRESSURE OF RESERVOIR, PSI
C
C     PVC       TOTAL NUMBER OF PORE VOLUMES INJECTED
C               UNTIL PROGRAM FLAGGED TO STOP
C
C*********SECOND LINE
C
C      IIT,IIB,PIT,PIB,FRACQP,FRACQI
C
C WHERE:
C
C     IIT       TOP GRID LAYER OF INJECTION PERFORATED
C                INTERVAL
C
C     IIT       TOP GRID BLOCK OF INJECTION PERFORATED
C                INTERVAL
C
C     IIB       BOTTOM GRID BLOCK OF INJECTION PERFORATED
C                INTERVAL
C
C     PIT       TOP GRID BLOCK OF PRODUCTION PERFORATED
C                INTERVAL
C
C     PIB       BOTTOM GRID BLOCK OF PRODUCTION PERFORATED
C                INTERVAL
C
C     FRACQP    FRACTION OF TOTAL FLOW RATE PRODUCED THROUGH
C                PERFORATED INTERVAL
C
C     FRACQI    FRACTION OF TOTAL FLOW RATE INJECTED THROUGH
C                PERFORATED INTERVAL
C
C*********THIRD LINE
C
C      AQ,L,DELH,NP,NPXS,NPYD
C
C WHERE:
C
```

```
C     AQ      TOTAL FLOW RATE, BARRELS PER DAY
C
C     L       TOTAL SYSTEM LENGTH, FEET
C
C     DELH    TOTAL SYSTEM HEIGHT, FEET
C
C     NP      TOTAL NUMBER OF MOVING POINTS
C
C     NPXD    NUMBER OF POINTS PER GRID IN X-DIRECTION
C
C     NPYD    NUMBER OF POINTS PER GRID IN Y-DIRECTION
C
C
C*********FOURTH LINE
C
C      W,DO,CM,ATEFF,ALEFF,CI
C
C WHERE:
C
C     W       SYSTEM WIDTH, FEET
C
C     DO      MOLECULAR DIFFUSION COEFFICIENT, SQUARE FEET/DAY
C
C     CM      FORMATION CEMENTATION FACTOR
C
C     ATEFF   TRANSVERSE DISPERSIVITY, FEET
C
C     ALEFF   LONGITUDINAL DISPERSIVITY, FEET
C
C     CI      INJECTED FLUID CONCENTRTION
C
C*********FIFTH AND SUBSEQUENT LINES
C
C      GRID PROPERTIES SHOULD BE LISTED
C      IN DESCENDING ORDER AS THEY APPEAR IN CROSS SECTION
C
C      EACH LINE CORRESPONDS TO ONE GRID LAYER
C
C      THE NUMBER OF LINES SHOULD CORRESPOND TO M INPUT
C       ABOVE
C
C      KX,KY,PHI
C
C WHERE:
C
C     KX      PERMEABILITY IN X-DIRECTION, MD
C
C     KY      PERMEABILITY IN Y-DIRECTION, MD
C
C     PHI     POROSITY
C
C****************************************
      DIMENSION A(136,55),B(136),X(136)
      DIMENSION DX(23),DY(28),PHI(28,23),K(28,23),Q(28,23),
     #TJ1(28,23),T1J(28,23),T1I(28,23),TI1(28,23),VP(28,23)
      DIMENSION K1J(28,23),K1I(28,23),KJ1(28,23),KI1(28,23)
      DIMENSION YP(28),XP(18)
      DIMENSION VX(136),VY(136),PCR(136),VPX(1601),VPY(1601),PX(1601),
     #PY(1601),PC(1601),CSTAR(136),V(136),DELC(136),C(136)
      DIMENSION KX(28,23),KY(28,23)
      DIMENSION DXX(136),DYY(136),DXY(136),DYX(136),DXX1I(136)
      DIMENSION DXXI1(136),DXY1I(136),DXYI1(136),DYX1J(136)
```

```
      DIMENSION DYXJ1(136),DYY1J(136),CYYJ1(136)
      DIMENSION UX(136),UY(136)
      DIMENSION PY1(1601),PX1(1601)
      DIMENSION CX(1000),XS(1000)
      DIMENSION PX2(1000),PY2(1000)
      DIMENSION AA(136,55),BB(136),XX(136)
      DIMENSION UXX(28,23),UYY(28,23)
      DIMENSION AAA(136,55)
      REAL K,KI1,K1I,KJ1,K1J
      REAL L
      INTEGER PIT,PIB
      REAL LBY,LBX
      REAL KX,KY,KSUM,KSUMI,KSUMP,KSUMPI
      IMI=0
      PVI=0.0
      IIII=0
      PCHECK=0.05
      IIZ=0
      IIJ=0
      TSUM=0.0
      CHECK=0.4
      AI=0.0
      AO=0.0
      TOUT=30.
      TSUM=0.0
      READ,M,N,DELT,CT,VIS,PI,PVC
      MN=M*N
      READ,IIT,IIB,PIT,PIB,FRACQP,FRACQI
      READ,AQ,L,DELH,NP,NPXD,NPYD
      DELY=DELH/M
      DELX=L/(N-1)
      READ,W,DO,CM,ATEFF,ALEFF,CI
      DO 7003 J=1,M
      READ,KX(J,1),KY(J,1),PHI(J,1)
7003  CONTINUE
      DO 8005 I=1,N
8005  DX(I)=DELX
      DO 8006 J=1,M
8006  DY(J)=DELY
      DO 7004 J=1,M
      DO 7005 I=1,N
      KX(J,I)=KX(J,1)
      KY(J,I)=KY(J,1)
      PHI(J,I)=PHI(J,1)
7005  CONTINUE
7004  CONTINUE
      PHISUM=0.0
      DO 8249 J=1,M
8249  PHISUM=PHISUM+PHI(J,1)*DELY
      PHIBAR=PHISUM/DELH
      DO 7001 I=1,N
      DO 7002 J=1,M
      Q(J,I)=0.0
7002  CONTINUE
7001  CONTINUE
      DO 6100 I=1,NP
6100  PC(I)=0.0
      N2=N*2
      M2=M*2
      DO 6101 I=1,N*NPXD
      DO 6102 J=1,M*NPYD
      MNC=M*NPYD*(I-1)+J
```

```
      XL=0.5*(DELX+DELX/NPXD)+(I-1)*DELX/NPXD
      YL=0.5*(DELY+DELY/NPYD)+(J-1)*DELY/NPYD
      PX(MNC)=XL
      PY(MNC)=YL
      PX1(MNC)=XL
      PY1(MNC)=YL
 6102 CONTINUE
 6101 CONTINUE
      KSUM=0.0
      KSUMI=0.0
      KSUMP=0.0
      KSUMPI=0.0
      IF(IIT .EQ. 1) GO TO 9500
      DO 1600 I=1,IIT-1
 1600 KSUM=KSUM+KX(I,1)
 9500 CONTINUE
      IF(IIB .EQ. M) GO TO 9501
      DO 1601 I=IIB+1,M
 1601 KSUM=KSUM+KX(I,1)
 9501 CONTINUE
      DO 1602 I=IIT,IIB
 1602 KSUMI=KSUMI+KX(I,1)
      IF(IIT .EQ. 1) GO TO 9502
      DO 1610 I=1,IIT-1
 1610 Q(I,1)=-AQ*(1.-FRACQI)*KX(I,1)/KSUM
 9502 CONTINUE
      DO 1611 I=IIT,IIB
 1611 Q(I,1)=-AQ*FRACQI*KX(I,1)/KSUMI
      IF(IIB .EQ. M) GO TO 9510
      DO 1612 I=IIB+1,M
 1612 Q(I,1)=-AQ*(1.-FRACQI)*KX(I,1)/KSUM
 9510 CONTINUE
      IF(PIT .EQ. 1) GO TO 9511
      DO 1613 I=1,PIT-1
 1613 KSUMP=KSUMP+KX(I,N)
 9511 CONTINUE
      IF(PIB .EQ. M) GO TO 9512
      DO 1614 I=PIB+1,M
 1614 KSUMP=KSUMP+KX(I,N)
 9512 CONTINUE
      DO 1615 I=PIT,PIB
 1615 KSUMPI=KSUMPI+KX(I,N)
      IF(PIT .EQ. 1) GO TO 9520
      DO 1616 I=1,PIT-1
 1616 Q(I,N)=AQ*(1.-FRACQP)*KX(I,N)/KSUMP
 9520 CONTINUE
      DO 1617 I=PIT,PIB
 1617 Q(I,N)=AQ*FRACQP*KX(I,N)/KSUMPI
      IF(PIB .EQ. M) GO TO 9521
      DO 1618 I=PIB+1,M
 1618 Q(I,N)=AQ*(1.-FRACQP)*KX(I,N)/KSUMP
 9521 CONTINUE
      QSUMP=0.0
      DO 9731 I=PIT,PIB
      QSUMP=QSUMP+Q(I,N)
 9731 CONTINUE
      SUMXP=DELX
      SUMYP=DELY
      YP(1)=DY(1)
      XP(1)=DX(1)
      DO 600 I=2,N
      SUMXP=SUMXP+(DX(I)+DX(I-1))/2.
```

```
600 XP(I)=SUMXP
    DO 601 J=2,M
    SUMYP=SUMYP+(DY(J)+DY(J-1))/2.
601 YP(J)=SUMYP
    DO 30 I=1,N
    DO 31 J=1,M
    VP(J,I)=DX(I)*DY(J)*W*PHI(J,I)
 31 CONTINUE
 30 CONTINUE
    DO 32 J=1,M
    DO 33 I=1,N-1
    KI1(J,I)=(DX(I)+DX(I+1))/(DX(I)/KX(J,I)+DX(I+1)/KX(J,I+1))
    TI1(J,I)=(0.00633*DY(J)*W*KI1(J,I))/(0.5*(DX(I)+DX(I+1))*VIS)
 33 CONTINUE
 32 CONTINUE
    DO 34 J=1,M
    DO 35 I=2,N
    K1I(J,I)=(DX(I)+DX(I-1))/(DX(I)/KX(J,I)+DX(I-1)/KX(J,I))
    T1I(J,I)=(0.00633*DY(J)*W*K1I(J,I))/(0.5*(DX(I)+DX(I-1))*VIS)
 35 CONTINUE
 34 CONTINUE
    DO 36 J=2,M
    DO 37 I=1,N
    K1J(J,I)=(DY(J)+DY(J-1))/(DY(J)/KY(J,I)+DY(J-1)/KY(J-1,I))
    T1J(J,I)=(0.00633*DX(I)*W*K1J(J,I))/(0.5*(DY(J)+DY(J-1))*VIS)
 37 CONTINUE
 36 CONTINUE
    DO 38 J=1,M-1
    DO 39 I=1,N
    KJ1(J,I)=(DY(J)+DY(J+1))/(DY(J)/KY(J,I)+DY(J+1)/KY(J+1,I))
    TJ1(J,I)=(0.00633*DX(I)*W*KJ1(J,I))/(0.5*(DY(J)+DY(J+1))*VIS)
 39 CONTINUE
 38 CONTINUE
    I=1
    DO 40 J=1,M
 40 T1I(J,I)=0.0
    I=N
    DO 41 J=1,M
 41 TI1(J,I)=0.0
    J=1
    DO 42 I=1,N
 42 T1J(J,I)=0.0
    J=M
    DO 43 I=1,N
 43 TJ1(J,I)=0.0
    M21=M*2+1
    MN=M*N
    DO 44 J=1,MN
    DO 45 I=1,M21
    A(J,I)=0.0
 45 CONTINUE
 44 CONTINUE
    II=0
    DO 46 I=1,N
    DO 47 J=1,M
    II=II+1
    A(II,1)=-T1I(J,I)
    A(II,M)=-T1J(J,I)
    A(II,M+1)=TI1(J,I)+TJ1(J,I)+T1I(J,I)+T1J(J,I)+VP(J,I)*CT/DELT
    A(II,M+2)=-TJ1(J,I)
    A(II,M21)=-TI1(J,I)
 47 CONTINUE
```

```
  46 CONTINUE
     DO 5907 J=1,M
     A(J,M+1)=A(J,M+1)+TI1(J,1)
5907 A(J,M21)=A(J,M21)-TI1(J,1)
     J=0
     DO 5908 II=MN-M+1,MN
     J=J+1
     A(II,M+1)=A(II,M+1)+T1I(J,N)
5908 A(II,1)=A(II,1)-T1I(J,N)
     DO 9998 I=1,MN
9998 X(I)=0.0
     II=0
     DO 49 I=1,N
     DO 50 J=1,M
     II=II+1
  50 B(II)=X(II)*VP(J,I)*CT/DELT-2.0*G(J,I)
  49 CONTINUE
     CALL ECOBAND(A,B,X,M,MN,IMI)
     DO 48 I=1,MN
  48 X(I)=PI+X(I)
     CALL OUTPUT(TSUM,X,M,N,XP,YP)
     MNC=0
     DO 6000 I=1,N
     DO 6001 J=1,M
     MNC=MNC+1
     POR(MNC)=PHI(J,I)
6001 CONTINUE
6000 CONTINUE
     III=0
     DO 1950 I=1,N-1
     DO 1951 J=1,M
     III=III+1
     UX(III)=0.00633*2.*(KX(J,I)*KX(J,I+1))/
    #((KX(J,I)+KX(J,I+1))*VIS*DELX)*(X(III)-X(III+M))
1951 CONTINUE
1950 CONTINUE
     III=0
     DO 9825 I=1,N
     DO 9826 J=1,M-1
     III=III+1
     UY(III)=0.00633*2.*(KY(J,I)*KY(J+1,I))/
    #((KY(J,I)+KY(J+1,I))*VIS*DELY)*(X(III)-X(III+1))
9826 CONTINUE
     III=III+1
9825 CONTINUE
     DO 1980 I=1,M
     UXIN=-Q(I,1)/(DELY*W)
1980 VX(I)=UXIN/POR(I)
     VELSUM=0.0
     DO 8251 J=1,M
     VELSUM=VELSUM+VX(J)*PHI(J,1)*DELY
8251 CONTINUE
     VELBAR=VELSUM/(DELH*PHIBAR)
     IF(IIII .GT. 1) GO TO 8253
     WRITE(6,8252) VELBAR
8252 FORMAT(1X,'VBAR= ',E12.4)
8253 CONTINUE
     DO 1981 I=M+1,MN-M
1981 VX(I)=0.5*(UX(I)+UX(I-M))/POR(I)
     II=0
     DO 1982 I=MN-M+1,MN
     II=II+1
```

```
      UXOUT=Q(II,N)/(DELY*W)
 1982 VX(I)=UXOUT/POR(I)
      II=0
      DO 1990 I=1,N
      II=II+1
      VY(II)=0.5*UY(II)/POR(II)
      DO 1991 J=2,M-1
      II=II+1
 1991 VY(II)=0.5*(UY(II-1)+UY(II))/POR(II)
      II=II+1
      VY(II)=0.5*UY(II-1)/POR(II)
 1990 CONTINUE
      DO 7311 J=1,M
 7311 UXX(J,1)=-Q(J,1)/(DELY*W)
      DO 7312 J=1,M
 7312 UXX(J,N+1)=Q(J,N)/(DELY*W)
      DO 7313 I=2,N
      DO 7314 J=1,M
      MNC=(I-2)*M+J
 7314 UXX(J,I)=UX(MNC)
 7313 CONTINUE
      DO 7315 I=1,N
      UYY(1,I)=0.0
      DO 7316 J=2,M
      MNC=(I-1)*M+(J-1)
 7316 UYY(J,I)=UY(MNC)
      UYY(M+1,I)=0.0
 7315 CONTINUE
      M1=M+1
      N1=N+1
      CALL OUTPUT(TSUM,VX,M,N,XP,YP)
      CALL OUTPUT(TSUM,VY,M,N,XP,YP)
      DO 1560 I=1,N
      DO 1561 J=1,M
      MNC=M*(I-1)+J
      V(MNC)=SQRT(VX(MNC)**2+VY(MNC)**2)
      DO=DO*(PHI(J,I)**(CM-1))
      DXX(MNC)=DO+ALEFF*(VX(MNC)**2)/ABS(V(MNC))
     #+ATEFF*(VY(MNC)**2)/ABS(V(MNC))
      DXY(MNC)=(ALEFF-ATEFF)*ABS(VX(MNC)*VY(MNC))/ABS(V(MNC))
      DYX(MNC)=(ALEFF-ATEFF)*ABS(VX(MNC)*VY(MNC))/ABS(V(MNC))
      DYY(MNC)=DO+ALEFF*(VY(MNC)**2)/ABS(V(MNC))
     #+ATEFF*(VX(MNC)**2)/ABS(V(MNC))
 1561 CONTINUE
 1560 CONTINUE
      DO 1570 I=1,M
      DXX1I(I)=DXX(I)*POR(I)
      DXY1I(I)=DXY(I)*POR(I)
 1570 CONTINUE
      DO 1571 I=M+1,MN
      IF(DXX(I) .LT. 1.0E-08) GO TO 5500
      DXX1I(I)=2.0*(POR(I-M)*DXX(I-M)*POR(I)*DXX(I))/
     #(POR(I-M)*DXX(I-M)+POR(I)*DXX(I))
      GO TO 5501
 5500 DXX1I(I)=0.0
 5501 CONTINUE
      IF(DXY(I) .LT. 1.0E-08) GO TO 5502
      DXY1I(I)=2.0*(POR(I-M)*DXY(I-M)*POR(I)*DXY(I))/
     #(POR(I-M)*DXY(I-M)+POR(I)*DXY(I))
      GO TO 5503
 5502 DXY1I(I)=0.0
 5503 CONTINUE
```

```
1571 CONTINUE
     DO 1572 I=1,MN-M
     IF(DXX(I) .LT. 1.0E-08) GO TO 5504
     DXXI1(I)=2.0*(POR(I)*DXX(I)*POR(I+M)*DXX(I+M))/
    #(POR(I)*DXX(I)+POR(I+M)*DXX(I+M))
     GO TO 5505
5504 DXXI1(I)=0.0
5505 CONTINUE
     IF(DXY(I) .LT. 1.0E-08) GO TO 5506
     DXYI1(I)=2.0*(POR(I)*DXY(I)*POR(I+M)*DXY(I+M))/
    #(POR(I)*DXY(I)+POR(I+M)*DXY(I+M))
     GO TO 5507
5506 DXYI1(I)=0.0
5507 CONTINUE
1572 CONTINUE
     DO 1574 I=1,N
     DO 1575 J=2,M
     MNC=M*(I-1)+J
     IF(DYY(MNC) .LT. 1.0E-08) GO TO 5508
     DYY1J(MNC)=2.0*(POR(MNC-1)*DYY(MNC-1)*POR(MNC)*DYY(MNC))/
    #(POR(MNC-1)*DYY(MNC-1)+POR(MNC)*DYY(MNC))
     GO TO 5509
5508 DYY1J(MNC)=0.0
5509 CONTINUE
     IF(DYX(MNC) .LT. 1.0E-08) GO TO 5510
     DYX1J(MNC)=2.0*(POR(MNC-1)*DYX(MNC-1)*POR(MNC)*DYX(MNC))/
    #(POR(MNC-1)*DYX(MNC-1)+POR(MNC)*DYX(MNC))
     GO TO 5511
5510 DYX1J(MNC)=0.0
5511 CONTINUE
1575 CONTINUE
1574 CONTINUE
     DO 1576 I=1,N
     DO 1577 J=1,M-1
     MNC=M*(I-1)+J
     IF(DYY(MNC) .LT. 1.0E-08) GO TO 5512
     DYYJ1(MNC)=2.0*(POR(MNC)*DYY(MNC)*POR(MNC+1)*DYY(MNC+1))/
    #(POR(MNC)*DYY(MNC)+POR(MNC+1)*DYY(MNC+1))
     GO TO 5513
5512 DYYJ1(MNC)=0.0
5513 CONTINUE
     IF(DYX(MNC) .LT. 1.0E-08) GO TO 5514
     DYXJ1(MNC)=2.0*(POR(MNC)*DYX(MNC)*POR(MNC+1)*DYX(MNC+1))/
    #(POR(MNC)*DYX(MNC)+POR(MNC+1)*DYX(MNC+1))
     GO TO 5515
5514 DYXJ1(MNC)=0.0
5515 CONTINUE
1577 CONTINUE
1576 CONTINUE
     DO 1880 I=1,MN,M
     DYY1J(I)=0.0
     DYX1J(I)=0.0
1880 CONTINUE
     DO 1881 I=M,MN,M
     DYYJ1(I)=0.0
     DYXJ1(I)=0.0
1881 CONTINUE
     DO 6683 J=MN-M+1,MN
     DXXI1(J)=0.0
6683 DXYI1(J)=0.0
     M21=M*2+1
     DO 7800 I=1,M21
```

```
      DO 7801 J=1,MN
      AA(J,I)=0.0
 7801 CONTINUE
 7800 CONTINUE
      DO 7802 I=1,MN
      XX(I)=0.0
 7802 CONTINUE
      MN1=MN-M
      DO 7803 J=1,MN1
      AA(J,M+1)=(DXXI1(J)+DXX1I(J))/(DELX**2)+
     #(DYYJ1(J)+DYY1J(J))/(DELY**2)+PCR(J)/DELT
 7803 CONTINUE
      DO 7804 J=M+1,MN1
      AA(J,1)=-(DXX1I(J))/(DELX**2)
 7804 CONTINUE
      DO 7805 J=1,MN
      AA(J,M)=-(DYY1J(J))/(DELY**2)
 7805 CONTINUE
      DO 7806 J=1,MN
      AA(J,M+2)=-(DYYJ1(J))/(DELY**2)
 7806 CONTINUE
      DO 7807 J=1,MN1
      AA(J,M21)=-(DXXI1(J))/(DELX**2)
 7807 CONTINUE
      DO 5909 J=MN1+1,MN
      AA(J,M+1)=2.0+DXX1I(J)/(DELX**2)+(DYY1J(J)
     #+DYYJ1(J))/(DELY**2)+PCR(J)/DELT
      AA(J,1)=-2.0+DXX1I(J)/(DELX**2)
      AA(J,M21)=0.0
 5909 CONTINUE
      DO 7989 J=1,MN
      DO 7990 I=1,M21
      AAA(J,I)=AA(J,I)
 7990 CONTINUE
 7989 CONTINUE
  101 CONTINUE
      IIII=IIII+1
      DO 7991 J=1,MN
      DO 7992 I=1,M21
      AA(J,I)=AAA(J,I)
 7992 CONTINUE
 7991 CONTINUE
      DO 1500 I=1,N
      DO 1501 J=1,M
      MNC=(I-1)*M+J
      LBX=(I-0.5)*DELX
      UBX=(I+0.5)*DELX
      LBY=(J-0.5)*DELY
      UBY=(J+0.5)*DELY
      DO 1502 II=1,NP
      IF(PX(II) .GE. LBX) GO TO 1503
      GO TO 1502
 1503 IF(PX(II) .LT. UBX) GO TO 1504
      GO TO 1502
 1504 IF(PY(II) .GE. LBY) GO TO 1505
      GO TO 1502
 1505 IF(PY(II) .LT. UBY) GO TO 1506
      GO TO 1502
 1506 CONTINUE
      IF(I .EQ. 1) GO TO 1960
      IF(I .EQ. N) GO TO 1961
      IF(PY(II) .GE. (LBY+(0.5*DELY))) GO TO 7323
```

```
      GO TO 7324
 7323 FACX=(PX(II)-LBX)/DELX
      FACXY=(PY(II)-(LBY+(0.5*DELY)))/DELY
      UPXL=UXX(J,I)*(1.-FACX)+UXX(J,I+1)*FACX
      IF(J .EQ. M) GO TO 7325
      UPXU=UXX(J+1,I)*(1.-FACX)+UXX(J+1,I+1)*FACX
      VPX(II)=(UPXL*(1.-FACXY)+UPXU*FACXY)/POR(MNC)
      GO TO 7326
 7325 VPX(II)=UPXL/POR(MNC)
 7326 CONTINUE
      GO TO 7358
 7324 FACX=(PX(II)-LBX)/DELX
      UPXU=UXX(J,I)*(1.-FACX)+UXX(J,I+1)*FACX
      IF(J .EQ. 1) GO TO 7329
      FACXY=(PY(II)-(LBY-(0.5*DELY)))/DELY
      UPXL=UXX(J-1,I)*(1.-FACX)+UXX(J-1,I+1)*FACX
      VPX(II)=(UPXL*(1.-FACXY)+UPXU*FACXY)/POR(MNC)
      GO TO 7330
 7329 VPX(II)=UPXU/POR(MNC)
 7330 CONTINUE
 7358 CONTINUE
      IF(PX(II) .GE. (LBX+(0.5*DELX))) GO TO 7321
      GO TO 7322
 7321 FACY=(PY(II)-LBY)/DELY
      FACYX=(PX(II)-(LBX+(0.5*DELX)))/DELX
      UPYL=UYY(J,I)*(1.-FACY)+UYY(J+1,I)*FACY
      UPYU=UYY(J,I+1)*(1.-FACY)+UYY(J+1,I+1)*FACY
      VPY(II)=(UPYL*(1.-FACYX)+UPYU*FACYX)/POR(MNC)
      GO TO 7328
 7322 FACY=(PY(II)-LBY)/DELY
      FACYX=(PX(II)-(LBX-(0.5*DELX)))/DELX
      UPYL=UYY(J,I-1)*(1.-FACY)+UYY(J+1,I-1)*FACY
      UPYU=UYY(J,I)*(1.-FACY)+UYY(J+1,I)*FACY
      VPY(II)=(UPYL*(1.-FACYX)+UPYU*FACYX)/POR(MNC)
      GO TO 7328
 1960 CONTINUE
      IF(PX(II) .LT. DELX) GO TO 7337
      IF(PY(II) .GE. (LBY+(0.5*DELY))) GO TO 7338
      FACX=(PX(II)-DELX)/(DELX/2.)
      UPXU=UXX(J,I)*(1.-FACX)+UXX(J,I+1)*FACX
      IF(J .EQ. 1) GO TO 7339
      FACXY=(PY(II)-(LBY-(0.5*DELY)))/DELY
      UPXL=UXX(J-1,I)*(1.-FACX)+UXX(J-1,I+1)*FACX
      VPX(II)=(UPXL*(1.-FACXY)+UPXU*FACXY)/POR(MNC)
      GO TO 7340
 7339 VPX(II)=UPXU/POR(MNC)
 7340 CONTINUE
      FACY=(PY(II)-LBY)/DELY
      FACYX=(PX(II)-DELX)/DELX
      UPYL=UYY(J,I)*(1.-FACY)+UYY(J+1,I)*FACY
      UPYU=UYY(J,I+1)*(1.-FACY)+UYY(J+1,I+1)*FACY
      VPY(II)=(UPYL*(1.-FACYX)+UPYU*FACYX)/POR(MNC)
      GO TO 7328
 7338 CONTINUE
      FACX=(PX(II)-DELX)/(DELX/2.)
      FACXY=(PY(II)-(LBY+(0.5*DELY)))/DELY
      UPXL=UXX(J,I)*(1.-FACX)+UXX(J,I+1)*FACX
      IF(J .EQ. M) GO TO 7341
      UPXU=UXX(J+1,I)*(1.-FACX)+UXX(J+1,I+1)*FACX
      VPX(II)=(UPXL*(1.-FACXY)+UPXU*FACXY)/POR(MNC)
      GO TO 7342
 7341 VPX(II)=UPXL/POR(MNC)
```

```
7342 CONTINUE
     FACY=(PY(II)-LBY)/DELY
     FACYX=(PX(II)-DELX)/DELX
     UPYL=UYY(J,I)*(1.-FACY)+UYY(J+1,I)*FACY
     UPYU=UYY(J,I+1)*(1.-FACY)+UYY(J+1,I+1)*FACY
     VPY(II)=(UPYL*(1.-FACYX)+UPYU*FACYX)/POR(MNC)
     GO TO 7328
1961 CONTINUE
     IF(PX(II) .GT. (DELX*N)) GO TO 7343
     IF(PY(II) .GE. (LBY+(0.5*DELY))) GO TO 7344
     FACX=(PX(II)-LBX)/(DELX/2.)
     UPXU=UXX(J,I)*(1.-FACX)+UXX(J,I+1)*FACX
     IF(J .EQ. 1) GO TO 7345
     UPXL=UXX(J-1,I)*(1.-FACX)+UXX(J-1,I+1)*FACX
     FACXY=(PY(II)-(LBY-(0.5*DELY)))/DELY
     VPX(II)=(UPXL*(1.-FACXY)+UPXU*FACXY)/POR(MNC)
     GO TO 7346
7345 VPX(II)=UPXU/POR(MNC)
7346 CONTINUE
     FACY=(PY(II)-LBY)/DELY
     FACYX=(PX(II)-(LBX-(0.5*DELX)))/DELX
     UPYL=UYY(J,I-1)*(1.-FACY)+UYY(J+1,I-1)*FACY
     UPYU=UYY(J,I)*(1.-FACY)+UYY(J+1,I)*FACY
     VPY(II)=(UPYL*(1.-FACYX)+UPYU*FACYX)/POR(MNC)
     GO TO 7328
7344 FACX=(PX(II)-LBX)/(DELX/2.)
     UPXL=UXX(J,I)*(1.-FACX)+UXX(J,I+1)*FACX
     IF(J .EQ. M) GO TO 7347
     UPXU=UXX(J+1,I)*(1.-FACX)+UXX(J+1,I+1)*FACX
     FACXY=(PY(II)-(LBY+(0.5*DELY)))/DELY
     VPX(II)=(UPXL*(1.-FACXY)+UPXU*FACXY)/POR(MNC)
     GO TO 7348
7347 VPX(II)=UPXL/POR(MNC)
7348 CONTINUE
     FACY=(PY(II)-LBY)/DELY
     FACYX=(PX(II)-(LBX-(0.5*DELX)))/DELX
     UPYL=UYY(J,I-1)*(1.-FACY)+UYY(J+1,I-1)*FACY
     UPYU=UYY(J,I)*(1.-FACY)+UYY(J+1,I)*FACY
     VPY(II)=(UPYL*(1.-FACYX)+UPYU*FACYX)/POR(MNC)
     GO TO 7328
7337 VPX(II)=UXX(J,I)/POR(MNC)
     VPY(II)=0.0
     GO TO 7328
7343 VPX(II)=UXX(J,N+1)/POR(MNC)
     VPY(II)=0.0
7328 CONTINUE
1502 CONTINUE
1501 CONTINUE
1500 CONTINUE
     DO 1520 J=1,NP
     PX(J)=PX(J)+DELT*VPX(J)
     PY(J)=PY(J)+DELT*VPY(J)
1520 CONTINUE
     DO 5803 I=1,NP
     PX2(I)=PX(I)
     PY2(I)=PY(I)
5803 CONTINUE
     DO 1521 I=1,NP
     IF(PX(I) .LT. ((N+0.5)*DELX)) GO TO 1521
     DO 9031 JJ=1,M
     DO 1522 J=1,NPYD
     NPC=0
```

```
      LBY=(JJ-0.5)*DELY+(J-1)*DELY/NPYD
      UBY=(JJ-0.5)*DELY+J*DELY/NPYD
      LBX=0.5*DELX
      UBX=0.5*DELX+DELX/NPXD
      DO 1523 II=1,NP
      IF(PX(II) .GE. LBX) GO TO 1524
      GO TO 1523
 1524 IF(PX(II) .LT. UBX) GO TO 1525
      GO TO 1523
 1525 IF(PY(II) .GE. LBY) GO TO 1526
      GO TO 1523
 1526 IF(PY(II) .LT. UBY) GO TO 1527
      GO TO 1523
 1527 NPC=NPC+1
 1523 CONTINUE
      IF(NPC .LT. 1) GO TO 1528
      GO TO 1522
 1528 IF(ABS(Q(JJ,1)) .LT. 1.0E-05) GO TO 1522
      PX(I)=LBX
      PY(I)=LBY+0.5*DELY/NPYD
      PC(I)=1.0
      GO TO 1521
 1522 CONTINUE
 9031 CONTINUE
 1521 CONTINUE
      DO 1550 I=1,N
      DO 1551 J=1,M
      MNC=M*(I-1)+J
      LBX=(I-0.5)*DELX
      UBX=(I+0.5)*DELX
      LBY=(J-0.5)*DELY
      UBY=(J+0.5)*DELY
      CSTARS=0.0
      ICO=0
      DO 1552 II=1,NP
      IF(PX(II) .GE. LBX) GO TO 1553
      GO TO 1552
 1553 IF(PX(II) .LT. UBX) GO TO 1554
      GO TO 1552
 1554 IF(PY(II) .GE. LBY) GO TO 1555
      GO TO 1552
 1555 IF(PY(II) .LT. UBY) GO TO 1556
      GO TO 1552
 1556 CONTINUE
      IF(PX(II) .GT. (DELX*N)) GO TO 1552
      ICO=ICO+1
      CSTARS=CSTARS+PC(II)
 1552 CONTINUE
      IF(ICO .EQ. 0) GO TO 2553
      CSTAR(MNC)=CSTARS/ICO
      GO TO 2554
 2553 CSTAR(MNC)=0.0
 2554 CONTINUE
 1551 CONTINUE
 1550 CONTINUE
      DO 7810 J=1,MN
      BB(J)=CSTAR(J)*POR(J)/DELT
 7810 CONTINUE
      DO 7811 J=1,M
      BB(J)=BB(J)+(DXX1I(J))/(DELX**2)*CI
 7811 CONTINUE
      IF(ALEFF .LT. 1.0E-05) GO TO 7820
```

```
      GO TO 7821
7820  IF(ATEFF .LT. 1.0E-05) GO TO 7822
7821  CONTINUE
      CALL ECOBAND(AA,BB,XX,M,MN,IMI)
      GO TO 7825
7822  CONTINUE
      DO 7826 J=1,MN
7826  DELC(J)=0.0
      GO TO 7827
7825  CONTINUE
      DO 7812 J=1,MN
      DELC(J)=XX(J)-CSTAR(J)
7812  CONTINUE
7827  CONTINUE
      DO 1583 I=1,N
      DO 1584 J=1,M
      MNC=M*(I-1)+J
      LBX=(I-0.5)*DELX
      UBX=(I+0.5)*DELX
      LBY=(J-0.5)*DELY
      UBY=(J+0.5)*DELY
      DO 1585 II=1,NP
      IF(PX(II) .GE. LBX) GO TO 1586
      GO TO 1585
1586  IF(PX(II) .LT. UBX) GO TO 1587
      GO TO 1585
1587  IF(PY(II) .GE. LBY) GO TO 1588
      GO TO 1585
1588  IF(PY(II) .LT. UBY) GO TO 1589
      GO TO 1585
1589  PC(II)=PC(II)+DELC(MNC)
1585  CONTINUE
1584  CONTINUE
1583  CONTINUE
      DO 1590 I=1,MN
      C(I)=CSTAR(I)+DELC(I)
1590  CONTINUE
      DO 5941 I=1,NP
      IF(PX(I) .LT. DELX) GO TO 5932
      GO TO 5941
5932  PC(I)=1.0
5941  CONTINUE
      CSUMP=0.0
      II=PIT-1
      DO 5931 J=MN1+PIT,MN1+PIB
      II=II+1
5931  CSUMP=CSUMP+C(J)*Q(II,N)
      CBARQ=CSUMP/QSUMP
      IF(CBARQ .LT. 0.0) GO TO 7533
      GO TO 7534
7533  CBARQ=0.0
7534  CONTINUE
      DO 6600 I=1,NP
      PX1(I)=PX(I)
      PY1(I)=PY(I)
6600  CONTINUE
      SUMC=0.0
      IC=M
      DO 513 I=2,N-1
      DO 514 J=1,M
      IC=IC+1
      SUMC=SUMC+C(IC)*POR(IC)
```

```
  514 CONTINUE
  513 CONTINUE
      DO 9514 J=1,M
 9514 SUMC=SUMC+C(J)*POR(J)*0.5
      DO 9515 J=MN-M+1,MN
 9515 SUMC=SUMC+C(J)*POR(J)*0.5
      AP=DELX*DELY*SUMC
      CONIN=0.0
      DO 515 J=IIT,IIB
  515 CONIN=CONIN-G(J,1)*CI+(DXX1I(J))*(CI-CSTAR(J))
     #/DELX*DELY
      AI=AI+DELT*CONIN
      PVSUM=0
      DO 9000 I=1,MN-M
 9000 PVSUM=PVSUM+DELX*DELY*POR(I)
      PV=PVSUM
      I=0
      PVI=AI/PV
      CONOUT=0.0
      DO 516 J=MN1+1,MN
      I=I+1
  516 CONOUT=CONOUT+G(I,N)*C(J)
      AO=AO+DELT*CONOUT
      IF(AP .LE. 1.0E-05) GO TO 7955
      PER=(AI-AO)/AP
      GO TO 7956
 7955 PER=0.0
 7956 CONTINUE
      TSUM=TSUM+DELT
      IF(PVI .LT. CHECK) GO TO 101
      CHECK=CHECK+0.0
      IIJ=IIJ+1
      CX(IIJ)=CBARO
      XS(IIJ)=PVI
      IF(PVI .GE. PCHECK) GO TO 9943
      GO TO 9944
 9943 PCHECK=PCHECK+0.05
      WRITE(6,7905) PVI,PER
 7905 FORMAT(3X,2F12.5)
      CALL OUTPUT(TSUM,C,M,N,XP,YP)
 9944 CONTINUE
      IF(PVI.GE.PVC) GO TO 8010
      GO TO 101
 8010 CONTINUE
      CALL OUTPT(CX,XS,M,N,TSUM,PVI,DELY,DELX,DELT,
     #ALEFF,ATEFF,PER,IIJ)
      CALL PLOTS(2,1,5LPLOTR)
      CALL SCALE(CX,6.,IIJ,1)
      CALL AXIS(1.5,9.5,4HCONC,4,5.,0.,CX(IIJ+1),CX(IIJ+2))
      CALL SCALE(XS,9.,IIJ,1)
      CALL AXIS(1.5,9.5,3HLEN,-3,8.,270.,XS(IIJ+1),XS(IIJ+2))
      CALL SYMBOL(4.5,4.5,0.14,11HAL=1.1390FT,270.,11)
      CALL SYMBOL(4.0,4.5,0.14,12HAT=0.0030 FT,270.,12)
      CALL SYMBOL(3.5,4.5,0.14,11HDELT=0.01 D,270.,11)
      CALL SYMBOL(3.0,4.5,0.14,5HNXP=3,270.,5)
      CALL PLOT(1.5,9.5,-3)
      DO 4115 I=1,IIJ
 4115 XS(I)=-XS(I)+0.4
      CALL LINE(CX,XS,IIJ,1,-1,2)
      CALL PLOT(0.0,0.0,999)
      STOP
      END
```

```
      SUBROUTINE OUTPT(XH,PHIS,M,N,TSUM,PVI,DELY,DELX,DELT,
     #ALEFF,ATEFF,PER,IIJ)
      DIMENSION XH(1000),PHIS(1000)
      WRITE(6,204)
      WRITE(6,205)
      WRITE(6,206) TSUM,PVI
      WRITE(6,207)DELY,DELX,DELT
      WRITE(6,208)ALEFF,ATEFF
      WRITE(6,212)PER
      WRITE(6,205)
      WRITE(6,204)
      WRITE(6,303)
  303 FORMAT(//)
  304 FORMAT(/)
      INC=8
      J=1
      IF(IIJ.GT.INC)GO TO 1
      WRITE(6,103)(PHIS(I),I=1,IIJ)
      WRITE(6,100)J,(XH(I),I=1,IIJ)
      GO TO 40
    1 CONTINUE
      JJ=INC
      IC=INC-7
      WRITE(6,103)(PHIS(I),I=IC,INC)
      WRITE(6,100)J,(XH(I),I=IC,JJ)
      INC=INC+8
      WRITE(6,304)
      IF(IIJ.GT.INC) GO TO 1
      IC=INC-7
      WRITE(6,103)(PHIS(I),I=IC,IIJ)
      WRITE(6,100)J,(XH(I),I=IC,IIJ)
   40 CONTINUE
  100 FORMAT(1X,I1,6X,8(E12.4))
  103 FORMAT(5X,*H(FT)*,3X,*K(MD)*,5X,*PHI*,4X,8(5X,F7.3))
  204 FORMAT(5X,40H****************************************
     #,15H***************)
  205 FORMAT(5X,1H*,53X,1H*)
  206 FORMAT(5X,1H*,10X,*TIME= *,F6.1,1X,*DAYS*,3X,*AMT INJ= *
     #,F5.3,*PV*,7X,1H*)
  207 FORMAT(5X,1H*,4X,*DELY=*,F5.1,1X,*FT*,2X,*DELX= *,
     #F5.2,1X,*FT*,2X,*DELT=*,F5.2,1X,*DAYS*,3X,1H*)
  208 FORMAT(5X,1H*,5X,*ALPHAL= *,F6.3,1X,*FT*,5X,*ALPHAT=*,
     #F8.5,1X,*FT*,7X,1H*)
  212 FORMAT(5X,1H*,13X,*MASS BALANCE FACTOR= *,F7.5,12X,1H*)
      RETURN
      END
      SUBROUTINE OUTPUT(TSUM,X,M,N,XP,YP)
      DIMENSION X(136),IXC(41)
      DIMENSION XP(23),YP(28)
      DO 100 I=1,N
  100 IXC(I)=I
      WRITE(6,206) TSUM
  206 FORMAT(10X,*TIME= *,F6.1,1X,*DAYS*)
      WRITE(6,103)
  103 FORMAT(//)
      INC=8
      MN=M*N
      IF(N.GT.INC) GO TO 1
      WRITE(6,207)(IXC(I),I=1,N)
  207 FORMAT(19X,9(10X,I2))
      WRITE(6,501)(XP(I),I=1,N)
  501 FORMAT(21X,8(4X,F8.1))
```

```
      WRITE(6,502)
  502 FORMAT(/)
      DO 10 J=1,M
   10 WRITE(6,208)J,YP(J),(X(I),I=J,MN,M)
  208 FORMAT(1X,I2,2X,F8.1,10X,8(E12.4))
      GO TO 40
    1 CONTINUE
      IC=INC-7
      JJ=INC*M
      WRITE(6,207)(IXC(I),I=IC,INC)
      WRITE(6,501)(XP(I),I=IC,INC)
      WRITE(6,502)
      DO 20 J=1,M
      II=(INC-8)*M+J
   20 WRITE(6,208)J,YP(J),(X(I),I=II,JJ,M)
      INC=INC+8
      WRITE(6,304)
  304 FORMAT(/)
      IF(N.GT.INC) GO TO 1
      IC=INC-7
      WRITE(6,207)(IXC(I),I=IC,N)
      WRITE(6,501)(XP(I),I=IC,N)
      WRITE(6,502)
      DO 30 J=1,M
      II=(INC-8)*M+J
   30 WRITE(6,208)J,YP(J),(X(I),I=II,MN,M)
   40 CONTINUE
      WRITE(6,103)
      RETURN
      END
      SUBROUTINE ECOBAND(A,B,X,M,MN,IMI)
      DIMENSION A(136,55),B(136),X(136),G(136)
      M21=M*2+1
      M1=M+1
      M2=M+2
      IF(IMI.GE.1) GO TO 82
      A(1,M2)=A(1,M2)/A(1,M1)
      IF(M.EQ.1) GO TO 99
      A(1,M21)=A(1,M21)/A(1,M1)
   99 CONTINUE
      DO 10 I=2,MN
      MJ=M+3-I
      IF(MJ.LT.2) MJ=2
      DO 20 J=MJ,M1
      SUML=0.0
      IF(MJ.EQ.2)GO TO 22
      IC=I
      GO TO 23
   22 IC=M+1
   23 DO 21 II=MJ-1,J-1
      IC=IC-1
   21 SUML=SUML+A(I,II)*A(I-IC,J+IC)
      A(I,J)=A(I,J)-SUML
   20 CONTINUE
      DO 30 J=M2,M21
      SUMU=0.0
      IF(MJ.EQ.2) GO TO 32
      IC=I
      GO TO 33
   32 IC=M+1
   33 DO 31 II=MJ-1,M
      IC=IC-1
```

```
      JIC=J+IC
      IF(JIC.GT.M21) GO TO 31
      SUMU=SUMU+A(I,II)*A(I-IC,JIC)
   31 CONTINUE
      A(I,J)=(A(I,J)-SUMU)/A(I,M1)
   30 CONTINUE
   10 CONTINUE
   82 CONTINUE
      G(1)=B(1)/A(1,M1)
      DO 40 I=2,MN
      JC=M+2-I
      IF(JC.LT.1) GO TO 42
      JJ=0
      GO TO 43
   42 JC=1
      JJ=I-M-1
   43 SUMG=0.0
      DO 41 II=JC,M
      JJ=JJ+1
   41 SUMG=SUMG+A(I,II)*G(JJ)
      G(I)=(B(I)-SUMG)/A(I,M1)
   40 CONTINUE
      X(MN)=G(MN)
      MROW=1
      DO 60 I=1,MN-1
      SUMX=0.0
      IC=MN-I
      JJ=IC
      MROW=MROW+1
      IF(MROW.GT.M1) GO TO 61
      GO TO 62
   61 MROW=M+1
   62 DO 63 II=M2,M+MROW
      JJ=JJ+1
   63 SUMX=SUMX+A(IC,II)*X(JJ)
      X(IC)=G(IC)-SUMX
   60 CONTINUE
      RETURN
      END
```

APPENDIX D

Fortran Listing of the Fixed Grid Simulator

```
      PROGRAM RORHIS(INPUT,OUTPUT,TAPE6=OUTPUT,PLOTR)
C*************************************************
C
C     FIXED GRID FINITE DIFFERENCE SIMULATOR
C
C     DATA SHOULD BE INPUT AS FOLLOWS:
C
C*********FIRST LINE
C
C     ATEFF,L,DO,VBAR,CM
C
C WHERE:
C
C    ATEFF    TRANSVERSE DISPERSIVITY, FEET
C
C    L        TOTAL SYSTEM LENGTH, FEET
C
C    DO       MOLECULAR DIFFUSTION COEFFICIENT, SQUARE FEET/DAY
C
C    VBAR     FLOW RATE AVERAGED INTERSTITIAL VELOCITY, FEET/DAY
C
C    CM       FORMATION CEMENTATION FACTOR
C
C*********SECOND LINE
C
C     M,N,DELT,PVC,CI,W
C
C WHERE:
C
C    M        NUMBER OF GRID BLOCKS IN Y-DIRECTION
C
C    N        NUMBER OF GRID BLOCKS IN X-DIRECTION
C
C    DELT     TIME STEP, DAY
C
C    PVC      TOTAL NUMBER OF PORE VOLUMES INJECTED
C              BEFORE PROGRAM FLAGGED TO STOP
C
C    CI       INJECTED FLUID CONCENTRATION
C
C    W        FIRST SPATIAL DERIVATIVE WEIGHTING FACTOR
C
C**********THIRD LINE AND SUBSEQUENT LINES
C
C     GRID PROPERTIES SHOULD BE LISTED IN ORDER THEY
C       APPEAR IN CROSS SECTION
C
C     EACH LINE CORRESPONDS TO ONE GRID LAYER
C
C     LAST LINE SHOULD BEGIN WITH  -1.0  TO SIGNAL
C      PROGRAM TO STOP READING.  THIS IS A DUMMY LINE.
C
C     H,K,APHI,ALEFF
C
C WHERE:
C
C    H        HEIGHT OF INDIVIDUAL LAYER
C
C    K        PERMEABILITY, MD
C
C    APHI     POROSITY
```

```
C
C     ALEFF    TRANSVERSE DISPERSIVITY, FEET
C
C*****************************************************0
      DIMENSION A(1450,35),B(1450),X(1450)
      DIMENSION V(18),PHI(18),KT(18),KL(18),H(18),K(18)
     #,C1J(18),C1I(18),C(18),CI1(18),CJ1(18),BC(18),
     #AV(18),APHI(18),AKL(18),AKT(18)
      DIMENSION CB(18),CI1B(18)
      DIMENSION XH(500),PHIS(500)
      DIMENSION ALEFF(18)
      REAL K,KL,KT,CM,JSTEP,JT,H
      REAL KBAR,L
      READ,ATEFF,L,DO,VBAR,CM
      READ,M,N,DELT,PVC,CI,W
      TSUM=0.0
      IMI=0
      CHECK=0.02
      IHIS=0
      AI=0.0
      AO=0.0
      JJ=1
      HTOT=0.0
      W1=1.-W
      WC=(2.*W)-1.
      I=0
    1 I=I+1
      READ,H(I),K(I),APHI(I),ALEFF(I)
      IF(H(I).LT.0.0) GO TO 2
      GO TO 1
    2 LYR=I-1
      POR=0.0
      DO 599 I=1,LYR
      POR=POR+H(I)*APHI(I)
  599 CONTINUE
      PV=L*POR
      CALL MEAN(KBAR,K,H,LYR)
      CALL MEAN(PHIBAR,APHI,H,LYR)
      DO 5 I=1,LYR
      AV(I)=K(I)*PHIBAR*VBAR/(APHI(I)*KBAR)
      AKL(I)=(DO*APHI(I)**(CM-1))+ALEFF(I)*AV(I)
      AKT(I)=(DO*APHI(I)**(CM-1))+ATEFF*AV(I)
      HTOT=HTOT+H(I)
    5 CONTINUE
      JSTEP=HTOT/M
      JT=-JSTEP/2.
      I=1
      AH=H(1)
      DO 6 J=1,M
      JT=JT+JSTEP
      IF(JT.GE.AH) GO TO 7
      V(J)=AV(I)
      KL(J)=AKL(I)
      KT(J)=AKT(I)
      PHI(J)=APHI(I)
      GO TO 8
    7 I=I+1
      V(J)=AV(I)
      KL(J)=AKL(I)
      KT(J)=AKT(I)
      PHI(J)=APHI(I)
      AH=AH+H(I)
```

```
  8 CONTINUE
  6 CONTINUE
    M1=M-1
    N1=N-1
    KT(M+1)=KT(M)
    DELY=JSTEP
    MN=M*N
    DELX=L/N
    MNM=MN-M
    DO 9 I=1,MN
    X(I)=0.0
  9 CONTINUE
    BC(1)=CI*V(1)/DELX
    IF(KT(1).GT.0.0001) GO TO 953
    CB(1)=1./DELT+W*V(1)/DELX+KL(1)/(DELX**2)
    GO TO 954
953 CONTINUE
    CB(1)=1./DELT+W*V(1)/DELX+KL(1)/(DELX**2)+
   #2.*((KT(1)*KT(2))/(KT(1)+KT(2)))/(DELY**2)
954 CONTINUE
    CI1B(1)=KL(1)/(DELX**2)-W1*V(1)/DELX
    IF(M.EQ.1) GO TO 207
    DO 911 J=2,M
    BC(J)=CI*V(J)/DELX
    IF(KT(J).GT.0.0001) GO TO 955
    CB(J)=1./DELT+W*V(J)/DELX+KL(J)/(DELX**2)
    GO TO 956
955 CONTINUE
    CB(J)=1./DELT+W*V(J)/DELX+KL(J)/(DELX**2)+2.*
   #((KT(J)*KT(J+1))/(KT(J)+KT(J+1)))/(DELY**2)+PHI(J-1)*2.*
   #((KT(J)*KT(J-1))/(KT(J)+KT(J-1)))/(PHI(J)*(DELY**2))
956 CONTINUE
    CI1B(J)=KL(J)/(DELX**2)-W1*V(J)/DELX
911 CONTINUE
207 CONTINUE
    C1I(1)=W*V(1)/DELX+KL(1)/(DELX**2)
    IF(KT(1).GT.0.0001) GO TO 957
    C(1)=1./DELT+WC*V(1)/DELX+2.*KL(1)/(DELX**2)
    GO TO 958
957 CONTINUE
    C(1)=1./DELT+WC*V(1)/DELX+2.*KL(1)/(DELX**2)
   #+2.*((KT(1)*KT(2))/(KT(1)+KT(2)))/(DELY**2)
958 CONTINUE
    CI1(1)=KL(1)/(DELX**2)-W1*V(1)/DELX
    IF(KT(1).GT.0.0001) GO TO 959
    CJ1(1)=0.0
    GO TO 960
959 CONTINUE
    CJ1(1)=2.*((KT(1)*KT(2))/(KT(1)+KT(2)))/(DELY**2)
960 CONTINUE
    IF(M.EQ.1) GO TO 208
    DO 10 J=2,M
    IF(KT(J).GT.0.0001) GO TO 961
    C1J(J)=0.0
    GO TO 962
961 CONTINUE
    C1J(J)=PHI(J-1)*2.*((KT(J)*KT(J-1))/(KT(J)+KT(J-1)))/
   #(PHI(J)*(DELY**2))
962 CONTINUE
    C1I(J)=W*V(J)/DELX+KL(J)/(DELX**2)
    IF(KT(J).GT.0.0001) GO TO 963
    C(J)=1./DELT+WC*V(J)/DELX+2.*KL(J)/(DELX**2)
```

```
      GO TO 964
  963 CONTINUE
      C(J)=1./DELT+WC*V(J)/DELX+2.*KL(J)/(DELX**2)+
     #2.*((KT(J)*KT(J+1))/(KT(J)+KT(J+1)))/(DELY**2)+
     #PHI(J-1)*2.*((KT(J)*KT(J-1))/(KT(J)+KT(J-1)))/
     #(PHI(J)*(DELY**2))
  964 CONTINUE
      CI1(J)=KL(J)/(DELX**2)-W1*V(J)/DELX
      IF(KT(J).GT.0.0001) GO TO 965
      CJ1(J)=0.0
      GO TO 966
  965 CONTINUE
      CJ1(J)=2.*((KT(J)*KT(J+1))/(KT(J)+KT(J+1)))/(DELY**2)
  966 CONTINUE
   10 CONTINUE
  208 CONTINUE
      M21=M*2+1
      DO 11 J=1,MN
      DO 12 I=1,M21
      A(J,I)=0.0
   12 CONTINUE
   11 CONTINUE
      IF(M.EQ.1) GO TO 97
      GO TO 98
   97 CONTINUE
      DO 211 I=2,MN
  211 A(I,1)=-CII(1)
      A(1,2)=CB(1)-CJ1(1)
      DO 212 I=2,MN-1
  212 A(I,2)=C(1)-CJ1(1)
      A(MN,2)=C(1)-CJ1(1)-CI1(1)
      DO 213 I=1,MN-1
  213 A(I,3)=-CI1(1)
      GO TO 214
   98 CONTINUE
      II=M
      DO 31 I=M+1,MN,M
      DO 30 J=1,M
      II=II+1
   30 A(II,1)=-CII(J)
   31 CONTINUE
      CIJ(1)=0.0
      II=0
      DO 40 I=1,MN,M
      DO 41 J=1,M
      II=II+1
   41 A(II,M)=-CIJ(J)
   40 CONTINUE
      DO 50 J=1,M-1
   50 A(J,M+1)=CB(J)
      A(M,M+1)=CB(M)-CJ1(M)
      II=M
      DO 51 I=M+1,MN-M,M
      DO 52 J=1,M-1
      II=II+1
   52 A(II,M+1)=C(J)
      II=II+1
      J=M
   51 A(II,M+1)=C(J)-CJ1(J)
      DO 53 J=1,M-1
      II=II+1
   53 A(II,M+1)=C(J)-CI1(J)
```

```
      II=II+1
      J=M
      A(II,M+1)=C(J)-CI1(J)-CJ1(J)
      CJ1(M)=0.0
      II=0
      DO 60 I=1,MN,M
      DO 61 J=1,M-1
      II=II+1
   61 A(II,M+2)=-CJ1(J)
      II=II+1
      A(II,M+2)=0.0
   60 CONTINUE
      II=0
      DO 72 I=1,MN-M,M
      DO 71 J=1,M
      II=II+1
   71 A(II,M21)=-CI1(J)
   72 CONTINUE
  214 CONTINUE
  101 CONTINUE
      DO 70 I=1,MN
      B(I)=X(I)/DELT
   70 CONTINUE
      J=1
      DO 80 I=1,M
      B(I)=B(I)+BC(I)
   80 CONTINUE
      CALL ECOBAND(A,B,X,M,MN,IMI)
      IMI=IMI+1
      SUMC=0.0
      DO 513 J=1,M
      DO 514 I=J,MN,M
      SUMC=SUMC+X(I)*PHI(J)
  514 CONTINUE
  513 CONTINUE
      AP=DELX*DELY*SUMC
      CONIN=0.0
      DO 515 J=1,M
  515 CONIN=CONIN+DELY*PHI(J)*V(J)*CI
      AI=AI+DELT*CONIN
      PVI=AI/PV
      I=0
      CONOUT=0.0
      DO 516 J=MN-M1,MN
      I=I+1
  516 CONOUT=CONOUT+DELY*V(I)*PHI(I)*X(J)
      AO=AO+DELT*CONOUT
      PER=(AI-AO)/AP
      TSUM=TSUM+DELT
      IF(PVI.LT.CHECK) GO TO 672
      IHIS=IHIS+1
      CHECK=CHECK+0.02
      XH(IHIS)=X(MN-9)
      PHIS(IHIS)=PVI
  672 CONTINUE
      IF(PVI.GE.PVC) GO TO 100
      GO TO 101
  100 CALL PLOTS(2,1,5LPLOTR)
      CALL SCALE(XH,6.,IHIS,1)
      CALL AXIS(1.5,9.5,4HCBAR,4,6.,0.,XH(IHIS+1),XH(IHIS+2))
      CALL SCALE(PHIS,9.,IHIS,1)
      CALL AXIS(1.5,9.5,3HPVI,-3,9.,270.,PHIS(IHIS+1),PHIS(IHIS+2))
```

```
      CALL SYMBOL(7.5,9.,0.14,4HMN=9,270.,4)
      CALL SYMBOL(7.0,9.0,0.14,9HAL=6.2 FT,270.,9)
      CALL SYMBOL(6.5,9.,0.14,10HAT=0.00 FT,270.,10)
      CALL SYMBOL(6.,9.,0.14,8HWELL 131,270.,8)
      CALL PLOT(1.5,9.5,-3)
      DO 4010 I=1,IHIS
 4010 PHIS(I)=-PHIS(I)
      CALL LINE(XH,PHIS,IHIS,1,2,2)
      CALL PLOT(0.0,0.0,999)
      DO 4020 I=1,IHIS
 4020 PHIS(I)=-PHIS(I)
      CALL OUTPUT(XH,PHIS,M,N,TSUM,PVI,DELY,DELX,DELT
     #,ALEFF,ATEFF,L,VBAR,W,CI,PER,HTOT,KBAR,PHIBAR,IHIS)
      STOP
      END
      SUBROUTINE OUTPUT(XH,PHIS,M,N,TSUM,PVI,DELY,DELX,DELT
     #,ALEFF,ATEFF,L,VBAR,W,CI,PER,HTOT,KBAR,PHIBAR,IHIS)
      DIMENSION XH(500),PHIS(500)
      DIMENSION ALEFF(19)
      REAL L,KBAR
      WRITE(6,204)
      WRITE(6,205)
      WRITE(6,206) TSUM,PVI
      WRITE(6,207)DELY,DELX,DELT
      WRITE(6,208)ALEFF(1),ATEFF
      WRITE(6,209) L,VBAR
      WRITE(6,210) W
      WRITE(6,211)CI
      WRITE(6,212)PER
      WRITE(6,205)
      WRITE(6,204)
      WRITE(6,303)
  303 FORMAT(//)
  304 FORMAT(/)
      INC=8
      J=1
      IF(IHIS.GT.INC)GO TO 1
      WRITE(6,103)(PHIS(I),I=1,IHIS)
      WRITE(6,100)J,HTOT,KBAR,PHIBAR,(XH(I),I=1,IHIS)
      GO TO 40
    1 CONTINUE
      JJ=INC
      IC=INC-7
      WRITE(6,103)(PHIS(I),I=IC,INC)
      WRITE(6,100)J,HTOT,KBAR,PHIBAR,(XH(I),I=IC,JJ)
      INC=INC+8
      WRITE(6,304)
      IF(IHIS.GT.INC) GO TO 1
      IC=INC-7
      WRITE(6,103)(PHIS(I),I=IC,IHIS)
      WRITE(6,100)J,HTOT,KBAR,PHIBAR,(XH(I),I=IC,IHIS)
   40 CONTINUE
  100 FORMAT(1X,I1,2X,F4.1,5X,F5.1,4X,F4.2,6X,8(E12.4))
  103 FORMAT(5X,*H(FT)*,3X,*K(MD)*,5X,*PHI*,4X,8(5X,F7.3))
  204 FORMAT(5X,40H****************************************
     #,15H***************)
  205 FORMAT(5X,1H*,53X,1H*)
  206 FORMAT(5X,1H*,10X,*TIME= *,F6.1,1X,*DAYS*,3X,*AMT INJ= *
     #,F5.3,*PV*,7X,1H*)
  207 FORMAT(5X,1H*,4X,*DELY=*,F5.1,1X,*FT*,2X,*DELX= *,
     #F5.2,1X,*FT*,2X,*DELT=*,F5.2,1X,*DAYS*,3X,1H*)
  208 FORMAT(5X,1H*,5X,*ALPHAL= *,F6.3,1X,*FT*,5X,*ALPHAT=*,
```

```
   #F9.5,1X,*FT*,7X,1H*)
209 FORMAT(5X,1H*,10X,*L= *,F6.1,1X,*FT*,4X,*VBAR= *,
   #F4.2,1X,*FT/SEC*,10X,1H*)
210 FORMAT(5X,1H*,15X,*WEIGHTING FACTOR= *,F5.2,15X,1H*)
211 FORMAT(5X,1H*,16X,*INITIAL CONC.= *,F6.3,16X,1H*)
212 FORMAT(5X,1H*,13X,*MASS BALANCE FACTOR= *,F7.5,12X,1H*)
    RETURN
    END
    SUBROUTINE MEAN(XB,X,H,N)
    DIMENSION X(18),H(18)
    SUM=0.0
    SUM1=0.0
    DO 1 I=1,N
    SUM1=SUM1+H(I)
 1  SUM=SUM+X(I)*H(I)
    XB=SUM/SUM1
    RETURN
    END
    SUBROUTINE ECOBAND(A,B,X,M,MN,IMI)
    DIMENSION A(1450,35),B(1450),X(1450),G(1450)
    M21=M*2+1
    M1=M+1
    M2=M+2
    IF(IMI.GE.1) GO TO 82
    A(1,M2)=A(1,M2)/A(1,M1)
    IF(M.EQ.1) GO TO 99
    A(1,M21)=A(1,M21)/A(1,M1)
 99 CONTINUE
    DO 10 I=2,MN
    MJ=M+3-I
    IF(MJ.LT.2) MJ=2
    DO 20 J=MJ,M1
    SUML=0.0
    IF(MJ.EQ.2)GO TO 22
    IC=I
    GO TO 23
 22 IC=M+1
 23 DO 21 II=MJ-1,J-1
    IC=IC-1
 21 SUML=SUML+A(I,II)*A(I-IC,J+IC)
    A(I,J)=A(I,J)-SUML
 20 CONTINUE
    DO 30 J=M2,M21
    SUMU=0.0
    IF(MJ.EQ.2) GO TO 32
    IC=I
    GO TO 33
 32 IC=M+1
 33 DO 31 II=MJ-1,M
    IC=IC-1
    JIC=J+IC
    IF(JIC.GT.M21) GO TO 31
    SUMU=SUMU+A(I,II)*A(I-IC,JIC)
 31 CONTINUE
    A(I,J)=(A(I,J)-SUMU)/A(I,M1)
 30 CONTINUE
 10 CONTINUE
 82 CONTINUE
    G(1)=B(1)/A(1,M1)
    DO 40 I=2,MN
    JC=M+2-I
    IF(JC.LT.1) GO TO 42
```

```
      JJ=0
      GO TO 43
   42 JC=1
      JJ=I-M-1
   43 SUMG=0.0
      DO 41 II=JC,M
      JJ=JJ+1
   41 SUMG=SUMG+A(I,II)*G(JJ)
      G(I)=(B(I)-SUMG)/A(I,M1)
   40 CONTINUE
      X(MN)=G(MN)
      MROW=1
      DO 60 I=1,MN-1
      SUMX=0.0
      IC=MN-I
      JJ=IC
      MROW=MROW+1
      IF(MROW.GT.M1) GO TO 61
      GO TO 62
   61 MROW=M+1
   62 DO 63 II=M2,M+MROW
      JJ=JJ+1
   63 SUMX=SUMX+A(IC,II)*X(JJ)
      X(IC)=G(IC)-SUMX
   60 CONTINUE
      RETURN
      END
```

APPENDIX E

Fortran Listing of the Layer Grouping Program TDISP

```
      PROGRAM  TDISP(INPUT,OUTPUT,TAPE6=OUTPUT)
C*************************************************
C
C     L AND H GROUPING METHOD PROGRAM
C
C      DATA SHOULD BE INPUT AS FOLLOWS
C
C*********FIRST LINE
C
C    ALEFF,ATEFF,L,DO,VBAR,M
C
C WHERE:
C
C    ALEFF       TRANSVERSE DISPERSIVITY, FEET
C
C    ATEFF       LONGITUDINAL DISPERSIVITY, FEET
C
C    L           TOTAL SYSTEM LENGTH, FEET
C
C    DO          MOLECULAR DIFFUSION COEFFICIENT,
C                 SQUARE FEET/DAY
C
C    VBAR        FLOW RATE AVERAGED INTERSTITIAL VELOCITY,
C                 FEET/DAY
C
C    M           FORMATION CEMENTATION FACTOR
C
C*********SECOND LINE AND SUBSEQUENT LINES
C
C
C      EACH LINE CORRESPONDS TO INDIVIDUAL LAYER PROPERTIES
C
C      LIST AS THEY APPEAR IN CROSS SECTION
C
C      LAST LINE SHOULD BEGIN WITH -1.0 TO FLAG PROGRAM
C       TO STOP. THIS IS A DUMMY LINE.
C
C    H,K,PHI
C
C WHERE:
C
C    H       LAYER HEIGHT, FEET
C
C    K       PERMEABILITY, MD
C
C    PHI     POROSITY
C
C*****************************************************************
      DIMENSION H(100),RHO(100),K(100),KL(100),KT(100),V(100),
     INTD(100),PHI(100)
      REAL K,KL,KT,K1,K2,L,NTD,KBAR,KT1,KT2,KLHT
      DATA EPHS/1.E-06/
      WRITE(6,100)
      READ,ALEFF,ATEFF,L,DO,VBAR,M
      IF(ALEFF.LT.0.0)STOP
      I = 0
      WRITE(6,101)
  1   I = I + 1
      READ, H(I),K(I),PHI(I)
      IF(H(I).LT.0.0)GO TO 2
      GO TO 1
```

```
 2    LYR = I - 1
      HTOT=0.0
      DO 5503 I=1,LYR
 5503 HTOT=HTOT+H(I)
      CALL MEAN(KBAR,K,H,LYR)
      CALL MEAN(PHIBAR,PHI,H,LYR)
      DO 5 I=1,LYR
      V(I) = K(I)*PHIBAR*VBAR/(PHI(I)*KBAR)
      KL(I) = (DO*PHI(I)**(M-1)) + ALEFF*V(I)
 5    KT(I) = (DO*PHI(I)**(M-1)) + ATEFF*V(I)
      CALL ALPHF(LYR,PHI,H,K,KBAR,PHIBAR,HTOT,ALPHA1,ATEFF,
     #VBAR,ALEFF,V)
      WRITE(6,5505) ALPHA1
 5505 FORMAT(1X,*ALPHA1 =*,F12.5)
 40   IF(LYR.EQ.1)GO TO 200
      LYR1 = LYR - 1
C
C     CALCULATE NTO
C
      DO 6 I=1,LYR1
      R = 14.*(L/(H(I)+H(I+1)))**2
      NTO(I) = R*KT(I+1)/(L*V(I))
 6    IF(V(I).LT.V(I+1))NTO(I) = R*KT(I)/(L*V(I+1))
C
C     FIND MAXIMUM NTO
C
      R = 0.0
      DO 7 I=1,LYR1
 7    R = AMAX1(R,NTO(I))
      IF(R.LT.5.0)GO TO 200
C
C     LOCATE LAYER-PAIR WITH MAXIMUM NTO
C
      DO 8 I=1,LYR1
      IF(ABS(R-NTO(I)).LT.EPHS)GO TO 9
 8    CONTINUE
 9    CONTINUE
      IF(V(I).LT.V(I+1))GO TO 10
      V1 = V(I)
      H1 = H(I)
      K1 = K(I)
      PHI1 = PHI(I)
      KT1 = KT(I)
      V2 = V(I+1)
      H2 = H(I+1)
      K2 = K(I+1)
      PHI2 = PHI(I+1)
      KT2 = KT(I+1)
      GO TO 11
 10   V1 = V(I+1)
      H1 = H(I+1)
      K1 = K(I+1)
      PHI1 = PHI(I+1)
      KT1 = KT(I+1)
      V2 = V(I)
      H2 = H(I)
      K2 = K(I)
      KT2 = KT(I)
      PHI2 = PHI(I)
 11   HT = H1 + H2
      PHT = (PHI1*H1 + PHI2*H2)/HT
      VHT = ((PHI1*V1*H1) + (PHI2*V2*H2))/(PHT*HT)
```

```
      A = (V1-VHT)/VHT
      B = (V2-VHT)/VHT
      KLHT = (KL(I)*H(I) + KL(I+1)*H(I+1))/HT
      C = 2.*A*A*((H1/HT)**3)*(PHI1/PHT)*VHT*L/KT1
      C = (3.*A*B*(H1*H2+H2/(HT**3))*(PHI1/PHT)*VHT*L/KT2) - C
      C = C + (B*B*(PHI2/PHT)*((H2/HT)**3)*VHT*L/KT2)
      PE = (KLHT/(VHT*L)) - ((HT/L)**2)*C/6.
      KL(I) = PE*VHT*L
      PHI(I) = PHT
      V(I) = VHT
      K(I) = (K(I)*H(I) + K(I+1)*H(I+1))/HT
      KT(I) = (KT(I)*HT*KT(I+1))/(KT(I)*H(I+1) + KT(I+1)*H(I))
      H(I) = HT
C
C     RE-INDEX LAYERS
C
      I = I + 1
      DO 12 J =I,LYR1
      H(J) = H(J+1)
      PHI(J) = PHI(J+1)
      K(J) = K(J+1)
      V(J) = V(J+1)
      KT(J) = KT(J+1)
 12   KL(J) = KL(J+1)
      LYR = LYR - 1
      GO TO 40
 200  CONTINUE
C
C     WRITE RESULTS
C
      WRITE(6,102)
      DO 15 I=1,LYR
      PE = KL(I)/(V(I)*L)
      ALPHA = PE*L
 15   WRITE(6,103)H(I),PHI(I),K(I),NTO(I),KL(I),KT(I),V(I),PE,ALPHA
 100  FORMAT(/* READ ALEFF,ATEFF,L,DO,VBAR,M *)
 101  FORMAT(/* READ H,K,PHI *)
 102  FORMAT(//* SUMMARY OF COMBINED LAYERS*/* H,PHI,K,NTO,KL,KT,V,PE,
     1ALPHA *)
 103  FORMAT(1X,2F6.3,F6.2,F6.1,2E12.4,F6.2,2E12.4)
      STOP
      END
      SUBROUTINE MEAN(XB,X,H,N)
      DIMENSION X(100),H(100)
      SUM = 0.
      SUM1 = 0.
      DO 1 I=1,N
      SUM1 = SUM1 + H(I)
 1    SUM = SUM + X(I)*H(I)
      XB = SUM/SUM1
      RETURN
      END
      SUBROUTINE ALPHE(M,PORIG,HORIG,KORIG,MEANK,MEANP,SUMH,ALPHA1,
     #ATEFF,VBAR,ALEFF,V)
      DIMENSION PORIG(200),HORIG(200),KORIG(200),V(200)
      REAL KORIG,MEANK,MEANP
      SUM=0.0
      DO 10 I=1,M
      SUML=ALEFF*V(I)*PORIG(I)*HORIG(I)/
     #(VBAR*MEANP*SUMH)
      SUMK=((KORIG(I)/PORIG(I))-(MEANK/MEANP))**2
      SUMT=((PORIG(I)**2)*SUMK*(HORIG(I)**3))
```

```
     #/(ATEFF*MEANK*KORIG(I)*SUMH*3.)
10    SUM=SUM+SUML+SUMT
      ALPHA1=SUM
      RETURN
      END
```

REFERENCES

1. Fried, J. J. and Combarnous, M. A., (1971), "Dispersion in Porous Media," Adv. in Hydrocarbon Science, vol. 7, pp. 169-282.

2. Fried, J. J., (1975), Groundwater Pollution, Elsevier Scientific Publishing Co., New York.

3. Perkins, T. K., and Johnson, O. C., (1963), "A Review of Diffusion and Dispersion in Porous Media," Soc. of Pet. Eng. J., vol. 3, no. 1, pp. 70-84, March.

4. Bird, R. B., Stewart, W. E., and Lightfoot, E. N., (1960), Transport Phenomena, Wiley, New York.

5. Bear, J. and Bachmat, Y., (1967), "A Generalized Theory on Hydrodynamic Dispersion in Porous Media," Proc. Int. Ass. Sci. Hydrol. Symp. Haifa, Pub. No. 72.

6. Taylor, G., (1953), "Dispersion of Soluble Matter in Solvent Flowing Slowly Through a Tube," Proc. Roy. Soc. Ser. A219, pp. 186-203.

7. Saffman, P. G., (1959), "A Theory of Dispersion in a Porous Medium," J. Fluid Mech., vol. 6, pp. 321-346.

8. De Josselin De Jong, G., (1958), "Longitudinal and Transverse Diffusion in Granular Deposits," Trans. Amer. Geophys. Un. vol. 39(1) pg. 67.

9. Bachmat, Y., (1969), "Hydrodynamic Dispersion in a Saturated Homogeneous Porous Medium at Low Peclet Numbers and Non Homogeneous Solution," Water Resour. Res. vol. 5(1) pg. 139.

10. Aris, R., (1956), "On the Dispersion of a Solute in a Fluid Flowing Through a Tube," Proc. Roy. Soc. Ser. A235, pg. 67.

11. Grane, F. E., and Gardner, G. H. F., (1961), "Measurements of Transverse Dispersion in Granular Media," Jour. Chem. Eng. Data, vol. 6, no. 2, pg. 283.

12. Brigham, W. E., et al., (1961), "Experiments on Mixing During Miscible Displacement in Porous Media," Soc. Pet. Eng. Jour., March, pg. 1.

13. Raimondi, P., et al., (1959), "Effect of Pore Structure and Molecular Diffusion on the Mixing of Miscible Liquids Flowing in Porous Media, Preprint 43 presented at AICHE-SPE Joint Symposium, San Francisco, Ca.

14. Handy, L. L., (1959), "An Evaluation of Diffusion Effects in Miscible Displacement," Trans. AIME, vol. 216, pg. 382.

15. Dieuhlin, A., (1980), "The Effect of Scale in the Propogation of Pollution in an Aquifer," Ph.D. dissertation, School of Mines in Paris, France.

16. Lake, L. W., and Hirasaki, G. J., (1979), "Taylor's Dispersion in Stratified Porous Media," SPE 8436, presented at 54th annual SPE convention Las Vegas, Nev., Sept. 23-26.

17. Lake, L. W., and Pope, G. A., et al., (1980), "Isothermal, Multiphase, Multicomponent Fluid in Permeable Media; Part I, Physical Description and Mathematical Formulation," The University of Texas.

18. Peaceman, D. W., (1966), "Improved Treatment of Dispersion in Numerical Calculation of Multidimensional Miscible Displacement," Soc. Pet. Eng. J., Sept., pp. 213-216.

19. McDonald, R. C., (1980), Class Notes.

20. Dake, L. P., (1978), Fundamentals of Reservoir Engineering, Elsevier Scientific Publishing Co., New York.

21. Intercomp Reservoir Simulation Training Manual, Houston, Tx.

22. Peaceman, D. W. (1977), Fundamentals of Numberical Reservoir Simulation, Elsevier Scientific Publishing Co., New York.

23. Naiki, M., (1979), "Numerical Simulation of Polymer Flooding including the effects of Salinity," Ph.D. dissertation, The University of Texas.

24. Lake, L. W., (1979-1981), Class Notes.

25. Garder, Jr., A. O., Peaceman, D. W. and Pozzi, A. L., (1964), "Numerical Calculation of Multidimensional Miscible Displacement by the Method of Characteristics," Soc. Pet. Eng. J., March, pp. 26-36.

26. El Dorado MiCellar-Polymer Demonstration Project Third Annual Report, June 1976-August 1977, by Cities Service Co.

27. Vairogs, J., (1980), Cities Service Co., Private Communications.

28. Weast, R. C., editor, (1969), CRC Handbook of Chemistry and Physics, Chemical Rubber Co., Cleveland, Oh.

29. Bennett, C. O., and Myers, J. E., (1962), Momentum, Heat, and Mass Transfer, McGraw-Hill, New York.

30. Settari, A., Price, H. S., and Dupont, T., (1977), "Development and Application of Variational Methods for Simulation of Miscible Displacement in Porous Media," Soc. Pet. Eng. J., June, pp. 228-246.

VITA

Robert Ravnaas was born in Rochelle, Illinois, on April 7, 1957, the son of Martin and Virginia Ravnaas. After completing his secondary education at Rochelle Township High School, Rochelle, Illinois, in 1975, he entered the University of Colorado in September, 1975. On January 6, 1979 he married Gina Marie Rushing and later received a B.S. in Chemical Engineering in August 1979. He began work on his M.S. in Petroleum Engineering in September 1979, and worked for Superior Oil during the summer of 1980 as an assistant engineer.

Permanent address: Rt. 3
Rochelle, IL 61068

This thesis was typed by Master Typist, Inc.